STANFORD
UNIVERSITY

Space Systems Development Laboratory
Robert Twiggs

Master Thesis

Design Of The Electrical Power System For The Rabbit Satellite

November 2003

Andy Hamm
AndyHamm@Stanford.Edu

Technical University of Munich
Institute of Astronautics

Prof. Dr.-Ing. U. Walter
Prof. Dr.-Ing. E. Igenbergs
Dr.-Ing. Kristian Pauly

Stanford University
Space Systems Development Laboratory

Prof. Robert J. Twiggs

Acknowledgement

I would like to acknowledge Prof. R. Twiggs, who hosted and supervised me at his *Space Development Laboratory* at Stanford University.

Prof. Dr. Ing. U. Walter, Prof. Dr.-Ing. E. Igenbergs, and Dr.-Ing. K. Pauly were my supervisors at the Technical University of Munich. They first initiated and helped arranging this project and have always been available for questions.

Especially I'd like to thank Mr. J. Ellis, mentor at Stanford University, for sharing his vast experience in power supply design.

The satellite design team of RabbitSat, lead by Scott Gorin, was involved in the EPS deign in the first place. Thanks to Scott Gorin, Dan Bhanderi, Yeefeng Ruan, Mark Featherstone, Mark Castanon, Mike Ingalls, and Lori Kahn for the good cooperation.

The professional support of Dr. Klinger contributed a great deal towards the completion of the RabbitSat design, in particular the prevailing RabbitSat EPS design.

Dan Bhanderi, who shared the office with me, made my stay at Stanford an even more pleasant and rich experience.

Last but not least the good cooperation with the financial supporters, Michael Enoch of Lockheed Martin and Keith Avery of Mission Research Cooperation, facilitated this work.

Funds facilitating my stay at Stanford came from: "Liselotte und Heinrich Muehlfenzl Stiftung", Germany.

Abstract

This paper is the complete documentation of the Electrical Power Subsystem (EPS) Design for the RabbitSat satellite.

As part of the Cubesat program, RabbitSat was being developed by a team of graduate students at the Space Systems Development Laboratory of Stanford University, United States of America. The RabbitSat project was conducted under the supervision of Cubesat inventor, Prof. Robert J. Twiggs.

In compliance with the general Cubesat idea, the specific goal of the prevailing EPS design was, to demonstrate the feasibility of a fully functional and reliable, yet highly efficient EPS, only consisting of COTS (Commercial-Of-The-Shelf) components.

This challenge was met with great success. This report presents the design of a complete and effectively tested Electrical Power Subsystem.

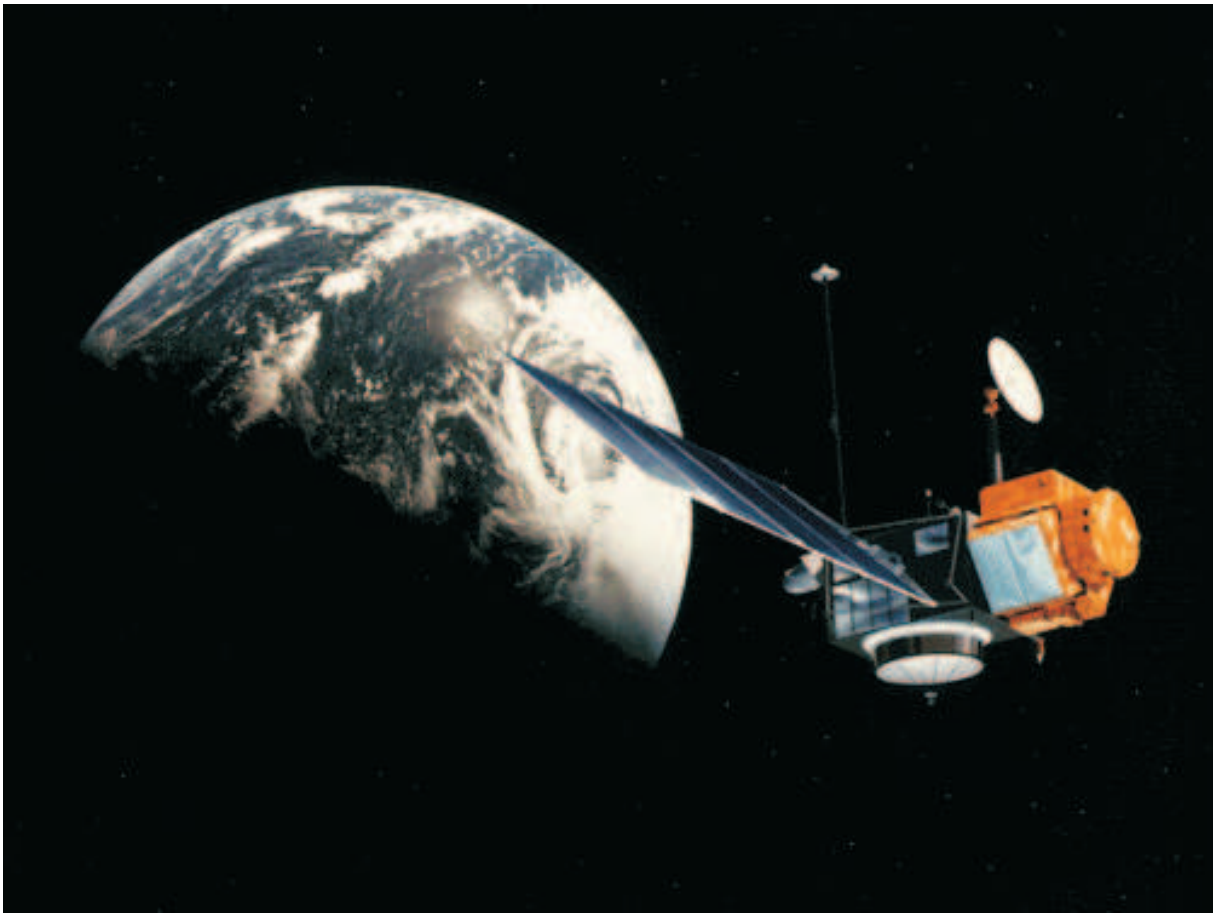

Contents

1 Introduction **9**

2 Background **11**

2.1 Introduction to the Cubesat Program 11

2.1.1 Cubesat Overview 12

2.1.2 Recent Cubesat Missions 13

2.2 RabbitSat Overview 19

2.2.1 The RabbitSat Mission 20

2.2.2 The RabbitSat Payloads 20

2.2.3 The RabbitSat Subsystems 21

2.3 RabbitSat Requirements 23

2.3.1 RabbitSat Top Level Requirements 23

2.3.2 Electrical Power Subsystem Functional Requirements 25

2.3.3 Electrical Power Subsystem Derived Requirements 26

2.4 RabbitSat Power Budget 27

2.4.1 Mission Type 27

2.4.2 Load Requirements for Electrical Power 30

3 RabbitSat Solar Array Layout and Design **32**

3.1 Power Source Options 32

3.2 Solar Panel Configuration 33

3.2.1 Estimation of the Required Solar Array Area 33

3.3 Solar Array Configuration Options 34

3.4 Solar Cell Choice 34

3.4.1 How a Solar Cell works 36

3.4.2 The Different Cell Types 37

3.5 Solar Panel Layout 41

3.5.1 The Trade Study 41

3.5.2 Evaluation of the Trade Study 45
3.6 Power Simulation for different Layouts 45
3.6.1 The Power Generation of Each Solar Panel 45
3.6.2 The Sun Vector 46
3.6.3 The Normal Vectors 47
3.6.4 The Angle of Incidence 49
3.6.5 Total Power Generation 49
3.6.6 Simulation Results 49
3.7 Solar Panel Design 52
3.8 Mounting the Solar Panels 55

4 RabbitSat EPS Power Storage 57
4.1 Power Storage Requirements 57
4.2 Selection of the Battery Type 58
4.3 Determining the Battery Capacity 59
4.4 Battery Charge/Discharge Characteristics 61
4.4.1 Battery Charging 61
4.4.2 Battery Discharging 61
4.4.3 Battery Self Discharge 61
4.5 Summary 63

5 RabbitSat Power Regulation, and Control 64
5.1 Customary EPS Control Schemes 65
5.2 RabbitSat EPS Control Scheme 66
5.3 RabbitSat Power Distribution 67
5.3.1 Cabling 67
5.3.2 Fault Protection 68
5.3.3 Switching Devices 68

6 RabbitSat EPS Electronic Board Design 71
6.1 The Power Source Unit 72
6.1.1 The DC/DC Converter 73
6.1.2 The Current Sensors 76
6.1.3 The Solar Array 78
6.2 The Power Distribution Unit 78
6.2.1 The DC/DC Converters 80

6.2.2 The Current Sensors 82
6.2.3 The Switches 82
6.2.4 The Delay Circuit 83
6.3 The EPS Test Board Design 86
6.4 The EPS Flight Board Design 88

7 Summary and Conclusions 93
References 94

A The Solar Panels 96
A.1 Mechanical Drawings 96

B The EPS Test Board 100
B.1 Schematics 100
B.2 Printed Circuit Board 103

C The EPS Flight Board 105
C.1 Schematics 105
C.2 Printed Circuit Board 110
C.3 EPS Board Component Lists 111

List of Figures

2.1 P-pod Design - Cubesat Deployer with 3-Cubesats Capacity [7] 12
2.2 QuakeSat [2] 13
2.3 QuakeSat EPS Configuration [2] 14
2.4 QuakeSat Solar Panel Configuration [2] 15
2.5 AAU-Cubesat [4] 16
2.6 AAU-Cubesat EPS Hardware Configuration [4] 18
2.7 3D Model of the RabbitSat structure 19
2.8 Structure Subsystem Functionality [10] 21
2.9 COMM Subsystem Functionality [10] 22
2.10 ADCS Subsystem Functionality 22
2.11 RabbitSat Requirements - Hierarchical Structure; the Requirements Marked Yellow are Listed Below 24
2.12 EPS basic functionality. [11]. 25
2.13 MEPSI Deployer Onboard the Space Shuttle, Payload Bay Integrated Truss Segment, Port1; Some Milliseconds after Cubesat Deployment 28
2.14 Power Allocation to the RabbitSat Subsystems. This Table is Part of the Power Simulation, available in Appendix CD, "Power Budget" 29
2.15 Power Allocation to the Subsystems. 31

3.1 Options for Solar Array Configuration 35
3.2 Principle of the Solar Cell Operation 36
3.3 Solar Cell Efficiency vs. Price per Watt of Maximum Power Output of the Solar Cell at Perpendicularly Incident Solar Radiation ($1365W/m^2$) 37
3.4 Basic Triple-Junction Cell Structure [15] 38
3.5 Utilization of the Sun Radiation by Solar Cells [14] 39
3.6 Histogram for 2000 Emcore Multi-Junction Cells [13] 41
3.7 Solar Panel Configuration Options I 42
3.8 Solar Panel Configuration Options II 43

3.9 Solar Cell Power Generation as a Function of the Angle of Incident Solar Radiation and the Solar Cell Normal (The data presented here stems from Spectrolab Triple Junction "Angle of Incidence Test Results", which is Spectrolab confidential information and not subject to publication) 46

3.10 Definition of the Sun Vector (Here in Green) in a Spherical Coordinate System 47

3.11 Definition of All Solar Panel Normal Vectors. The Solar Panel Vectors, $\vec{p}_1$ through $\vec{p}_6$ are Static through the Simulation, Only the Sun Vector $\vec{s}_{IN}$ is "Tumbling". Here, $\vec{s}_{IN}$ is Shown in it's Null Position 48

3.12 In/Out-put Window of the Excel Incoming Power Simulation 50

3.13 Excel Output of the Power Simulation 51

3.14 Solar Panel Design - The (SL) Solar Cell Dimensions (All Dimensions in Inch) 52

3.15 Solar Panel Design - The Panel's Electrical Configuration. Left: Two Large Panels in Series per Large Face of the Satellite. Right: One Small Panel per Small Face of the Satellite 53

3.16 Solar Panel Design - The Small Panels (All Dimensions in Inch) 54

3.17 Solar Panel Design - The Large Panels (All Dimensions in Inch) 54

3.18 The Solar Panel Structure 55

3.19 Solar Cell, Used for the Test Panels [15] 55

4.1 Showcase Power Usage Chart 58

4.2 Common Battery Types 59

4.3 Depth-of-Discharge vs. cycle life for Secondary Batteries. Increased Cycle Life Reduces the Amount of Energy Available from the Batteries During Each Cycle - DOD Decreases with Cycle Life [11] 60

4.4 Charging NiCd Batteries at Different Charge Currents [16] 61

4.5 Discharging of NiCd Batteries [16] 62

4.6 Typical NiCd self discharge characteristics [16] 62

5.1 The Main Spacecraft Power Control Schemes; Derived from [11] 65

5.2 First-cut RabbitSat Control Scheme Configuration 66

5.3 RabbitSat Power Control Scheme 69

5.4 RabbitSat Power Control Scheme 70

6.1 First-cut RabbitSat Control Scheme Configuration 72

6.2 The MAX1771 DC/DC Converter [17] 73

6.3 MAX1771 - Maximum Output Current vs. Input Voltage 75

6.4 The RabbitSat MAX1771 Layout 75

6.5 MAX471 Typical Operating Circuit [17] 76
6.6 MAX4172 Typical Operating Circuit [17] 77
6.7 DC/DC Converter Efficiency Characteristics of the below Discussed Parts [17] 79
6.8 DC/DC Converter Typical Operating circuits [17] 79
6.9 The EPS Switching Tasks 82
6.10 IRF4905 - Application as Switches for RabbitSat 83
6.11 The EPS Delay Circuit 84
6.12 The EPS Delay Circuit 85
6.13 Functionality of the EPS Circuit Test Board 86
6.14 The EPS Circuit Test Board with Components 87
6.15 The EPS Circuit Test Board 87
6.16 The EPS Flight Board 89
6.17 Connector Pin Allocation 90
6.18 Connector Pin Allocation 90
6.19 Connector Pin Allocation 91
6.20 Connector Pin Allocation 91
6.21 Connector Pin Allocation 92
6.22 Connector Pin Allocation 92

List of Tables

2.1 Orbit Parameters as Defined Above 28

3.1 Effects of System Level Parameters on the Electrical Power Subsystem Design 33
3.2 Solar Cell Prices 40
3.3 Solar Panel Layout Configurations - Evaluation Table 44

Abbreviations

AAU	Aalborg University
ACS	Attitude Control Subsystem
ADCS	Attitude Determination and Control Subsystem
BCR	Battery Charge Regulator
BDR	Battery Discharge Regulator
CIC	Coverglass Inter Connect
COMM	Communications Subsystem
C&DH	Computer and Data Handling Subsystem
COTS	Commercial Of The Shelf
DC	Direct Current
DET	Direct Energy Transfer
DJ	Dual Junction
DOD	Depth of Discharge
DOD	Department of Defence
EC	Emcore
EOL	End Of Life
EPS	Electrical Power Subsystem
FPGA	Field Programmable Gate Array
LEO	Low Earth Orbit
IC	Integrated Circuit
ITJ	Improved Triple Junction
NiCd	Nickel Cadmium
NiMH	Nickel Metal Hydrate
MCU	Micro Controller Unit
MEPSI	Micro Electromechanical System-Based Pico Satellite Launcher
MOSFET	Metal Oxide Field Effect Transistor
MPPT	Maximum Power Point Tracker
MRC	Mission Research Corporation
MUX	Multiplexer
OBC	Onboard Computer
RabbitSat	Rapid Application and Basic Bus Integrated Test Bed
PC	Protection Circuit
PCB	Printed Circuit Board
SCR	Semiconductor Controlled Rectifier
SL	Spectrolab
SQ	Space Quest Inc.
TBD	To Be Determined
TBR	To Be Reviewed
TJ	Triple Junction

Chapter 1

Introduction

Scope

This document is the Master Thesis of Andy Hamm. The thesis was conducted at the Department of Aeronautics and Astronautics of Stanford University, California, USA.

Subject of the Master thesis is the design of the Electrical Power Subsystem of RabbitSat, a "Cubesat"-type pico-satellite, developed at Stanford's Space Systems Development laboratory under Professor Robert J. Twiggs.

RabbitSat represents a team effort of Stanford Graduate students in collaboration with the customer of Lockheed Martin.

The first RabbitSat team meeting in April, 2003 was the official start of the project. The RabbitSat design is anticipated to be completed by December, 2003.

Contents Overview

In order to maintain a clear overview of this document, this section summarizes the contents of all chapters.

Chapter 1 - Introduction The introduction describes the scope of the thesis at hand and summarizes the subsequent chapters.

Chapter 2 - Background In this chapter, the reader is first introduced to the Cubesat program. A general Cubesat description is followed by two outstanding examples of successfully completed Cubesat missions, Quakesat and AAUSat.

This done, the focus will be the RabbitSat mission itself, whose Electrical Power Subsystem design is subject of this thesis. You will find a general mission description and a detailed discussion of the RabbitSat requirements. The EPS specific derived requirements, together with a description of mechanical mission parameters, lead to a comprehensive, preliminary power budget table which concludes this chapter.

Chapter 3 - RabbitSat Solar Array Layout and Design After introducing customary spacecraft power sources, this chapter treats the design process of the RabbitSat solar array. A rough estimation of the total required solar array area eventually leads

to a trade study of practical layout options. The description of the layout choice process is followed by a discussion of the solar panel design for RabbitSat. This chapter concludes with the description of building test solar panels.

Chapter 4 - RabbitSat EPS Power Storage This chapter considers power storage requirements, battery chemistry and configuration options followed by a technical discussion of battery properties.

Chapter 5 - RabbitSat Power Regulation and Control After presenting an introduction to customary satellite power control schemes, the reader will be guided along the design path towards the control scheme for RabbitSat.

Chapter 6 - RabbitSat Electronic Board Design After defining the functionality of the EPS system in the previous chapters, the goal of this chapter is to guide the reader through the design process of the Electronic hardware. The hardware includes the power source unit to condition the current for usage and the power distribution unit, responsible for providing power at certain voltage levels to the end users.

Chapter 7 - Summary and Conclusions ...description coming soon

Chapter 2

Background

2.1 Introduction to the Cubesat Program

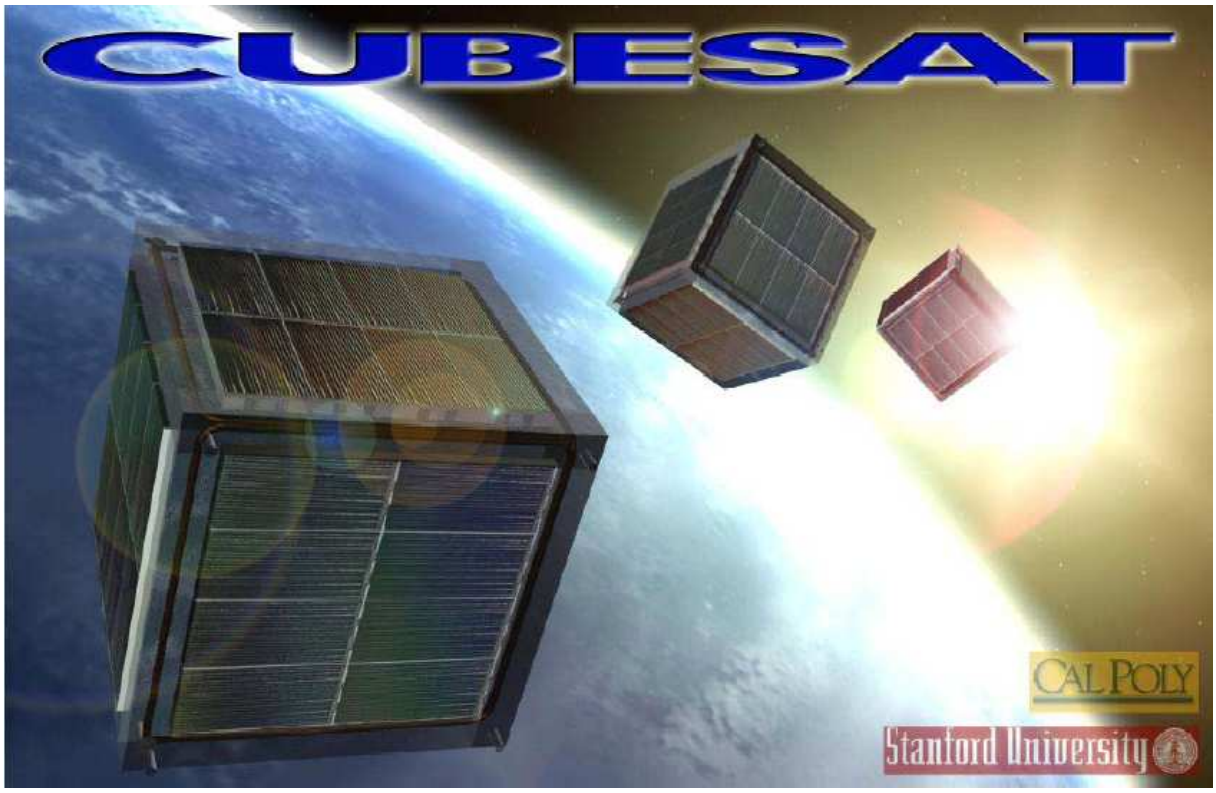

2.1.1 Cubesat Overview

The CubeSat program was started in 1999 so as to facilitate access to space for universities that are building pico-satellites by standardizing launch integration using the Poly Picosat Orbital Deployer (P-pod) launcher (see Figure 2.1). The flight-certified P-POD launcher can accommodate three CubeSats and may be easily integrated as a secondary payload on many types of launches. By standardizing size and mass requirements ($10 \cdot 10 \cdot 10cm^3$ cube, $1kg$), the collaborative initiative by California Polytechnic University and the Space Systems Development Lab at Stanford has encouraged dozens of international teams to develop satellites in this common CubeSat form factor [1].

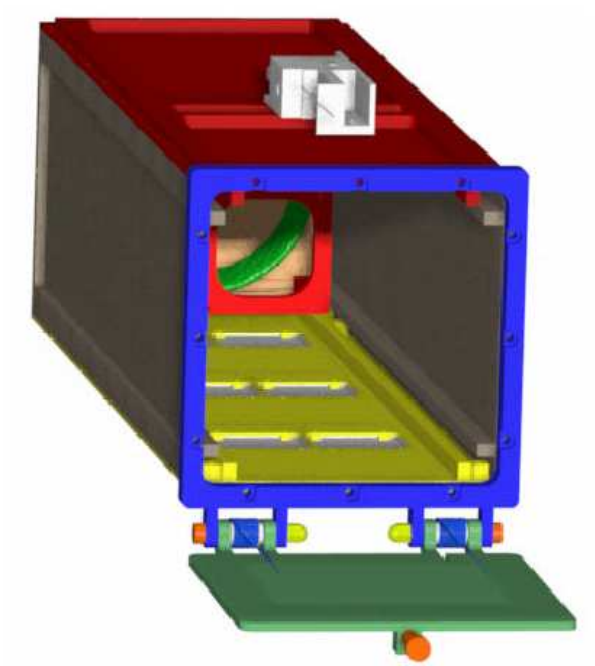

Figure 2.1: P-pod Design - Cubesat Deployer with 3-Cubesats Capacity [7]

2.1.2 Recent Cubesat Missions

This year, six Cubesat satellites have been successfully launched onboard the Russian *Rockot* rocket, operated by Eurockot Company. The mechanical interface with the *Rockot-Breeze* upper stage was provided by the usage of three P-pod deployers. The negotiations with Eurockot were done solely by Calpoly University, southern California.

The author would like to introduce the "Quakesat" mission by Stanford University as well as the "AAU-Cubesat" mission by Aalborg University, Denmark, as tw examples od especially outstanding missions. The focus in the subsequent description will be on the Electrical Power Subsystems of these satellites.

Quakesat Mission

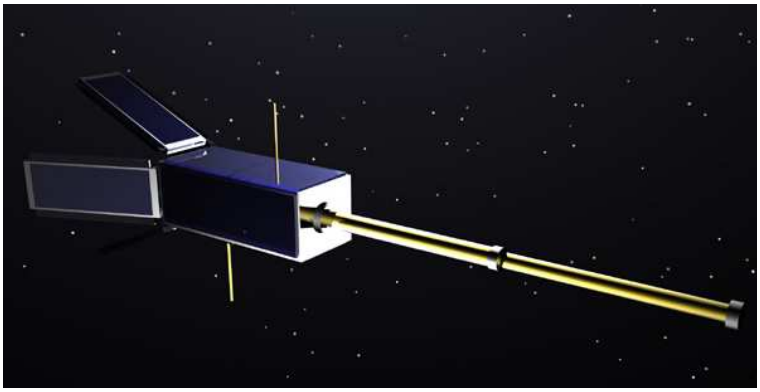

Figure 2.2: QuakeSat [2]

The Mission

Earthquakes are a global concern. Not only are they a major threat to life, but they also present a great danger to regional infrastructure. Yet, currently there are no means of accurately forecasting imminent earthquake activity. The mission of QuakeSat is to change all that. Using an innovative space based technique to search for the emission of Extremely Low Frequency (ELF) magnetic signals, which have shown to be an earthquake precursor phenomenon, groundbreaking methods for predicting earthquake activity may become plausible in the near future[2].

The three primary *mission objectives* for the QuakeSat Nano-Sat are:

1. To detect, record, and downlink earthquake ELF emission data
2. Demonstrate that the CubeSat Nano-Sat design is a cost-effective platform for conducting significant space science research experiments
3. Demonstrate the feasibility of utilizing commercially-off-the-shelf (COTS) parts to construct a reliable, short mission micro-satellite [2]

The Electrical Power Subsystem

The QuakeSat Electrical Power System (EPS) includes three subsystems: a power source, power storage, and a power regulator.

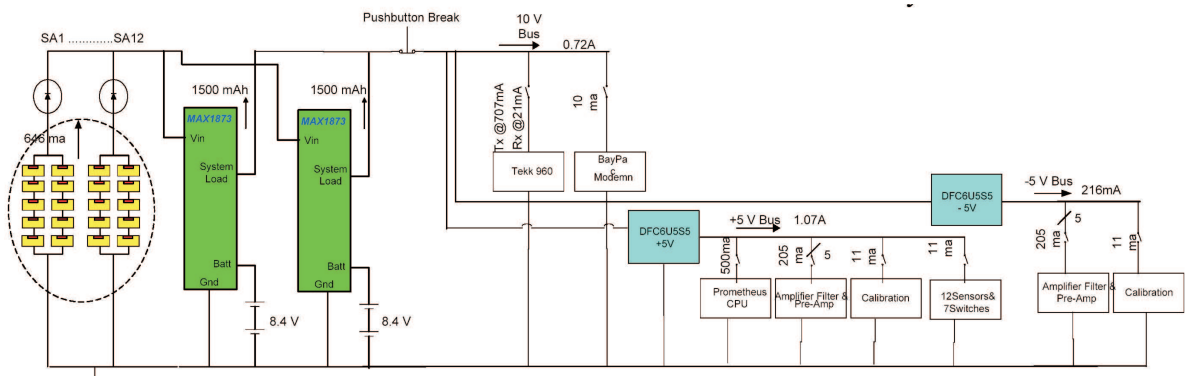

Figure 2.3: QuakeSat EPS Configuration [2]

Figure 2.3 shows the configuration of the EPS system, as described in [2]. The power source consists of a solar array with twelve solar panels: four body mounted panels and four double-sided deployable wings (see Figure 2.2). The double-sided arrays are canted at 150deg relative to the QuakeSat body. The 150deg cant angle was found through a power/attitude simulation to yield the maximum amount of power due to the high sun angle experienced in the sun synchronous orbit. The simulation showed that the solar arrays at a 150deg cant angle would generate between 7.90W to 19.05W, depending on the time of year. These power levels will adequately cover the system loads, which are expected to be between 2.8W (min) and 12.6W (peak). Each solar panel measures $330 \cdot 86mm^2$ and the ten multi junction solar cells on each panel have an efficiency of 22.9%. The cells on each panel are made up of two electrically parallel strings, five cells in series per string (see Figure 2.4). They produce 6.46W per panel.

The power storage subsystem includes two MAX1873 Li+ charge controllers and four Li+ Ion batteries, 2-series Li+ batteries per branch and 2 parallel-branches[1]. The MAX1873 is capable of supplying power to the system load during daylight, while charging 3 Li+ cells in series. A chip in the MAX1873 kit was replaced so that 2 instead of 3 Li+ batteries could be charged. Each charge controller limits the total source current and the maximum charging current to 3A, to charge 2-series Li+ cells up to 4.2V each, and to power the satellite function. The power regulator consists of two DFC6U5S5 voltage regulators that convert the unregulated solar panel bus voltages of 9.6V and 7.5V during daylight and eclipse respectively, to regulated +5V and -5V payload buses. The +5 V bus supplies the power to the CPU and the payload, and the -5V bus supplies the payload only. The system bus also supplies the power directly to the radio.

[1] 2 Li+ batteries in series for each of the 2 parallel branches

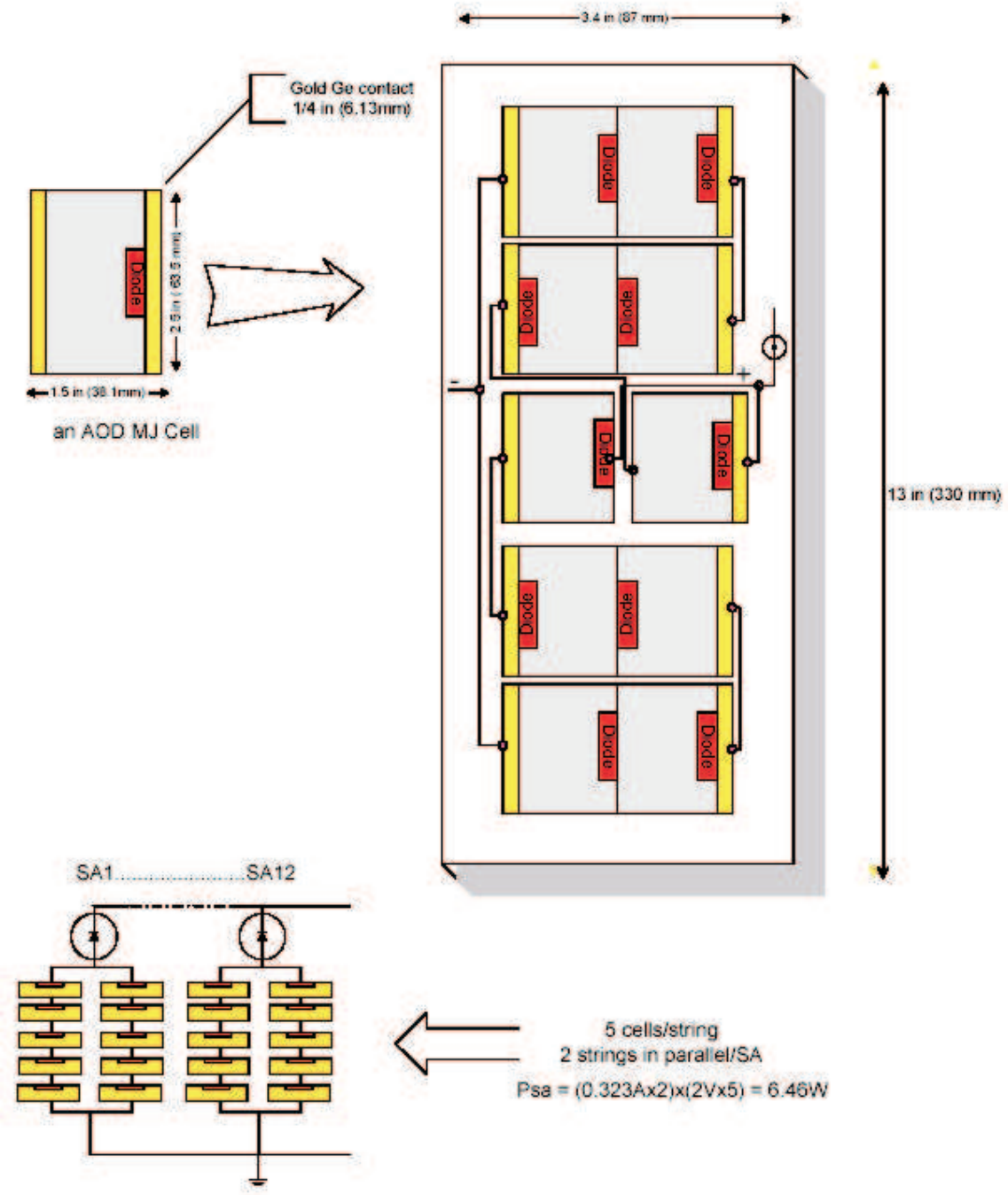

Figure 2.4: QuakeSat Solar Panel Configuration [2]

AAU-Cubesat Mission

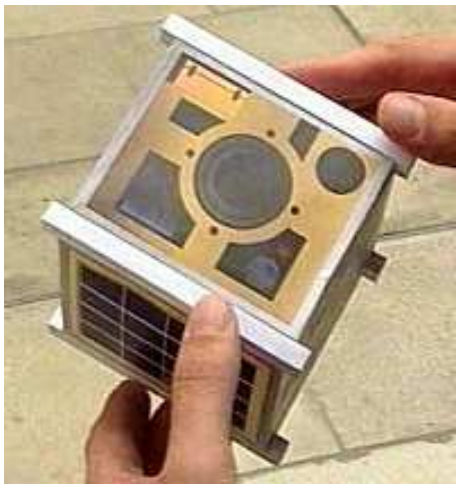

Figure 2.5: AAU-Cubesat [4]

The Mission

The "scientific" mission of the AAU-Cubesat (AAlborg University-Cubesat) is to take pictures of the surface of the Earth, and particularly of Denmark, by using the on-board camera. The images recorded by the satellite will later be transmitted to the ground station, located at Aalborg University, from where they will be distributed over the Internet and made accessible to the general public. Several success criteria have been defined. A basic success criterion in this case, is to develop and build a satellite that will be able to survive the launch and the hazardous environment in its orbit. Another success criterion is the establishment of a communication link with the ground station informing about the status of the satellite. Being able to point the on-board camera towards a specific target on the ground, to take an image and to send this data down to the ground station, represents the final success criteria [4].

The AAU-Cubesat Subsystems

The subsequent list gives a brief overview of the AAU-Cubesat subsystems that are referred to in the following section.

OBC The Onboard Computer handles information from subsystems and controls the satellite.

ACS The Attitude Control Subsystem is responsible for controlling the orientation of the satellite, such that camera and antennas are pointed in a specified direction.

CAM The Camera Payload is responsible for the part of the satellite mission which is to take pictures of Denmark.

COM The Communications Subsystem is responsible for transmitting and receiving communication between the satellite and the ground station. The COM unit consists of the radio as well as a modem.

EPS The Electrical Power Subsystem, as subsequently discussed in more detail [4].

Introduction to the AAU-Cubesat Electrical Power Subsystem

The AAU-Cubesat Electrical Power Subsystem is rather complex for a Cubesat-type satellite. The author finds that this EPS design sets a good standard, and believes that its understanding will be of great value for the understanding of the RabbitSat EPS design as presented in this paper. This section gives an overview of the AAU-Sat design. In depth documentation can be found online at [4].

The AAU EPS is a fully autonomous system that receives power from a number of solar arrays with photo-voltaic cells, and conditions and distributes this power to a number of users, which are the other electronic subsystems on board the satellite. If more power is obtained from the solar cells than that consumed by the connected subsystems, then this power must be stored in a number of batteries, and when power consumption exceeds the power input, the batteries should discharge in order to provide the required power output. If a subsystem draws a current from the EPS that is large enough to suggest a malfunction of that user, then the EPS must cut the current to the users and inform the Onboard Computer (OBC). Further it must be possible for the OBC to specify which users are allowed to receive power at a given time. In addition to this main functionality the EPS has a set of secondary functions that must be fulfilled:

1. Collect housekeeping information, including satellite temperatures
2. Act as boot-master and external watchdog for the OBC [4]

Functionality of the AAU-Cubesat Electrical Power Subsystem

This section is a brief discussion of the AAU-Cubesat hardware functionality. It provides an overview of the hardware configuration by extending the information given in the previous introduction with more details regarding the configuration of solar arrays and battery pack. The EPS is depicted in Figure 2.6, including all hardware modules. The following will explain the modules of Figure 2.6.

Solar Arrays The solar arrays are configured such that the cells of each side on the satellite are connected in series and the five sides are connected in parallel. This configuration has been chosen because it was found that this is the best tradeoff between ease of Maximum Power Point Tracking (MPPT) and improved converter performance. The voltage across the parallel connection will, in this configuration, be approximately 4.0V, depending on the incident solar radiation. The diodes protect the cells from conducting a reverse current.

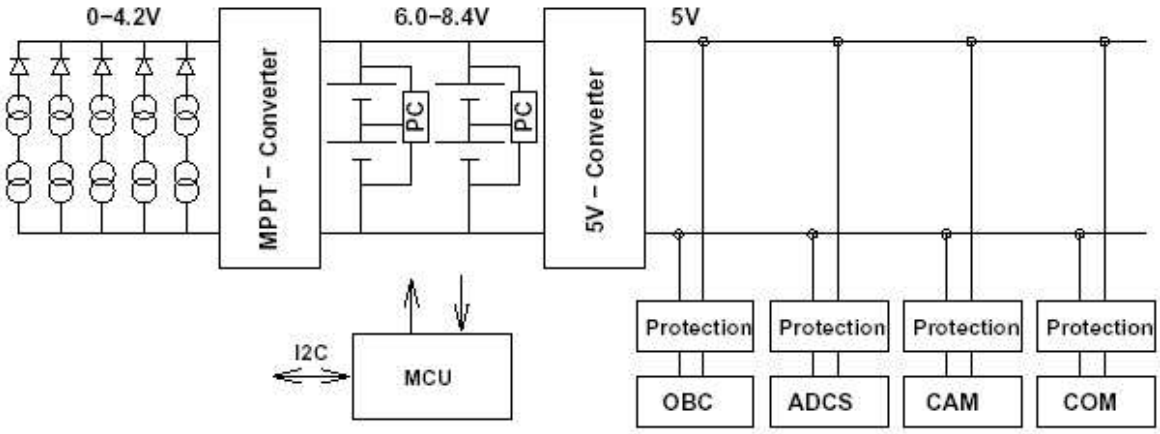

Figure 2.6: AAU-Cubesat EPS Hardware Configuration [4]

MPPT-Converter The MPPT-converter performs MPPT on the solar array i.e. it transfers the maximum obtainable power from the solar array to the output side of the converter. Furthermore, it steps up the voltage to fit the level of the battery pack.

Battery Pack The battery pack consist of 2·2 batteries connected in two parallel strings of two batteries in series. This gives a voltage of between 6.0V and 8.4V depending on the state of the batteries. The battery is also responsible for voltage control of the intermediate power bus between the two converters. The batteries keep the average voltage in the range 6.0V to 8.4V. Protection-circuits (PC), protecting the batteries from over- and under-voltage, are placed across the batteries.

5V-Converter The 5V-converter conditions the voltage for the main 5V power bus by stepping down the voltage from the intermediate power bus.

Remove-Before-Flight-Pin Amongst the smaller things that are included in the EPS, the "Remove before flight" pin is quite important. When this pin, which consists of 4 jumpers is inserted, the EPS is off. There is a jumper for each battery protection circuit that - when inserted - disconnects the batteries from the rest of the satellite. Also, there is a jumper for each converter that - when inserted - switches off the converter.

User Protection Each load has an associated protection circuit which will shut down the user, i.e. disconnect it from the power bus, if the load draws a current that is higher than a specified maximum for the respective load. This could happen if the load would have suffered from an internal latch-up due to radiation effects. The load protection circuit also serves as a controllable on/off switch that lets the EPS Micro Control Unit (MCU) switch loads on and off according to the orders that it receives from the OBC, with which the MCU communicates through the I^2C Bus.

Digital Hardware The digital hardware, i.e. the Micro Controller Unit (MCU) is shown in the bottom of Figure 2.6. The MCU is responsible for measuring physical

values of the system depicted in Figure 2.6 and measurement of temperatures at various locations in the satellite. These measurements serve distinct purposes, and they are sent to the OBC for housekeeping information. [4]

2.2 RabbitSat Overview

RabbitSat stands for Rapid Application and Basic Bus Integrated Testbed. RabbitSat is being developed by a team of graduate students at Stanford University's Space Systems Development Laboratory (SSDL). The project is being conducted in cooperation with the customers, who provide two electronic payload boards. The development of the RabbitSat Electrical Power Subsystem is subject of the hereby presented thesis. This chapter gives an overview of the RabbitSat mission and requirements; it briefly introduces all RabbitSat subsystems and presents the thereof derived power requirements.

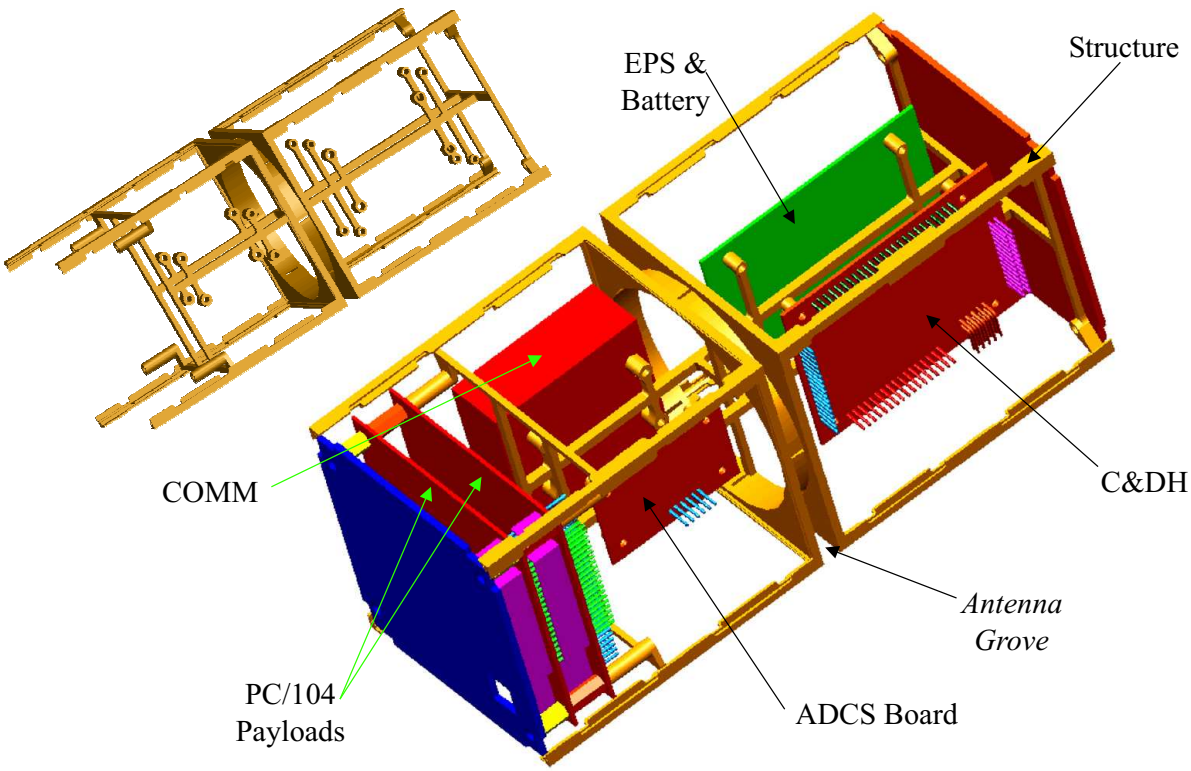

Figure 2.7: 3D Model of the RabbitSat structure

2.2.1 The RabbitSat Mission

The *primary objective* of the RabbitSat mission is to collect in-orbit performance data of payload space electronic components. *Secondary objectives* are: to utilize rapid prototyping technologies; and to provide additional data to support the analysis of the payload through direct measurement. These data include spacecraft orbit/position, spacecraft attitude, temperature, local magnetic field strength, ionizing dose rate, and total ionizing dose (accumulated) [5].

2.2.2 The RabbitSat Payloads

Two payloads will be flown onboard the RabbitSat satellite. These are the

- Mission Research Cooperation (MRC) Design Hardened Test Board, and the
- Field Programmable Gate Array (FPGA) Test Board

Our payloads are being provided by the RabbitSat through the Agile program from the Lockheed Martin Advanced Technology Center.

Agile, short for Agile Design and Development, is a Lockheed Martin Advanced Technology Center unclassified research and development effort being executed for the Advanced Science and Technology division of the National Reconnaissance Office. The purpose of the Agile program is to investigate alternative processes for rapid development of space systems, including model based contracting, simulation based acquisition, model based design and rapid prototyping manufacturing techniques [9].

The MRC Board

The objective of this payload is to collect data on the on-orbit performance of space electronic components developed using design hardened techniques. The spacecraft will be expected to provide power and communications for the experiment. In addition, the spacecraft will provide positional data, space environment and dosimetry data to be used to analyze the data collected from the payload. The Principal Investigator for this payload is Mr. Keith Avery of Mission Research Corporation (MRC) in Albuquerque, NM [9].

The FPGA Board

The objective of this payload is to collect data on the on-orbit performance of Commercial Of The Shelf (COTS) derived Field Programmable Gate Array (FPGA) space electronic components. The spacecraft will be expected to provide power and communications for the experiment. The Principal Investigators for this payload are Mr. Michael Enoch of the Lockheed Martin Advanced Technology Center in Albuquerque, NM and Mr. Carl Carmichael of Xilinx in San Jose, CA [9].

2.2.3 The RabbitSat Subsystems

This section provides an overview of the definition and the functions of the respective RabbitSat subsystems.

The Structure Subsystem

The RabbitSat structure is the backbone of the spacecraft, both figuratively and in reality. It provides the strength for mounting of all other subsystems, as well as handling launch and transportation loads. Figure 2.8 shows the functions of the structure subsystem. The RabbitSat structure will be made out of titanium, manufactured through the shape metal deposition process [10].

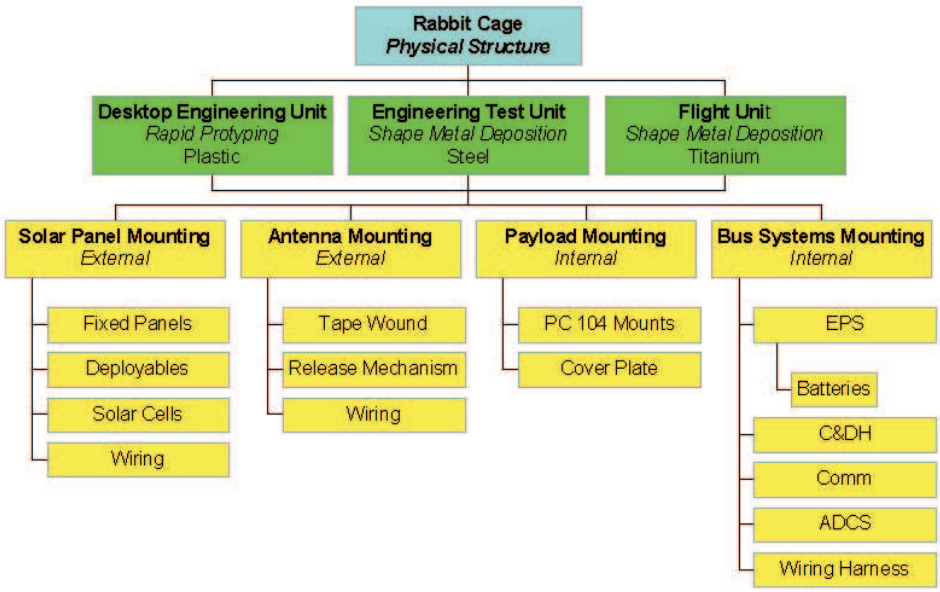

Figure 2.8: Structure Subsystem Functionality [10]

The EPS Subsystem

The Electrical Power Subsystem (EPS) will provide power to the other subsystems. The design of the EPS is the subject of this paper and will be discussed in detail through the following chapters.

The C&DH Subsystem

The Command and Data Handling Subsystem (C&DH) integrates and regulates the other Sub-Systems through various modes of operation throughout the life of the satellite [10].

The COMM Subsystem

The Communications Subsystem (COMM) provides the interface between the spacecraft and ground systems. The Communication subsystem receives and demodulates uplink signals and modulates and transmits downlink signals. Figure 2.9 shows the basic functionality of the RabbitSat COMM Subsystem [10].

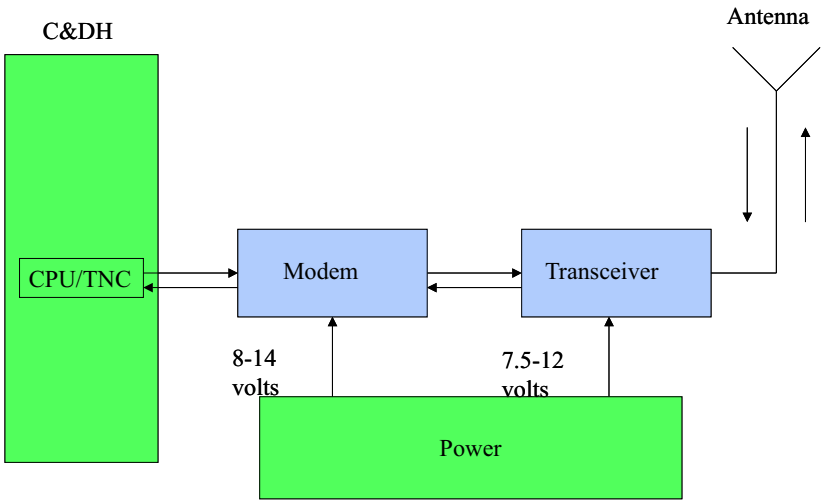

Figure 2.9: COMM Subsystem Functionality [10]

The ADCS Subsystem

The Attitude Determination and Control Subsystem (ADCS) provides the necessary determination of attitude and orbit of the satellite. There will be no attitude control onboard RabbitSat, hence the attitude data will be evaluated on ground. As depicted in Figure 2.10, the raw data will be the solar panels power outcomes as well as magnetometer data.

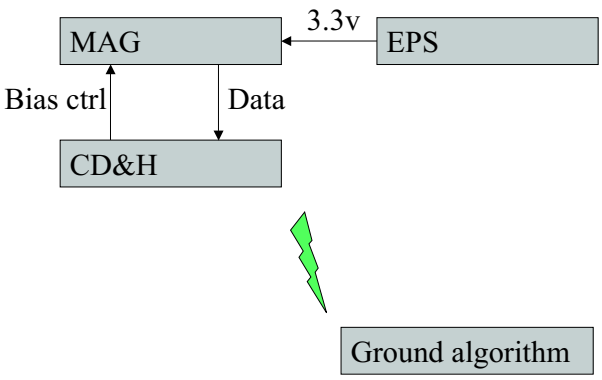

Figure 2.10: ADCS Subsystem Functionality

2.3 RabbitSat Requirements

Requirements for the RabbitSat have been derived through a process (mission analysis and functional/physical architecture definition) that has identified requirements associated with the Agile mission. The RabbitSat requirements have been formatted by direct inclusion of requirement tables from a RabbitSat System Requirements Database. This database is an EXCEL spreadsheet database [6].

This chapter gives an overview of the RabbitSat Requirements. The specific Electrical Power Subsystem (EPS) Requirements are discussed in more detail.

Figure 2.11 shows the RabbitSat requirements structure. There are essentially three documents that precede all subsequent RabbitSat requirements. These are: the Cubesat Specifications; the customer provided Agile Technical Requirements Document [8] and the Agile Mission Requirements Document [9]; and the Stanford AA236 course requirements.

The *Cubesat Specifications* document is a guideline for all Cubesat developers, exactly defining the Cubesat standard. Please see Section 2.1.1 for information about the Cubesat program and [7] for information regarding the document. The *Agile Technical Requirements Document* and the *Agile Mission Requirements Document* were prepared by our primary customer M. Enoch of Lockheed Martin Space Systems Company. These documents include requirements for the spacecraft (SC) design and fabrication, payload integration, space vehicle (SV) testing, launch vehicle (LV) integration, launch site testing, ascent and early orbit operations support (SV checkout and initialization), and mission operations support for the space vehicle. All requirements herein are mandatory requirements. The latter documents are not public domain, and are proprietary to the Lockheed Martin Space Systems Company.

The AA236 course requirements are rather organizational requirements regarding the AA236 class. They include, for instance, the minimum workhour requirements for the development team members, or the obligatory integration of customary space systems engineering methods. They are not of immediate concern for the technical design of the RabbitSat satellite.

The second level of Figure 2.11 includes the RabbitSat top-level requirements: the System Requirements and the Programmatic Requirements. These are listed in Section 2.3.1 and are consistent with the listings of [6].

The lowest level requirements in Figure 2.11 are the respective subsystem requirements, referred to as Functional Requirements. To maintain an overview, Section 2.3.2 includes only the specific functional requirements of the EPS subsystem.

Not shown in figure 2.11 are the Derived Requirements of section 2.3.3 which are the lowest level requirements of the RabbitSat requirements hierarchy. Derived requirements exist for each subsystem. They are not part of the System Requirements Document [6], but are maintained by the subsystem leads, respectively.

2.3.1 RabbitSat Top Level Requirements

The Top Level requirements are here split up into two categories: the Programmatic Requirements and the System Level Requirements. This is primarily to enhance the

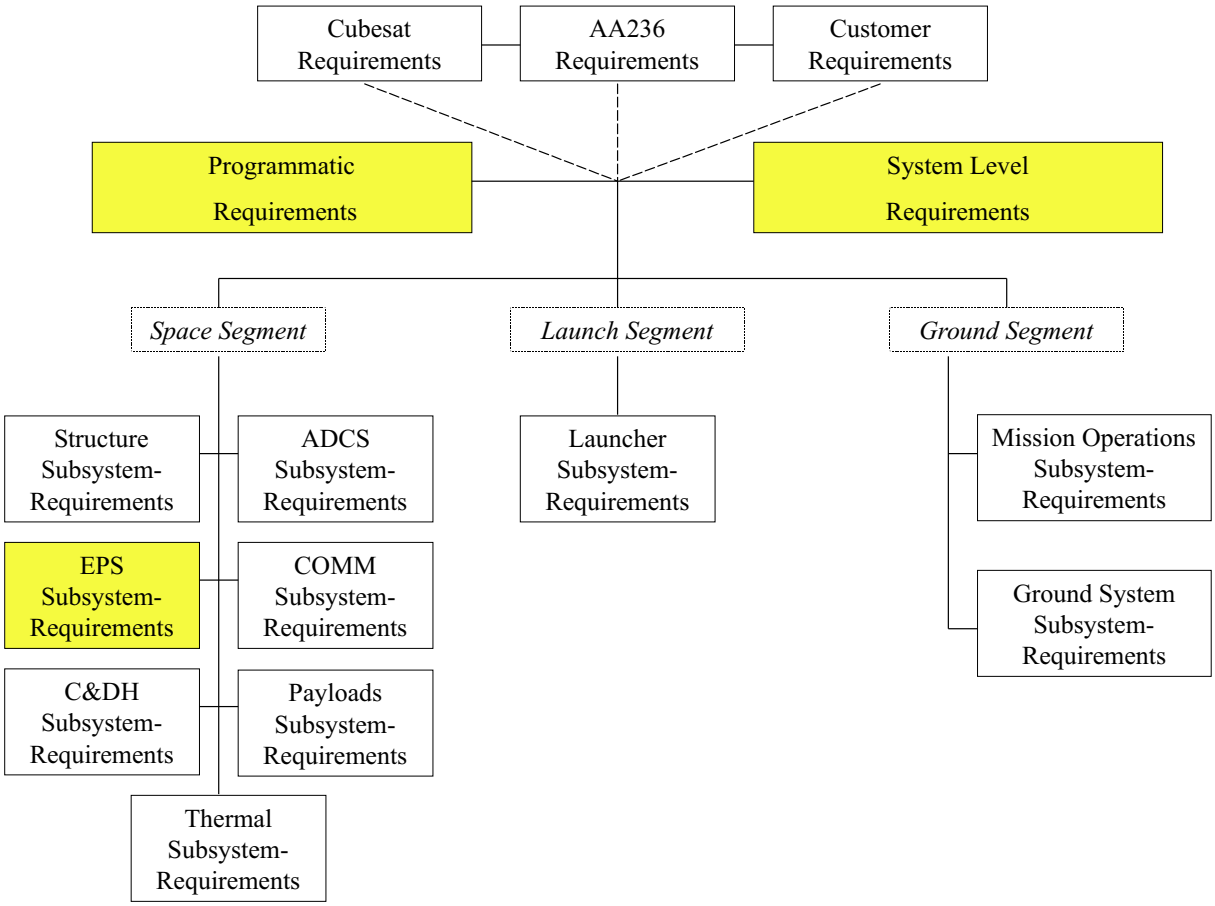

Figure 2.11: RabbitSat Requirements - Hierarchical Structure; the Requirements Marked Yellow are Listed Below

overview. Whereas the Programmatic Requirements mainly deal with requirements that originate from the Stanford Cubesat program intents, the System Level Requirements address rather technical issues.

Programmatic Requirements

1. The Team shall develop a CubeSat to fly a customer provided payload.
2. The RABBIT CubeSat shall fly 2 payloads - LMSS-ATC & MRC to each provide 1 payload.
3. The CubeSat shall conform to the P-POD Launcher in foot-print but not exceed MEPSI Launcher in length.
4. The CubeSat shall utilize Rapid Prototyping Technologies.
5. The Team shall implement full systems engineering to the CubeSat Project.
6. The Team shall conduct appropriate level development reviews throughout the CubeSat System Design Process.

7. The Project and its operation shall conform to all local, federal and international laws and regulations.
8. The CubeSat shall utilize COTS parts to minimize costs.
9. The CubeSat shall conform to the intent of the CubeSat Design Specifications Document.
10. The Team shall implement the 11 Steps of SMAD throughout the design and development.

System Level Requirements

1. The System shall collect performance data to support the payload data.
2. They System shall have an on-orbit operational life minimun of 6 months.
3. The System shall have a LEO orbit with a preference of 250 km - 400 km.
4. The System shall be compatible with a Stanford Ground Station.
5. The System shall have up-link and down-link communication capabilities.
6. The System Link Margin shall be greater than or equal to 10E-6 bit error rate (BER) for up-link and down-link.
7. All data processing shall be done on the ground by the customer.

2.3.2 Electrical Power Subsystem Functional Requirements

Figure 2.12 gives an overview of the functional requirements of the Electrical Power System (EPS). These are to store, distribute, and control power within the spacecraft.

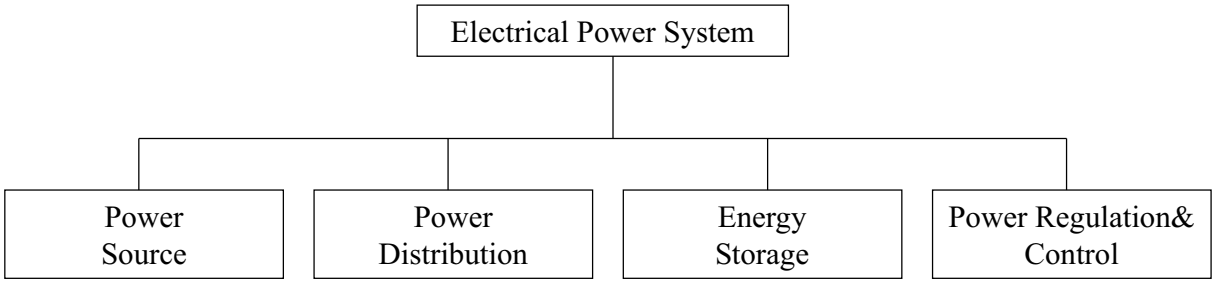

Figure 2.12: EPS basic functionality. [11].

Below is a more detailed list of the functional requirements. These are directly derived from the RabbitSat system level requirements of Section 2.3.1. The Subsystem Functional Requirements are the framework guideline for the EPS design. In Section 2.3.3 you will find the Derived Requirements. These represent the technical interpretation of the functional requirements.

1. The EPS shall supply a continuous source of electrical power to the spacecraft and payload loads.

2. The EPS shall control and distribute power to the spacecraft and payloads.

3. The EPS shall meet the average and peak power demands of the spacecraft and payloads

4. The EPS shall energize the satellite's electrical loads after deployment with a delay

5. The EPS shall provide solar cell current and voltage data to ADCS

6. The EPS shall provide for command and handling capacity by the FPGA

7. The EPS shall cut the solar cell/batteryconnections after EOL

2.3.3 Electrical Power Subsystem Derived Requirements

The Derived Requirements are the lowest level requirements in the RabbitSat requirements hierarchy. They are the technical interpretation of the Functional requirements as presented in Section 2.3.2. The Derived Requirements serve as the baseline for the RabbitSat Electrical Power Subsystem design. They are:

1. Provide TJ solar cells on each, top and bottom panel

2. Provide DJ solar cells on 4 side panels

3. Provide deployment switches to isolate the batteries from all circuits

4. Provide master switch to isolate the batteries from all circuits (mechanically activated during deployment)

5. povide for minimum two time delay from deployment to start of satellite operations

6. Provide battery overcharging protection

7. Supply power to the COMM at 7.2 to 14V

8. Supply power to the FPGA at 5V

9. Supply power to the MRC at 3.3V and 5V

10. Supply power to the ADCS at 3.3V

11. Supply power to the C&DH at 3.3V

12. Supply power to the Sensors at 3.3V and 5V

2.4 RabbitSat Power Budget

2.4.1 Mission Type

The RabbitSat is anticipated to be launched as a secondary payload within the "Micro-Electromechanical System - Based Pico Satellite Inspector" (MEPSI) deployer onboard the Space Shuttle (Payload Bay Integrated Truss Segment, Port1, see Figure 2.13). To make up for the uncertainty regarding the resumption of the Shuttle flights, RabbitSat shall also have the capability of adapting to the P-Pod launcher launched on Eurockot from Plesetsk, Russia. The P-Pod launcher is the standard Cubesat payload adapter, as discussed in Chapter 2.1. Three Cubesat satellites fit in one P-Pod. P-Pod launch integration is done by CalPoly University under J. Puig-Suari.

Considering the possibility of a launch onboard the Space Shuttle as well as onboard a Russian launcher, our design shall account for a 300km to 700km LEO orbit at *TBD* inclination.

To estimate the minimum incoming power for this type of orbit, we have to determine the average eclipse period. As the average eclipse period lies close to the maximum eclipse period, we will use this value. All formulas in this and the following section, unless stated otherwise, are taken from [11]. Let ρ be the angular radius of the Earth, and you find for the maximum eclipse duration in a circular orbit, T_E,

$$T_E = P \cdot \frac{\rho}{180deg} \tag{2.1}$$

where ρ may be calculated by

$$\sin\rho = \frac{R_E}{R_E + H} \tag{2.2}$$

P is the orbit period, given by

$$P = 1.658669 \cdot 10^{-4} \cdot (R_E + H)^{3/2} \tag{2.3}$$

H is the altitude of the circular orbit in km, and R_E is the radius of the earth ($R_E = 6378.14km$). By choosing $H = 400km$, and therefore $\rho = 70.22deg$ and $P = 92.56min$ we obtain $T_E = 36.10min$.

Table 2.1 summarizes the orbital data we assume as a worst case scenario for the subsequent power calculations. The revolutions per day are computed by

$$R = \frac{1436.07}{P} \tag{2.4}$$

Parameter	**Symbol**	**Value**	**Unit**
Radius of the Earth	R_E	6378.14	km
Altitude	H	400	km
Orbital Period	P	92.56	min
Maximum Eclipse	P_E	36.10	min
Minimum Daylight	P_S	56.46	min
Revolutions per Day	R	15.56	#
Cycles after six Months	C	2839	#

Table 2.1: Orbit Parameters as Defined Above

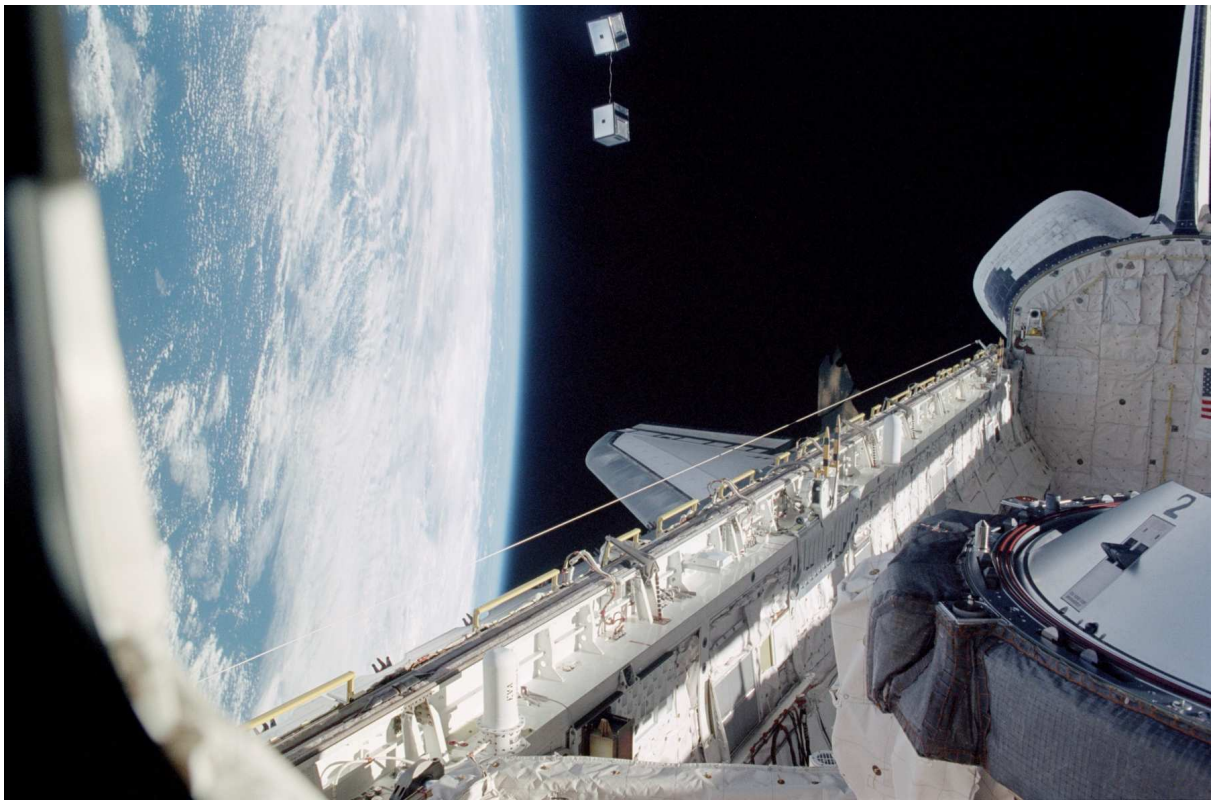

Figure 2.13: MEPSI Deployer Onboard the Space Shuttle, Payload Bay Integrated Truss Segment, Port1; Some Milliseconds after Cubesat Deployment

Power Allocation										
Subsystem	**Component**	**Duty Cycle**	**Duty Cycle Fraction**	**Voltage (V)**	**Current (mA)**	**Operational Power (mW)**	**Orbit Avrg. Power [mW]**	**Energy/Orbit (mW-hrs)**	**Power per day [mWhr]**	
ADCS	Magnetometer	continuous	1	5	5	25.00	25.00	38.57	600	**ADCS**
						0.00	0.00	0.00	0	
						0.00	0.00	0.00	0	
						0.00	0.00	0.00	0	
						0.00	0.00	0.00	0	
						0.00	0.00	0.00	0	
C&DH	CPU operational	continuous	1	5	20	100.00	100.00	154.27	2400	**C&DH**
					0	0.00	0.00	0.00	0	
						0.00	0.00	0.00	0	
						0.00	0.00	0.00	0	
						0.00	0.00	0.00	0	
						0.00	0.00	0.00	0	
COMM	Transmitter	10 min per day	0.006944444	9.6	850	8160.00	56.67	87.42	1360	**COMM**
	Modem	continuous	1	9.6	10	96.00	96.00	148.10	2304	
	Receiver	only if no transmiss.	0.993055556	9.6	20	192.00	190.67	294.14	4576	
						0.00	0.00	0.00	0	
						0.00	0.00	0.00	0	
	Transmitter/Beacon	1 min per 30 min	0.033333333	9.6	850	8160.00	272.00	419.61	6528	
MRC - Payload	Board/ Low	all but 8min per orb	0.913570101	5	16	80.00	73.09	112.75	1754.054594	**MRC - Payload**
	Board/ High	8 min per orbit	0.086429899	5	80	400.00	34.57	53.33	829.7270311	
	Board/High	0	0	3.3	0	0.00	0.00	0.00	0	
						0.00	0.00	0.00	0	
						0.00	0.00	0.00	0	
FPGA - Payload	Board/ Low	all but 10min per orb	0.891962626	5	100	500.00	445.98	688.00	10703.55151	**FPGA - Payload**
	Board/ High	10 min per orbit	0.108037374	5	150	750.00	81.03	125.00	1944.672729	
						0.00	0.00	0.00	0	
						0.00	0.00	0.00	0	
						0.00	0.00	0.00	0	
						0.00	0.00	0.00	0	
Other				0	0	0.00	0.00	0.00	0	**Other**
						0.00	0.00	0.00	0	
						0.00	0.00	0.00	0	
						0.00	0.00	0.00	0	
						0.00	0.00	0.00	0	
						0.00	0.00	0.00	0	
						Operational Power (mW)	Orbit Avrg. Power [mW]	Energy/Orbit (mW-hrs)	Power per day [mWhr]	
			Total design load			18463.00	1375.00	2121.18	33000.00587	
			Margin of Error (%)			**30**				
			Total required load			24001.90	1787.50	2757.53	42900.00763	

Figure 2.14: Power Allocation to the RabbitSat Subsystems. This Table is Part of the Power Simulation, available in Appendix CD, "Power Budget"

2.4.2 Load Requirements for Electrical Power

Before selecting a suitable type and design of the power source, the load requirements for electrical power of each single subsystem including the MRC and FPGA payloads were drafted (refer to Section 2.2.2 for information about these payloads). Figure 2.14 presents these preliminary values. Whereas some columns are mainly for reference, the most important columns in this overview are the *Subsystems* and their respective *Components*, the *Duty Cycles*, and particularly the *Orbit Average Powers*. The *Operational Power* (=Maximum Power) will be the basis for the battery capacity sizing, the *Voltages* will determine the optimum bus voltage and the required voltage converters.

It follows a detailed description of the columns of Figure 2.14.

Component The power consumption values are listed for the relevant components for each respective subsystem.

Duty Cycle The duty cycle column includes descriptions of the operational modes.

Duty Cycle Fraction The duty cycle fraction X_{DC} is here defined as

$$X_{DC} = \frac{P_C}{P_A} \quad [-], \tag{2.5}$$

where P_C refers to the Period of Operation during a representative considered period P_A. The duty cycle fraction becomes one for continuously operated components. The values for X_{DC} are part of the equations for the Operational Power, the Orbit Average Power, and the Power per Day.

Voltage The voltage V refers to the voltage the component is anticipated to run on.

Current The Current I specifies the current that a component is assumed to, or specified to, consume.

Operational Power The Operational Power or the maximum power P_{max} is here calculated as

$$P_{max} = V \cdot I \quad [mW] \tag{2.6}$$

Orbit Average Power The Orbit Average Power is the product of the Operational Power and the Duty Cycle. It is the average power consumption of a component, averaged independently of daylight and eclipse periods.

$$P_{mean} = P_{max} \cdot X_{DC} \quad [mW] \tag{2.7}$$

Energy per Orbit The Energy per Orbit averages the total amount of energy per orbit with the period P as in Table 2.1.

$$P_{orb} = P_{mean} \cdot P \quad [mWH] \tag{2.8}$$

Power per Day The Energy per Day averages the total amount of energy per day.

$$P_{day} = P_{mean} \cdot 24hrs \quad [mWH] \tag{2.9}$$

Figure 2.15 visualizes the breakdown of power amongst the different RabbitSat subsystems.

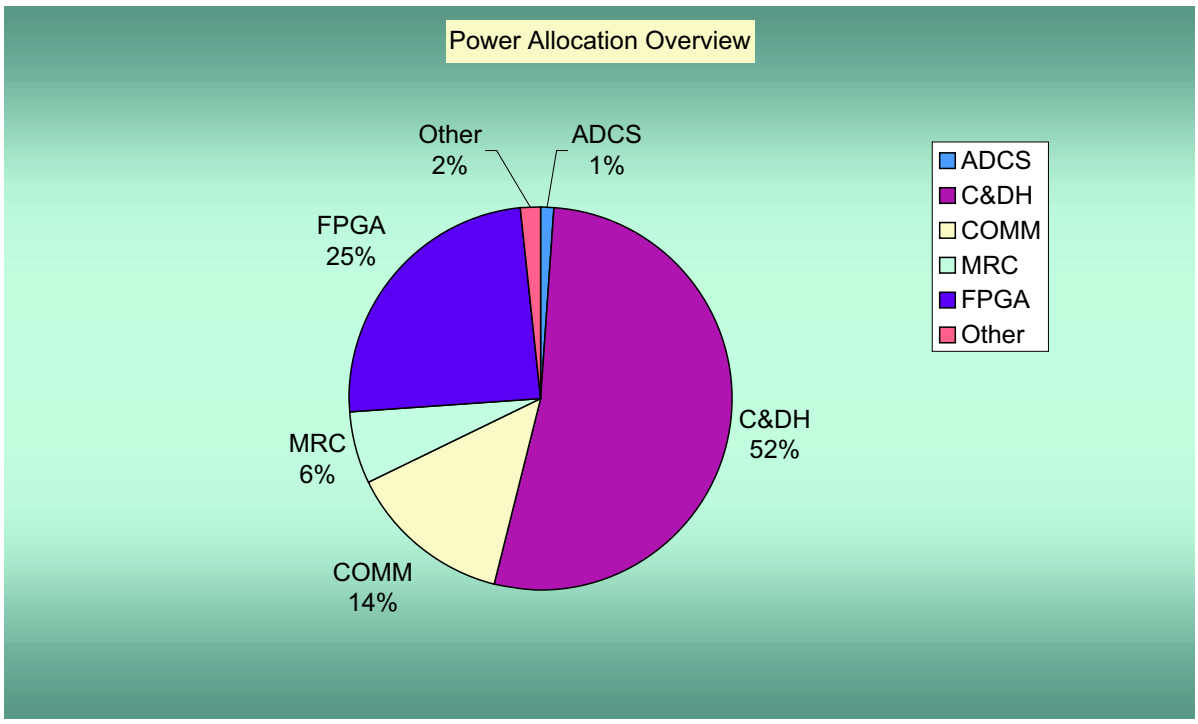

Figure 2.15: Power Allocation to the Subsystems.

Chapter 3

RabbitSat Solar Array Layout and Design

Various parameters influence the design of the Electrical Power Subsystem. The effects of different parameters on the design are being summarized in Table 3.1. [11].

3.1 Power Source Options

The power source generates electrical power within the spacecraft. Four different types of power sources are commonly used in spacecraft:

1. Solar Photovoltaic
2. Static Sources
3. Dynamic Sources
4. Fuel Cells

Solar photovoltaic is the most common power source for earth orbiting spacecraft. Incident solar radiation is directly converted to electrical current. *Static* power sources convert heat directly to electrical power, utilizing the thermoelectric principle (Currently at low conversion efficiencies of 5 to 8% [11]). *Dynamic* power sources use a heat source to drive a thermodynamic power cycle. *Fuel cells* have very high specific power ($275W/kg$ in the Space Shuttle [11]). Chemical energy is directly converted to electrical energy. Fuel cells are especially useful for manned space missions, as they produce water as a valuable by-product.

For the Rabbit Satellite though, the choice of the power source is — at the current state of the art — limited to photovoltaic. The other options listed above require additional periphery which needs space that is not available on a satellite of Cubesat-size.

Parameter	Effects on Design
Average Electrical Power Requirement	Sizes the power-generation system (e.g. number of solar cells, primary battery size) and possibly the energy-storage system gives the eclipse period and depth of discharge
Peak Electrical Power Required	Sizes the energy-storage (e.g., number of batteries, capacitor bank size) and the power-processing and distribution equipment
Mission Life	Longer mission life (>7 years) implies extra redundancy design, independent battery charging, longer capacity batteries, and larger arrays
Orbital parameters	defines incident solar energy, Eclipse/Sun periods, and radiation environment
Spacecraft configuration	Spinner typically implies body mounted solar cells; 3-axis stabilized typically implies body fixed and deployable solar panels

Table 3.1: Effects of System Level Parameters on the Electrical Power Subsystem Design

3.2 Solar Panel Configuration

As a first step towards the solar panel configuration, we will subsequently estimate the required solar array area according to [11]. This is to give us a better understanding of our specific power requirements. Starting from there, we will perform detailed trades on some configuration options.

3.2.1 Estimation of the Required Solar Array Area

The first thing to determine is the power P_{sa} that the spacecraft must provide during daylight:

$$P_{sa} = \frac{\frac{P_e \cdot T_e}{X_e} + \frac{P_d \cdot T_d}{X_d}}{T_d}, \tag{3.1}$$

where P_e and P_d are the spacecraft's power during eclipse and daylight, and T_e and T_d are the respective periods in minutes. X_e and X_d represent the efficiency of the current path from source to loads. Assuming Direct Energy Transfer, these efficiencies may be approximated as $X_e = 0.65$ and $X_d = 0.85$. The higher efficiency during daylight is because the current to the loads is directly provided by the solar cells and does not have to go through the battery cycle. Using the values from the power requirements table (Figure 2.14), we obtain $P_{sa} = 4054mW$.

As solar cells for our estimation, we selected GaAs cells, commonly with efficiencies in the 18.5% range. Thus, the power output P_0 of GaAs cells of the incident sun normal to the surface of the cells becomes

$$P_0 = 0.185 \cdot 1367W/m^2 = 253W/m^2. \tag{3.2}$$

Given a cubic non-stabilized satellite with body-mounted solar cells, the beginning-of-life power per unit area is

$$P_{BOL} = 1/4 \cdot P_0 \cdot I_d \cdot \cos\theta = 41.79W/m^2, \tag{3.3}$$

where $\cos\theta$ is the so-called cosine loss and $I_d = 0.77$ the inherent degradation. Here, θ is the angle between the incident solar radiation and the normal to the solar panel. As a worst case value, we choose $\theta = 23.5deg$.

To determine the end-of-life power production capability, we must take into account the lifetime degradation, Ld,

$$L_d = (1 - \frac{degradation}{year})^{satellitelife} = 0.986 \tag{3.4}$$

where the degradation per year is 2.75% for GaAs cells, and the lifetime 0.5 years. The end-of-life performance per unit area becomes

$$P_{EOL} = P_{BOL} \cdot L_d = 41.21W/m^2. \tag{3.5}$$

Eventually, we obtain the total required solar array area

$$A_{sa} = \frac{P_{sa}}{P_{EOL}} = 983cm^2. \tag{3.6}$$

As our assumption was a cubic spacecraft, we have to divide A_{sa} by six, so as to obtain the array area per face. Thus, we would meet the power requirements with *6 body mounted solar arrays of 13cm by 13cm* each.

This approximation now shall be the basis for the solar array design, discussed in the subsequent chapters. The calculated panel size is larger than what the Rabbit Satellite could allow for body-mounted solar cells. Yet, the number is not totally out of reach.

3.3 Solar Array Configuration Options

There are many ways to arrange solar panels on the satellite. Three examples are shown in Figure 3.1. Deployable arrays increase the surface area and thereby increase the electrical power income, while reducing the heat load within the satellite. The drawback is that they also increase complexity, space requirements, mass, and risk of failure. While deployable arrays may be a very reasonable and necessary choice for 3-axis stabilized spacecraft, they are even less useful for a tumbling satellite such as RabbitSat. Nonetheless, we will investigate the power increase of two sideways-deployable panels as in Figure 3.1(c) in Section 3.6. However, for the reasons above, our first choice will be body-mounted solar panels.

3.4 Solar Cell Choice

In this section, we will begin with a short overview of how a solar cell works. After briefly discussing the different cell types, we will go through concrete manufacturers' price quotes, which will be part of the subsequent trade study for the optimum Solar Array layout.

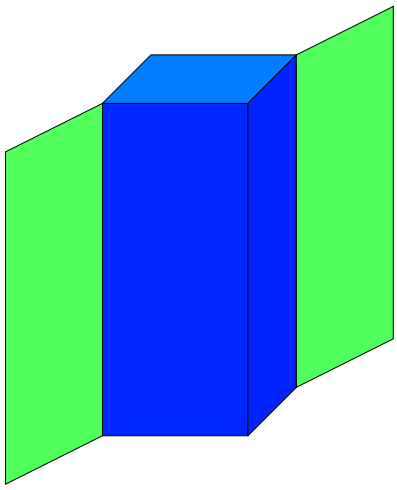

(a) Configuration with Sideways Deployable Panels

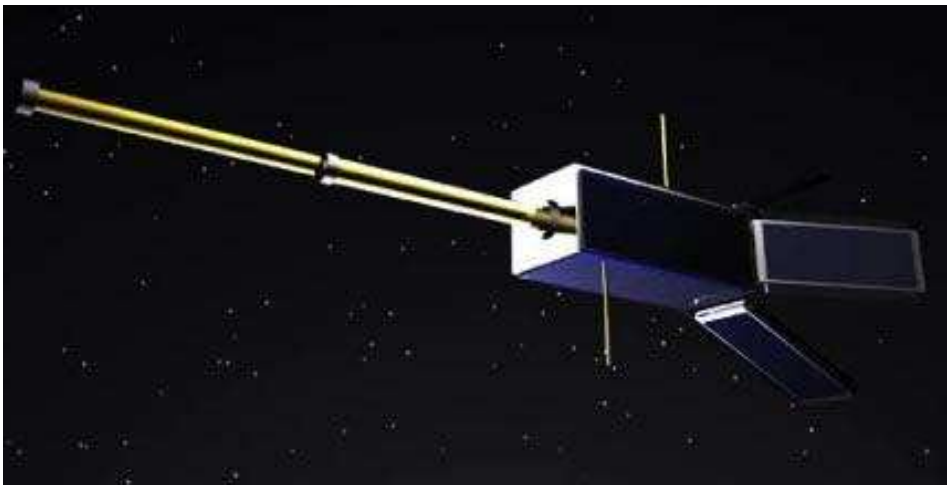

(b) Configuration with Bottom Deployable Panels

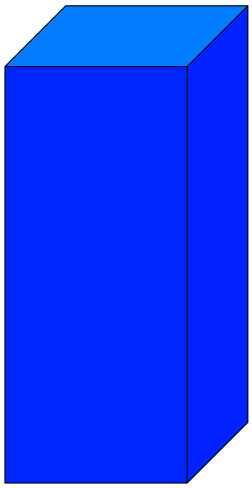

(c) Configuration with Sole Body-Mounted panels

Figure 3.1: Options for Solar Array Configuration

3.4.1 How a Solar Cell works

Solar cells are made of special materials called semiconductors, such as silicon, which is currently the most commonly used. When light strikes the cell, a certain portion of it is absorbed within the semiconductor material. This means that the energy of the absorbed light is transferred to the semiconductor. The energy knocks electrons loose, allowing them to flow freely. Solar cells also all have one or more electric fields that act to force electrons freed by light absorption to flow in a certain direction. This flow of electrons is a current, and by placing metal contacts on the top and bottom of the Solar cell, we can draw that current to use externally (See Figure 3.2). This current, together with the cell's voltage, defines the power that the solar cell can produce [12].

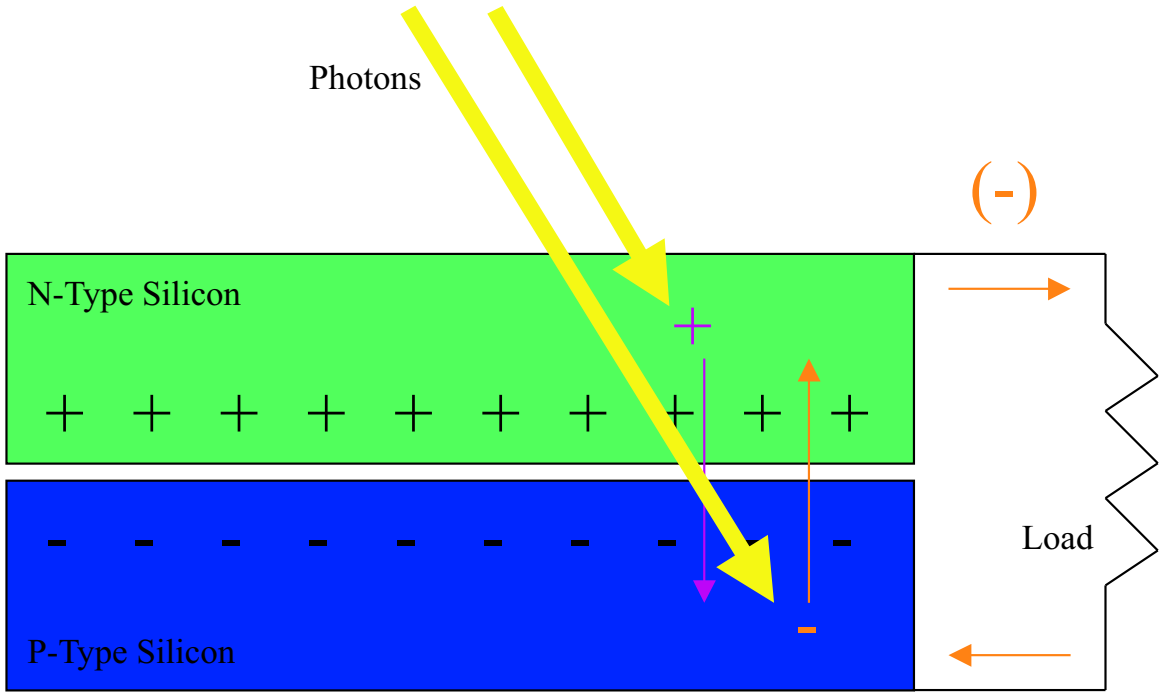

Figure 3.2: Principle of the Solar Cell Operation

As the voltage of each single cell is usually too low (0.5V to 2.5V) to be used it directly, the manufacture of solar panels for both space and terrestrial applications involves stringing cells together such that they are connected electrically in series.

Stringing the cells in series though involves one problem; if only one solar cell in a string is in the shade, with the remaining cells still in the light, the cell is forced into reverse bias breakdown to be able to conduct the current of the string. This reverse biasing of the cell into breakdown can permanently damage the cell. This may be prevented by connecting discrete bypass diodes in parallel to the cell, but with opposite polarity, such that when the cell in the string is in the shade, the bypass diode is forward biased and the current of the string safely passes through the cell-bypass diode combination. Thus, the cell is prevented from being reverse biased into breakdown. Several different approaches to attaching a discrete diode to the solar cell have been proposed and are in use, including front mounted, corner mounted (in-plane with the cell), and back mounted diodes [13].

Solar cells with built-in diodes, interconnects, and cover-glass are commonly referred to as CIC-cells (Coverglass-Inter-Connect).

3.4.2 The Different Cell Types

While silicon solar cells are the most well known and the most commonly used, more efficient Gallium Arsenide (GaAs) cells are replacing silicon cells in the aerospace sector. Hoever, as Figure 3.3 shows, the price per watt of power increases exponentially with the cell performance. The data here comes from Price quotes of the Solar Cell manufacturers, and the prices underlying this chart are as of Table3.2. Abbreviations in this chart are: SL for Spectrlab and EM for Emcore (See Section 3.4.2). DJ stands for Dual Junction cells, TJ and ITJ for Triple Junction and Improved Triple Junction, respectively.

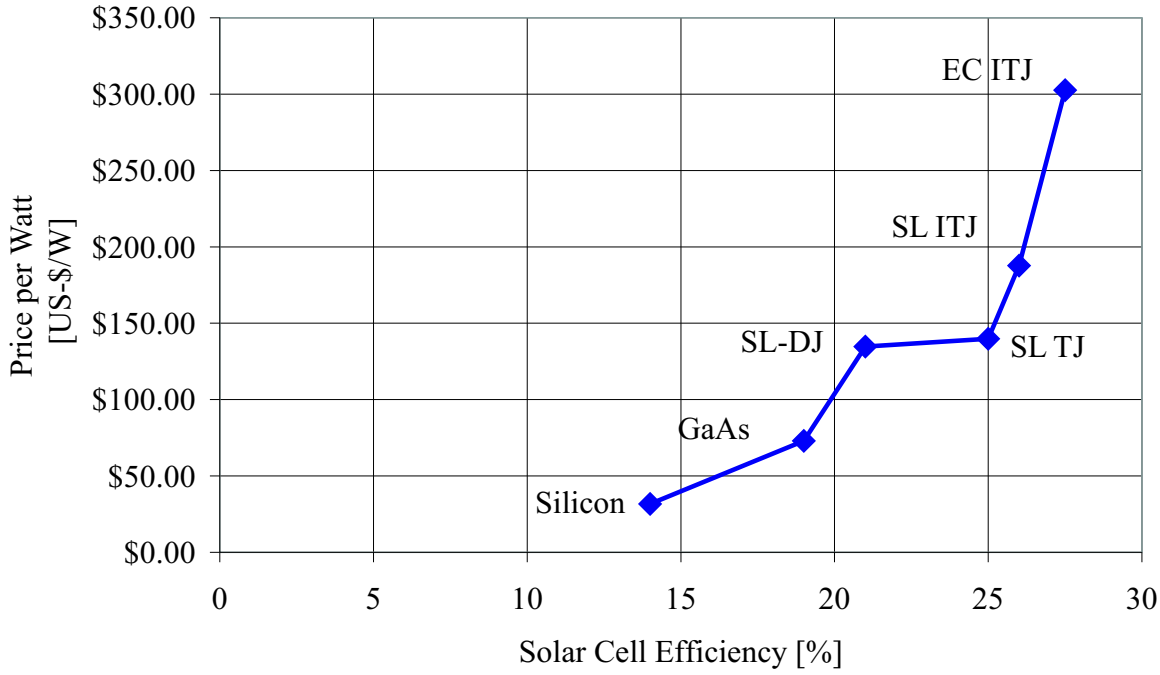

Figure 3.3: Solar Cell Efficiency vs. Price per Watt of Maximum Power Output of the Solar Cell at Perpendicularly Incident Solar Radiation ($1365W/m^2$)

The reason for the surprisingly low maximum efficiencies of solar cells in general is that a certain cell material (e.g. Silicon or GaAs) can only convert a small wavelength range of the total sunlight spectrum, as shown in Figure 3.5(a). To mitigate this problem, so-called Multi-junction cells were invented. These cells have two or three layers of different materials, such as $GaInP_2$, $GaAs$ and Ge, that utilize different parts of the sunlight spectrum, respectively. Figure 3.4 shows the structure of a Triple Junction solar cell. As can be seen from Figure 3.5(b), the single energy conversion efficiencies of each material in its wavelength range are close to 100%. With triple junction solar cells, maximum efficiencies of about 28% were reached.

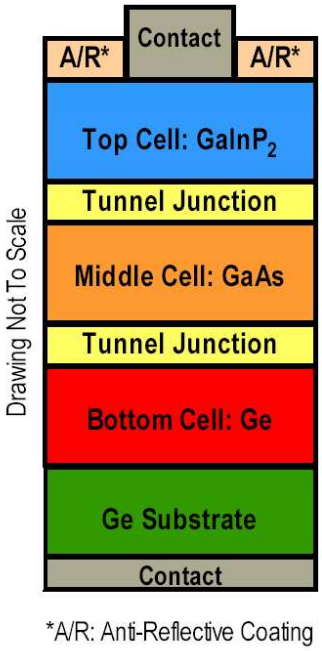

Figure 3.4: Basic Triple-Junction Cell Structure [15]

The Space Solar Cell Marked

There are two relevant space solar cell manufacturers in the United States, Emcore and Spectrolab:

Emcore Solar Cell Operations
10420 Research Road SE
Albuquerque NM 87123
Tel: (505) 332 5000
Fax: (505) 332 5038
<www.emcore.com>

Contact: Robert Langdon
Tel: (626) 934-6541

Spectrolab, Inc.
12500 Gladstone Avenue
Sylmar, CA 91342
Tel: (818) 365-4611
Fax: (818) 361-5102
<www.spectrolab.com>

Contact: Mike Kalachian
Tel: (818) 898-7540

Both companies offer comparable products - both companies are currently working on launching high-end "Ultra Triple Junction" cells with efficiencies in the 28% range.

The available cells with price quotes are listed in Table 3.2.

An important thing to keep in mind after buying solar cells is that the single cells don't all

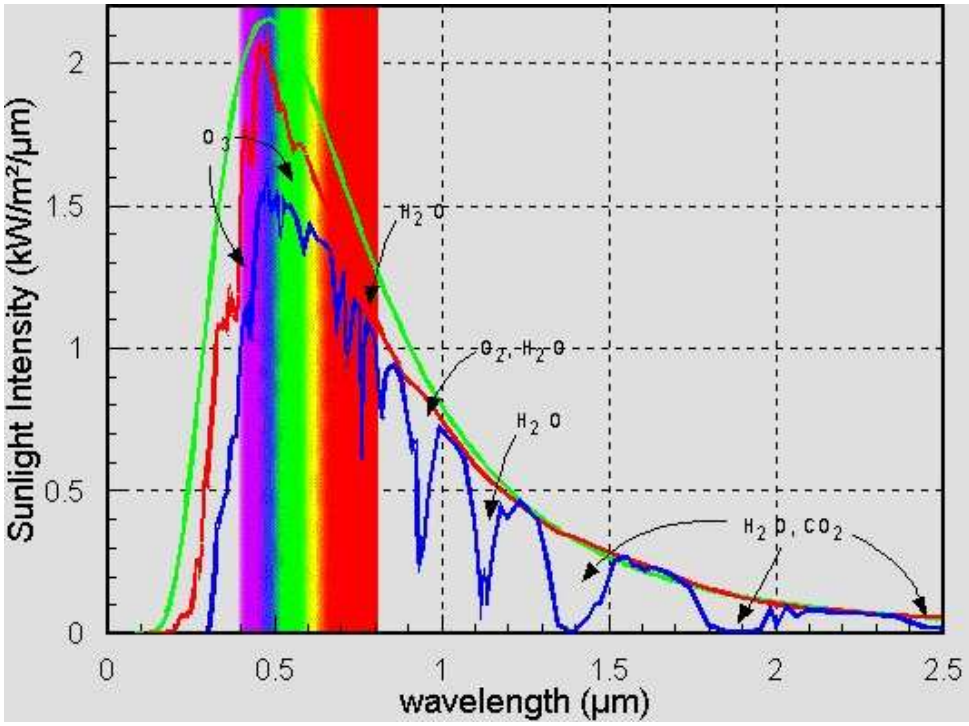

(a) Spectrum of the Sunlight

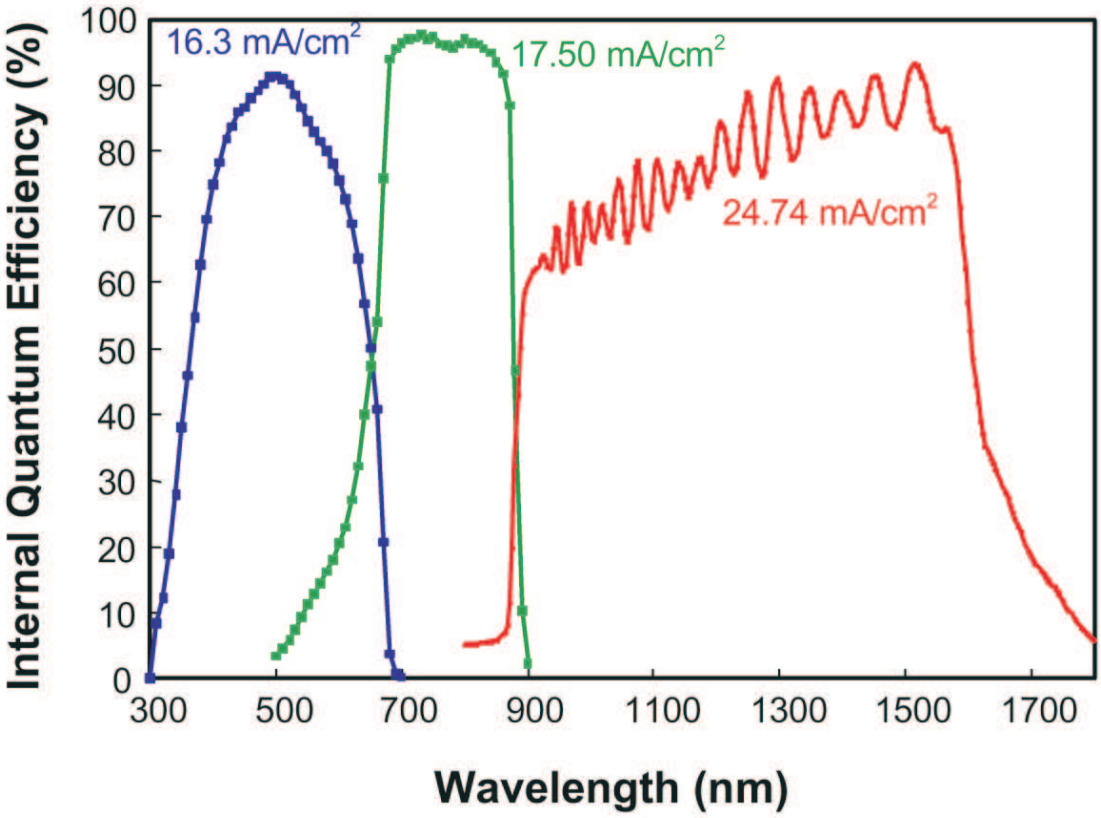

(b) Bandwidth Ranges of Light that is Utilized by Different Layers of the Solar Cell

Figure 3.5: Utilization of the Sun Radiation by Solar Cells [14]

Manufacturer	**Cell Type**	**Efficiency [%]**	**Cell Dimensions**[a] $[cm^2]$	**Retail Prize**	**Reduced Prize**[b]
Techstar[c] (Emcore)	Dual Junction	21 to 22	$6.3 * 3.84$	-	\$35[d]
Emcore	Triple Junction	~ 28	$6.89 * 3.95$	-	\$300
Emcore	Triple Junction	~ 28	$7.60 * 3.70$[e]	-	\$300
Spectrolab	Silicon	14	$3.93 * 6.89$	\$16[f]	-
Spectrolab	GaAs Single Junction	19	$3.93 * 6.89$	\$50	-
Spectrolab	Dual Junction	21	$3.93 * 6.89$	\$102	\$50[g]
Spectrolab	Triple Junction	25	$3.93 * 6.89$	\$126	-
Spectrolab	Improved Triple Junction	26.8	$3.93 * 6.89$	\$176	\$150

[a]Note that the effective cell area may be smaller, as most cells have cropped corners
[b]Prices with educational discount for the SSDL, Stanford University
[c]Techstar was bought up by Emcore, cell remainders are sold by Emcore
[d]Quote from July 10, 2003, by R. Langbon
[e]Limited availability
[f]Quote at a minimum \$500 order volume from July 14, 2003, by M. Kalachian
[g]Quote at a minimum \$500 order volume from August 21, 2003, by M. Kalachian

Table 3.2: Solar Cell Prices

have the same efficiency. The cell manufacture produces cells with an efficiency distribution according to the Gaussian Distribution (See Figure 3.6). Hence you'll always receive cells with a guaranteed minimum efficiency, but varying single cell efficiencies. Note that the efficiency of a series string of solar cells is driven by the efficiency of the least efficient cell, respectively.

Space Quest

Space Quest is a small company in VA, providing micro-satellite components. Space Quest gave us a quote for providing complete solar panels, including solar cells and mounting. They are using solar cells from Spectrolab or Emcore, thereby guaranteeing a minimum 27% efficiency.

SpaceQuest, Ltd.
3554 Chain Bridge Road
Suite 103
Fairfax, VA 22030
<http://www.spacequest.com>

Contact: Mark Kawanati
Tel: (703) 273-7010

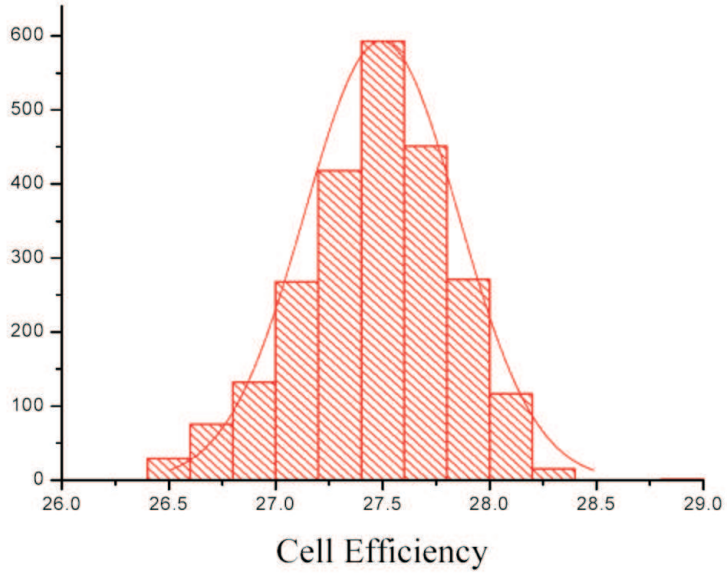

Figure 3.6: Histogram for 2000 Emcore Multi-Junction Cells [13]

3.5 Solar Panel Layout

3.5.1 The Trade Study

This section presents a comprehensive overview of the trade study that lead to our solar panel layout. First, you'll see two figures, Figure 3.7 and 3.8, showing four promising cell configurations which seemed to make sense. Making sense here means that the maximum power point voltages V_{MP}, of small and large panels respectively, match (Figures 3.7(a) through 3.8(a)). One exception to this principle may be found in the concept shown in Figure 3.8(b). Here, the voltages are 4V and 12V, for the small and large panels respectively (Please see Table 3.3, option 6 for further comments). You may be wondering, why the previously mentioned options with deployable solar panels are not part of this discussion. Now, as deployable solar panels add considerable complexity and thus cost and development time to every satellite, we intended here to do without deployables, as long as the power budget allowed. Hence, body-mounted solar arrays are our preliminary goal here.

Now the Figures are being followed by a table (Table 3.3), listing 6 layout options, directly derived from the Figures. Table 3.3 shows the relevant (technical) factors for each layout option.

The last row in the table contains the Average Sunlight Power output capability of each layout. This value is the result of a simulation, described in the following section.

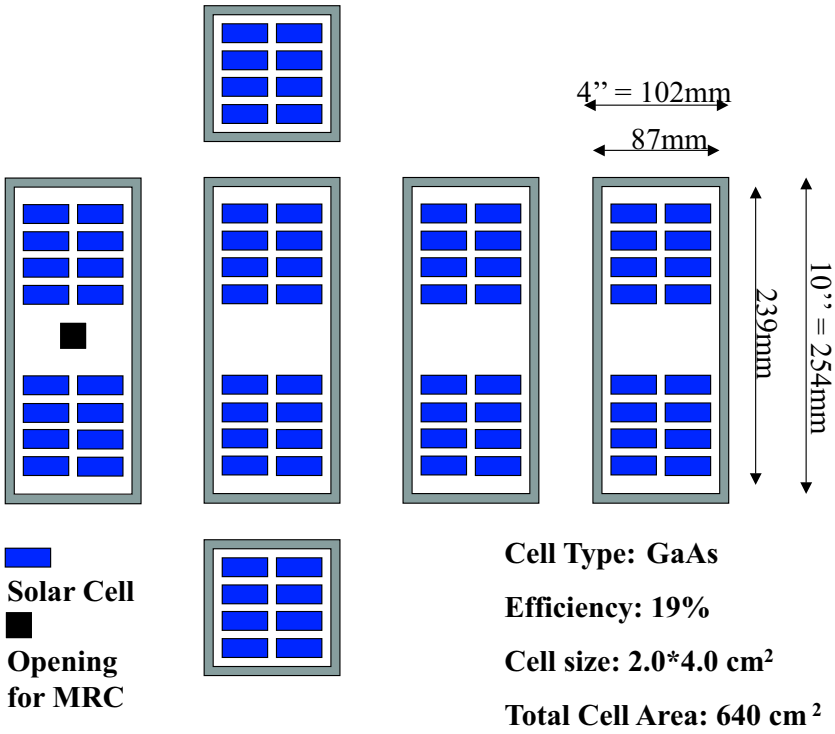

(a) Configuration 1

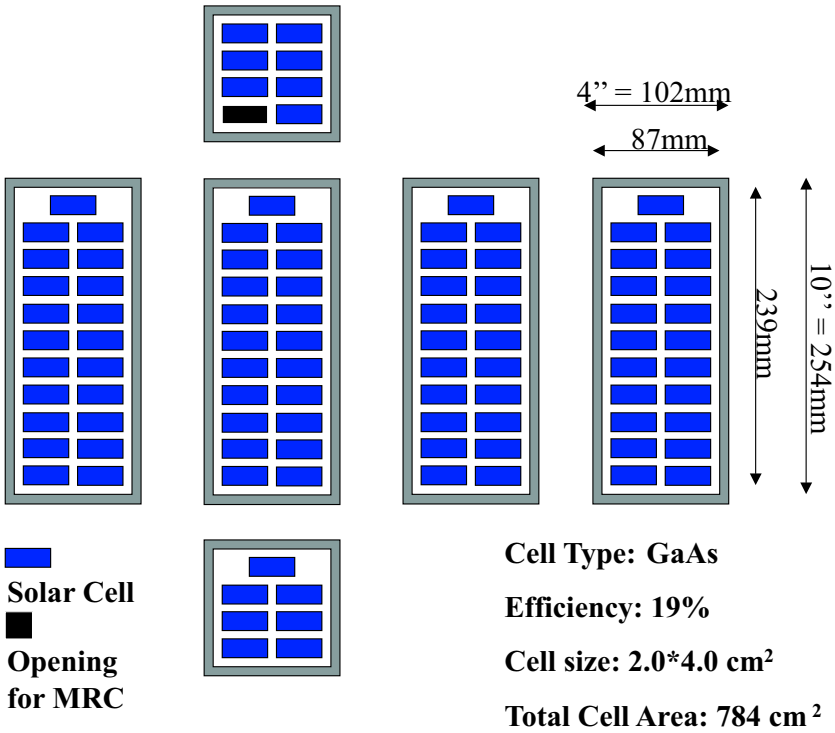

(b) Configuration 2

Figure 3.7: Solar Panel Configuration Options I

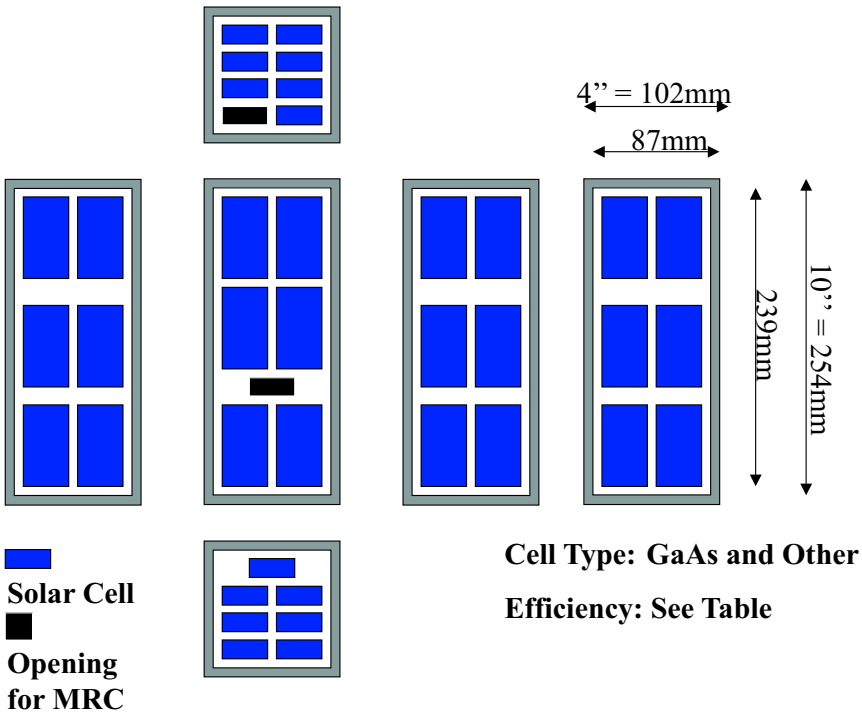

(a) Configuration 3

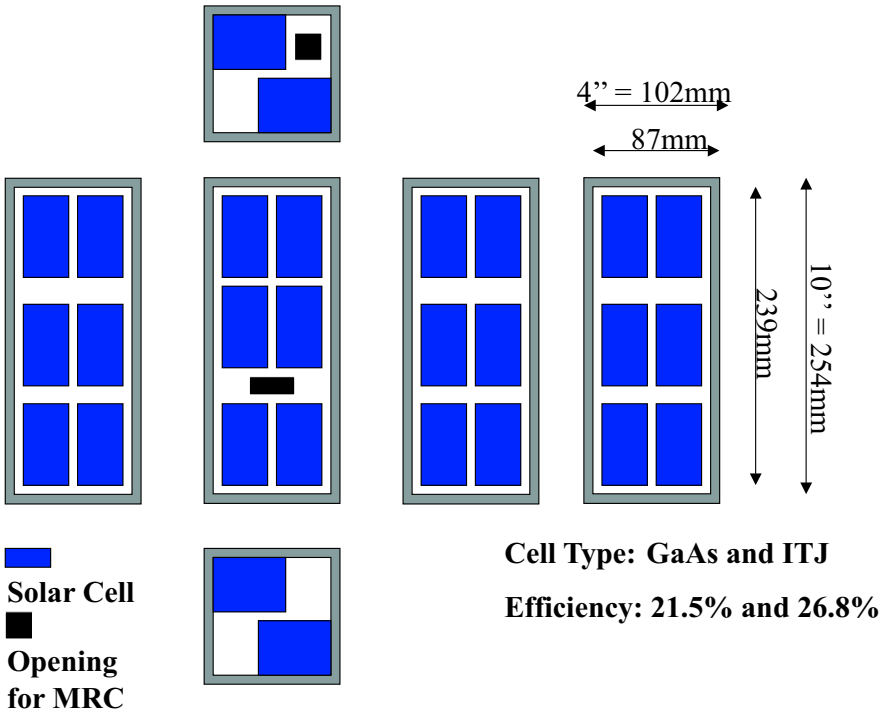

(b) Configuration 4

Figure 3.8: Solar Panel Configuration Options II

	Option 1		**Option 2**		**Option 3**	
Reference Figure	3.7(a)		3.7(b)		3.8(a)	
Panel [a]	S	L	S	L	S	L
Cell Type	GaAs	GaAs	GaAs	GaAs	GaAs	DJ
Make	SL	SL	SL	SL	SL	EC [b]
Cell Size $[cm^2]$	$2.0 \cdot 4.0$	$2.0 \cdot 4.0$	$2.0 \cdot 4.0$	$2.0 \cdot 4.0$	$2.0 \cdot 4.0$	$3.84 \cdot 6.3$
Cell Efficiency [%]	19	19	19	19	19	21.5
Cells per String [#]	8	8	7	7	7	3
Cells per Panel [#]	8	16	7	21	7	6
V_{MP} **per string** $[V]$	7.2	7.2	6.3	6.3	6.3	6.24
Price per Cell [$]	N/A [c]	N/A	N/A	N/A	N/A	35
Price for all Cells[d] [$]	N/A		N/A		1100	
Sunlight Avrg. Power[e] $[W]$	2.42		2.84		2.79	

	Option 4		**Option 5**		**Option 6**	
Reference Figure	3.8(a)		3.8(a)		3.8(b)	
Panel	S	L	S	L	S	L
Cell Type	GaAs	TJ	GaAs	TJ	TJ	DJ
Make	SL	EC	SL	SQ [f]	SL	SL
Cell Size $[cm^2]$	$2.0 \cdot 4.0$	$3.9 \cdot 6.9$	$2.0 \cdot 4.0$	$2.0 \cdot 4.0$	$3.9 \cdot 6.9$	$3.9 \cdot 6.89$
Cell Efficiency [%]	19	25.4	19	27	26.8	21.6
Cells per String [#]	8	3	8	3	2	6
Cells per Panel [#]	8	6	8	6	2	6
V_{MP} **per string** $[V]$	7.2	6.84	7.2	6.75	4.5	12.2
Price per Cell [$]	N/A	300	N/A	360	150	50
Price for all Cells [$]	9400		8800		2340	
Sunlight Avrg. Power[g] $[W]$	3.59		3.76		3.1 (3.3)[h]	

Table 3.3: Solar Panel Layout Configurations - Evaluation Table

[a] S refers to each of the two small panels, and L to each of the four large panels, respectively

[b] Reminders of stock by Techstar, see Table 3.2 for details

[c] Cells available as overstock from the SSDL, Stanford University

[d] This number includes a 30% margin

[e] These values stem from the simulation, discussed in Section 3.6

[f] SQ refers to Space Quest Company of Virginia. SQ is not a solar cell maufacturer - the price here is the panel price incl. mounting of the cells by SQ

[g] These values stem from the simulation, discussed in Section 3.6

[h] In this design the voltage levels have to be assim 3.1W is the Power, if the Power of the small panels is derated by a factor of 0.8. 80% is a reasonable efficiency for boosting the voltage from 4V to 12V

3.5.2 Evaluation of the Trade Study

The results of the trade study show that we cannot completely cover our current power requirements ($P_{sa} = 4054mW$, as of Section 3.2.1) with any of the designs.Regarding the 30% margin of error which is already included in the above value for P_{sa} though, we are rather close to the anticipated number. Due to the constraints in development time and financial budget, it was not possible to go for deployable arrays. The team decided to cut power requirements wherever possible, and declare the power production capability of the chosen array a constraint. As for the layout selection, the team decided to go with Configuration 4 (Figure 3.8(b)), design option 6 (Table 3.3). Reasons for this layout being advantageous were:

Price The total solar cell price is relatively low for the power production capability.

Panel Mounting The mounting of the solar panels will be easier, as only using this design, all solar cells come as CIC-cells (see Section 3.4.1). The smaller GaAs cells of the other layout proposals are basically pure solar cells, without back-bias diodes and without cover-glass or interconnects. Also, the Lockheed Martin Solar Array Center would have the capability of mounting the type of CIC cells, employed in this layout. They could not mount non-CIC cells.

Small Panels In this layout, even the small side panels provide a relatively large amount of power. This is desirable, in case the slowly tumbling satellite will rest in a close to worst-case position towards the sun, i.e. one of the small panels directly facing the sun for a long time.

3.6 Power Simulation for different Layouts

So as to simulate the power income for the different solar panel configurations, we created a complex Excel simulation (Available in Appendix CD, "Power Budget").

The simulation works in time steps, i.e. for each time increment, the power income of the solar panels is computed. The satellite power income is the sum of the power generation of each solar panel which, in turn, is calculated via the angle of the incident sun radiation and the normal of the respective panel surfaces.

3.6.1 The Power Generation of Each Solar Panel

The Power generation of each of the solar panels P_{in} is a function of the incidence angle of the sun γ and the normal to the solar cell plane. The generated solar cell power is expressed as a geometric function.

$$P_{in} = cos\gamma \cdot \eta_{SC} \cdot A_{SP} \cdot S \tag{3.7}$$

where η_{SC} refers to the solar cell efficiency, A_{SP} to the total effective solar panel area, and S to the Solar Constant, at $S = 1365W/m^2$.

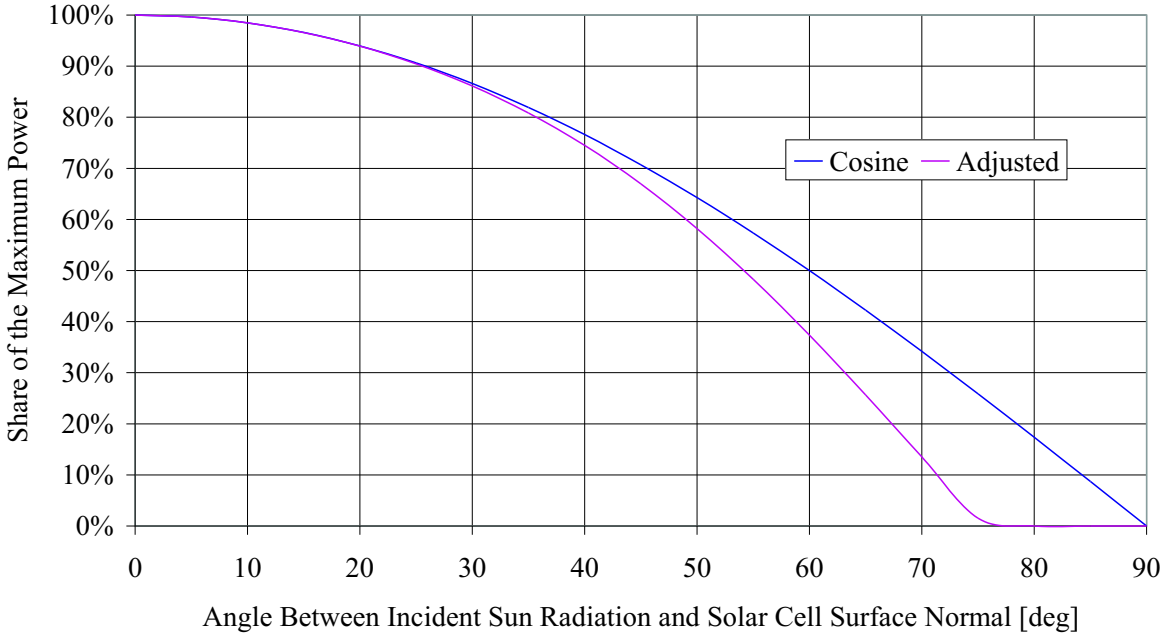

Figure 3.9: Solar Cell Power Generation as a Function of the Angle of Incident Solar Radiation and the Solar Cell Normal (The data presented here stems from Spectrolab Triple Junction "Angle of Incidence Test Results", which is Spectrolab confidential information and not subject to publication)

In reality though, as the angle γ increases towards 90deg, the solar cell power decreases faster than the pure cosine function would prescribe. This effect is shown in Figure 3.9. The curves stem from Spectrolab experimental data. The reason for this behavior may be sought in reflection losses. For our simulation, we derived the following approximation for the true power function:

$$P_{in} = (cos\gamma - 0.3 \cdot sin^6\gamma) \cdot \eta_{SC} \cdot A_{SP} \cdot S \tag{3.8}$$

Now we discussed how to calculate the solar panel incoming power from the angle of incidence γ and solar cell specific and general constants.

The following will show how γ may be obtained from two vectors in spherical coordinates, namely, the sun vector and the normal vector to the solar panel. Therefore, we first define these two vectors:

3.6.2 The Sun Vector

As the RabbitSat will not have attitude control, it will be tumbling in orbit. To account for the tumbling, the simulation provides a tumbling sun vector, this vector being controlled by the angles ϑ and ϕ in a spherical coordinate system (See Figure 3.10). The proceeding of ϑ and ϕ throughout the simulation period is being controlled by two input values, the rotational frequencies f_ϑ "Theta Rotations per minute" and f_ϕ "Psi Rotations per minute", as shown in Figure 3.12. For a time step width of one minute, the sun vector

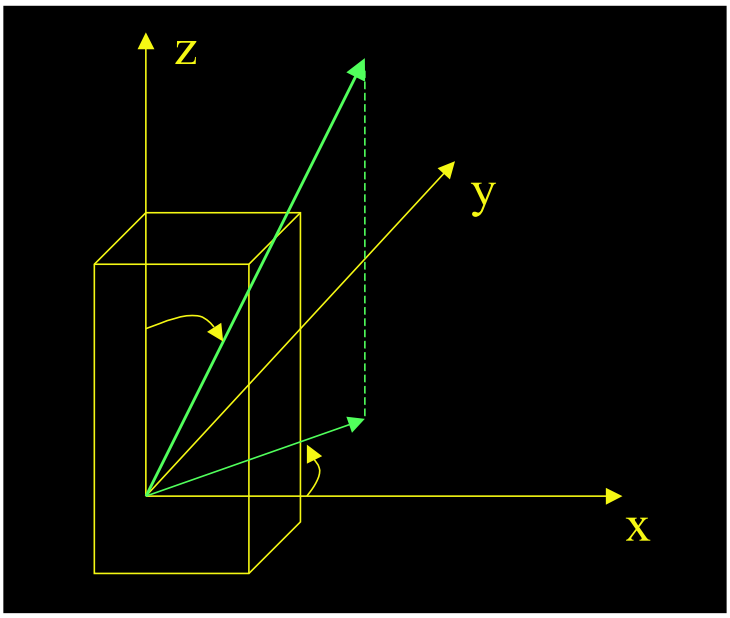

Figure 3.10: Definition of the Sun Vector (Here in Green) in a Spherical Coordinate System

becomes

$$\vec{s}_{IN} = \begin{pmatrix} R \\ \vartheta_{n+1} \\ \phi_{n+1} \end{pmatrix} = \begin{pmatrix} R \\ \vartheta_n + f_\vartheta \cdot 360 deg/min \\ \phi_n + f_\phi \cdot 360 deg/min \end{pmatrix} \tag{3.9}$$

where R is a constant and of no relevance for this consideration, and n is the sequential number of the time step.

The option of setting the tumbling frequencies is important to us, because we don't know what tumbling frequency we will obtain.

The simulation is a rough simplification of reality, in that it does not account for the satellite attitude changes due to its movement around the earth. This shall be provided for when setting reasonable tumbling frequencies.

3.6.3 The Normal Vectors

The vectors normal to the respective solar panels is offset for each one of the six solar panels of the satellite. Figure 3.11 mirrors the definition of the Power Simulation with the static vectors:

$$\vec{p}_1 = \begin{pmatrix} R \\ \vartheta_1 \\ \phi_1 \end{pmatrix} = \begin{pmatrix} R \\ 0^o \\ 0^o \end{pmatrix} \tag{3.10}$$

$$\vec{p}_2 = \begin{pmatrix} R \\ \vartheta_2 \\ \phi_2 \end{pmatrix} = \begin{pmatrix} R \\ 0^o \\ 180^o \end{pmatrix} \tag{3.11}$$

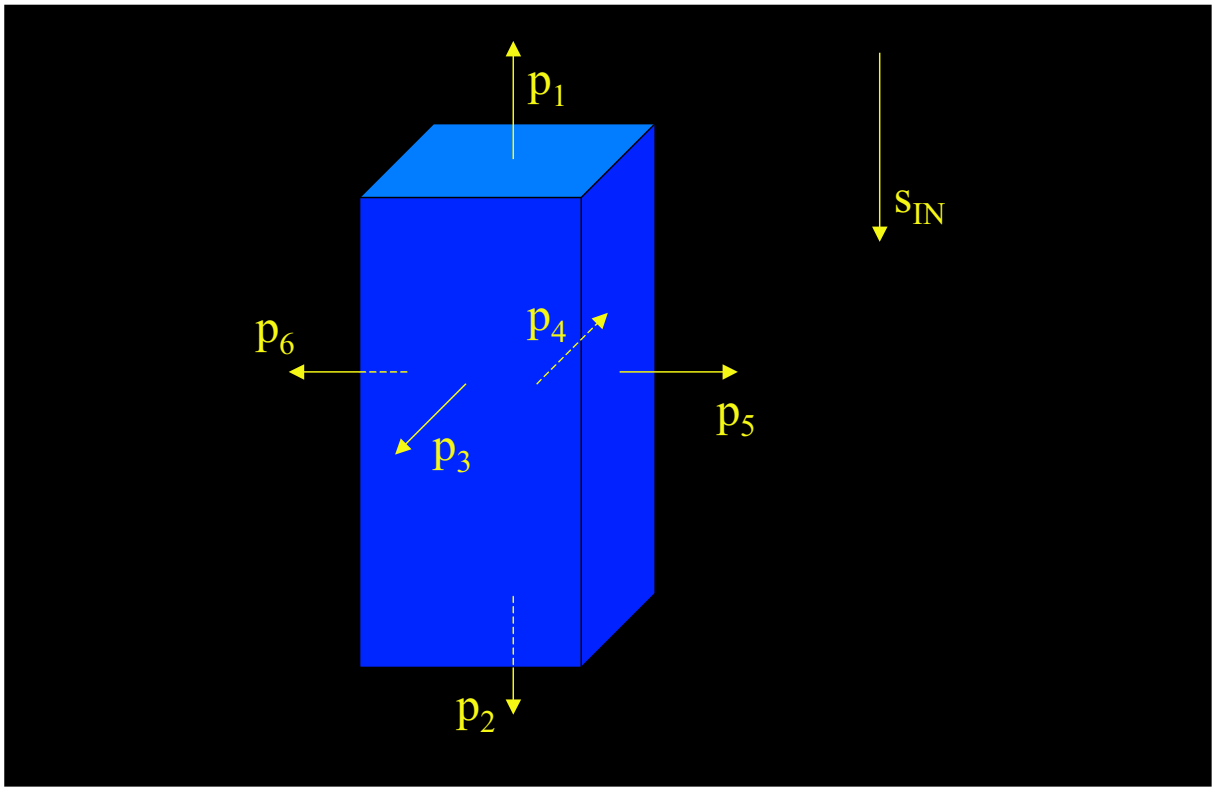

Figure 3.11: Definition of All Solar Panel Normal Vectors. The Solar Panel Vectors, $\vec{p}_1$ through $\vec{p}_6$ are Static through the Simulation, Only the Sun Vector $\vec{s}_{IN}$ is "Tumbling". Here, $\vec{s}_{IN}$ is Shown in it's Null Position

$$\vec{p}_3 = \begin{pmatrix} R \\ \vartheta_3 \\ \phi_3 \end{pmatrix} = \begin{pmatrix} R \\ -90^o \\ 90^o \end{pmatrix} \tag{3.12}$$

$$\vec{p}_4 = \begin{pmatrix} R \\ \vartheta_4 \\ \phi_4 \end{pmatrix} = \begin{pmatrix} R \\ 90^o \\ 90^o \end{pmatrix} \tag{3.13}$$

$$\vec{p}_5 = \begin{pmatrix} R \\ \vartheta_5 \\ \phi_5 \end{pmatrix} = \begin{pmatrix} R \\ 0^o \\ 90^o \end{pmatrix} \tag{3.14}$$

$$\vec{p}_6 = \begin{pmatrix} R \\ \vartheta_6 \\ \phi_6 \end{pmatrix} = \begin{pmatrix} R \\ 180^o \\ 90^o \end{pmatrix} \tag{3.15}$$

3.6.4 The Angle of Incidence

Now we have defined all required vectors, and therefore we can calculate the *angle of incidence* γ_i, the angle between $\vec{s}_{IN}$ and $\vec{p}_i$. Using the basic laws of geometry, we obtain

$$\begin{aligned} \cos\gamma_i &= \cos\vartheta \cdot \cos\vartheta_i \cdot \sin\phi \cdot \sin\phi_i + \\ &\quad + \sin\vartheta \cdot \sin\vartheta_i \cdot \sin\phi \cdot \sin\phi_i + \cos\phi \cdot \cos\phi_i \end{aligned} \tag{3.16}$$

whereby the Greek letters without symbols refer to the sun vector.

3.6.5 Total Power Generation

With the definitions obtained in the previous subsections, the total generated satellite power at a time step n becomes

$$P_{in,n} = S \cdot \sum_{i=1}^{6} \left((cos\gamma_i - 0.3 \cdot sin^6\gamma_i) \cdot \eta_{SC,i} \cdot A_{SP,i} \right) \tag{3.17}$$

3.6.6 Simulation Results

There are two principal outputs to this power simulation. First, we obtain the sunlight average power output of the solar panels in $[WHr]$, secondly, Excel creates a chart, showing the power vs. time. This chart allows us to view the minimum, maximum and average power production vs. time. This chart does not allow us to read the sunlight average power, as the sunlight average power also accounts for Daylight and Eclipse periods. A sample power output chart is shown in Figure 3.13.

Solar Array: Spectrolab, TJ, 9.3*3.94cm^2 ,6 cells per face, no cells on top and bottom

Area Definition					Legend	
	# of cells	Area per cell cm2	Area [cm^2]	Cell efficency		User Input Values
Area 1	2	27.3654	14.77732	0.27		
Area 2	2	27.3654	14.77732	0.27		Comments
Area 3	6	27.3654	35.30137	0.215		
Area 4	6	27.3654	35.30137	0.215		needs to be rev
Area 5	6	27.3654	35.30137	0.215		
Area 6	6	27.3654	35.30137	0.215		Output Values

Orbit Data	
Radius of Earth (km)	6378.15
Altitude (km above surface)	400
Orbital Velocity (km/s)	7.67
period (minutes)	92.56
maximum eclipse (fraction of orbit)	0.390
maximum eclipse (minutes)	36.11
minimum daylight (minutes)	56.45
rev/day	15.56
Cycles after 6 months:	2839
visable sky angle (degrees)	39.56

Irradiation and Efficiency Values		
Earth Albedo [W/m^2]	40.95	Value from Experiments of Space Quest Ltd.
Solar Constant [W/m^2]	1365	
Irradiation Total [W/cm^2]	0.140595	Including Earth Albedo
Solar Cell Efficiency [%]	99.99	
Temperature Degradation [%]	80	

Calculated from this Simulation	
Average Power Output [W]	**3.33008**
Aver. Energy Output per day [Wh]	48.7444
	2.03102

Tumbling Frequencies	
Theta Rotations per minute	0.067
Psi Rotations per minute	0.56

Figure 3.12: In/Out-put Window of the Excel Incoming Power Simulation

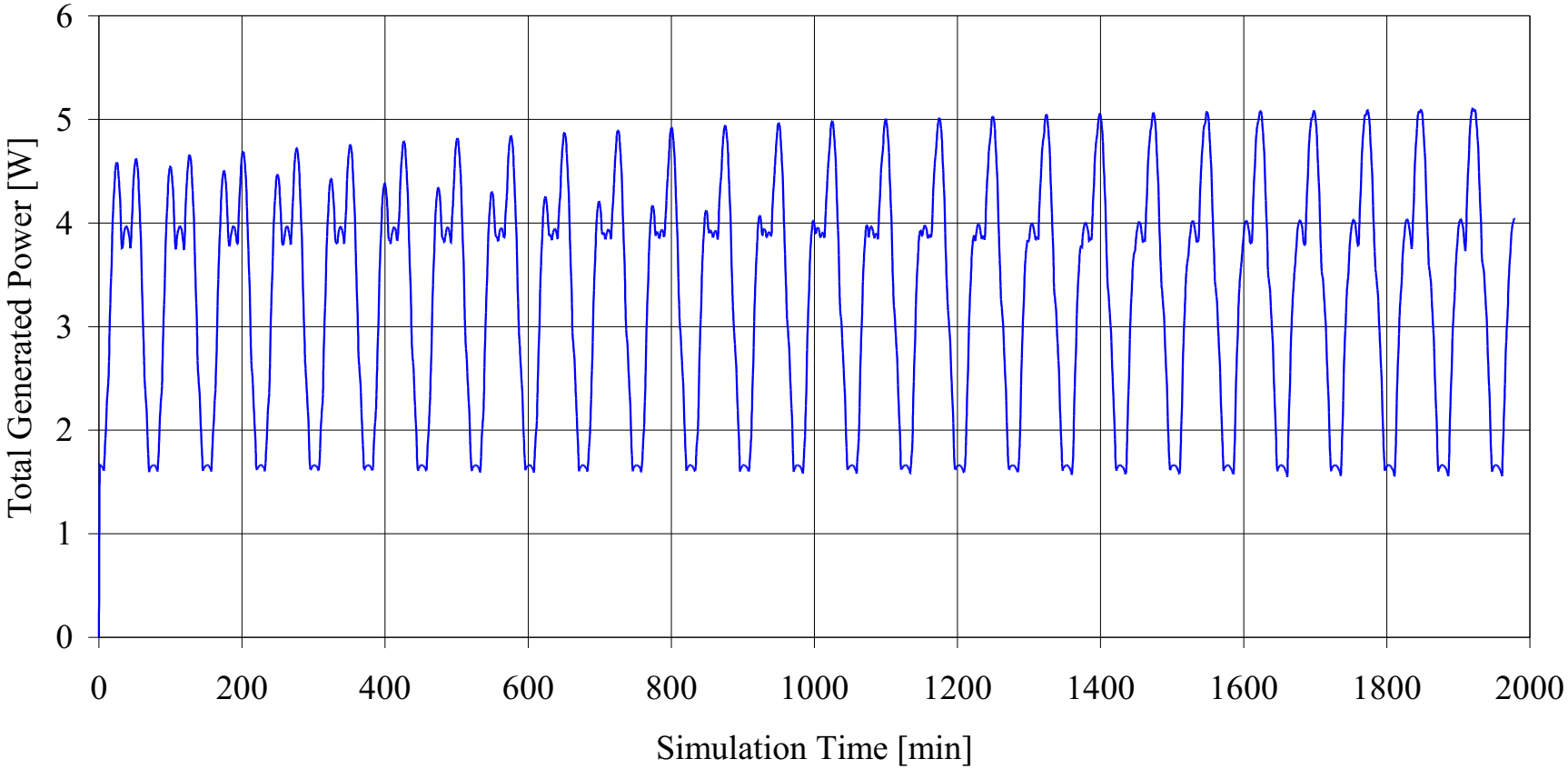

Figure 3.13: Excel Output of the Power Simulation

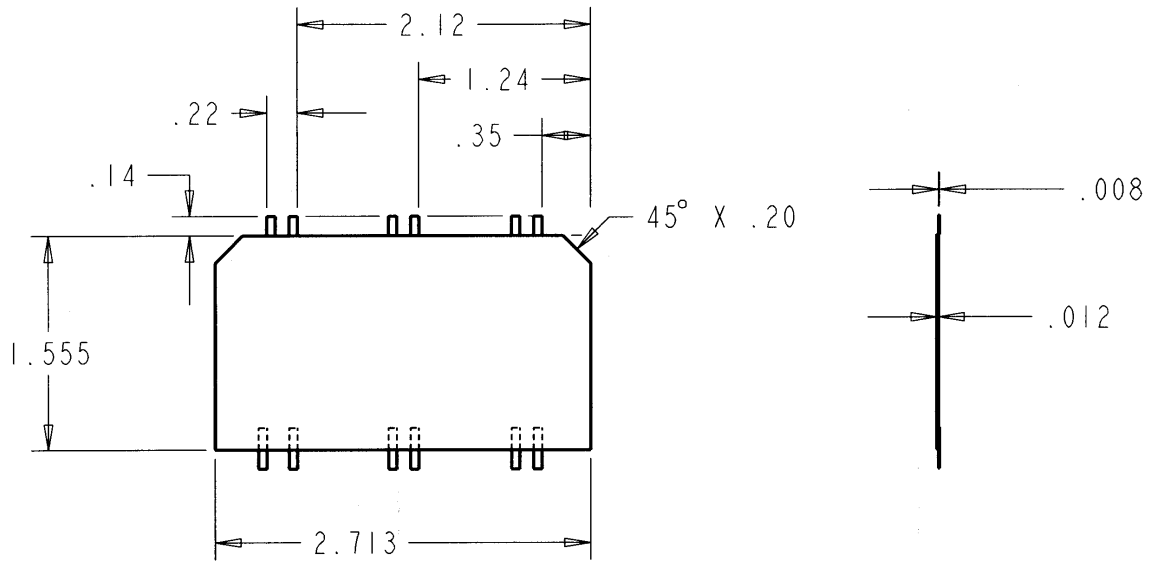

Figure 3.14: Solar Panel Design - The (SL) Solar Cell Dimensions (All Dimensions in Inch)

3.7 Solar Panel Design

This section will explain the design of the solar panels, based upon the general layout selection of the previous chapter. The design of the panels was simultaneous to the design of the structure. It has been an iterative process, driven by solar cell selection, possible solar cell arrangements, antenna design, MRC payload opening[1] sizing and placement and structure skeleton design. The result were the designs for the panels of four large side faces and the two small top and bottom faces of the satellite. As the antennas obtain an optimum omni-directional gain pattern if mounted around the middle of the satellite's large faces, the respective panels on the large faces were split in two. (See Figure 3.15). The design is shown in Figure 3.16 for the small-side panels and Figure 3.17 for the large-side panels, respectively. A more detailed description of this design is part of the next section. The following list shall summarize some technical details for this design.

Solar Cells 'S' The Solar cells for the *small panels* are *Triple Junction* Cells by Spectrolab. The cells measure $3.9 \cdot 6.89 cm^2$ and are rated at 26.8% efficiency. The Maximum Power Point voltage is 2.25V per cell. The cell area is $26.41 cm^2$. The cell thickness is $7mil$ for the cell plus 3 to $6mil$ for the cover-glass[2]. The cells are CIC cells, that is, cover-glass, diodes, and interconnects are part of the cell as delivered. The solar cell dimensions are also shown in Figure 3.14.

Solar Cells 'L' The solar cells for the *large panels* are *Dual Junction* Cells by Spectrolab. The cells are rated at 21.5% efficiency. The Maximum Power Point voltage is 2.05V per cell. The geometrical dimensions are as in the previous cells for the small panels.

[1]The MRC payload requires a small opening above their payload board to allow the operation of a one-shot camera

[2]Mil is a technical unit derived from the Imperial System, i.e. $1mil = 1/1000inch$

Electrical Interface The cells are connected in strings as follows: The small panel has two solar cells connected in series. The large panel includes three solar cells, connected in series, whereby each of the four large faces of the satellite includes two large panels in series respectively. Figure 3.15 illustrates the panel arrangement, showing one large face and one small face of the satellite with the respective solar panels.

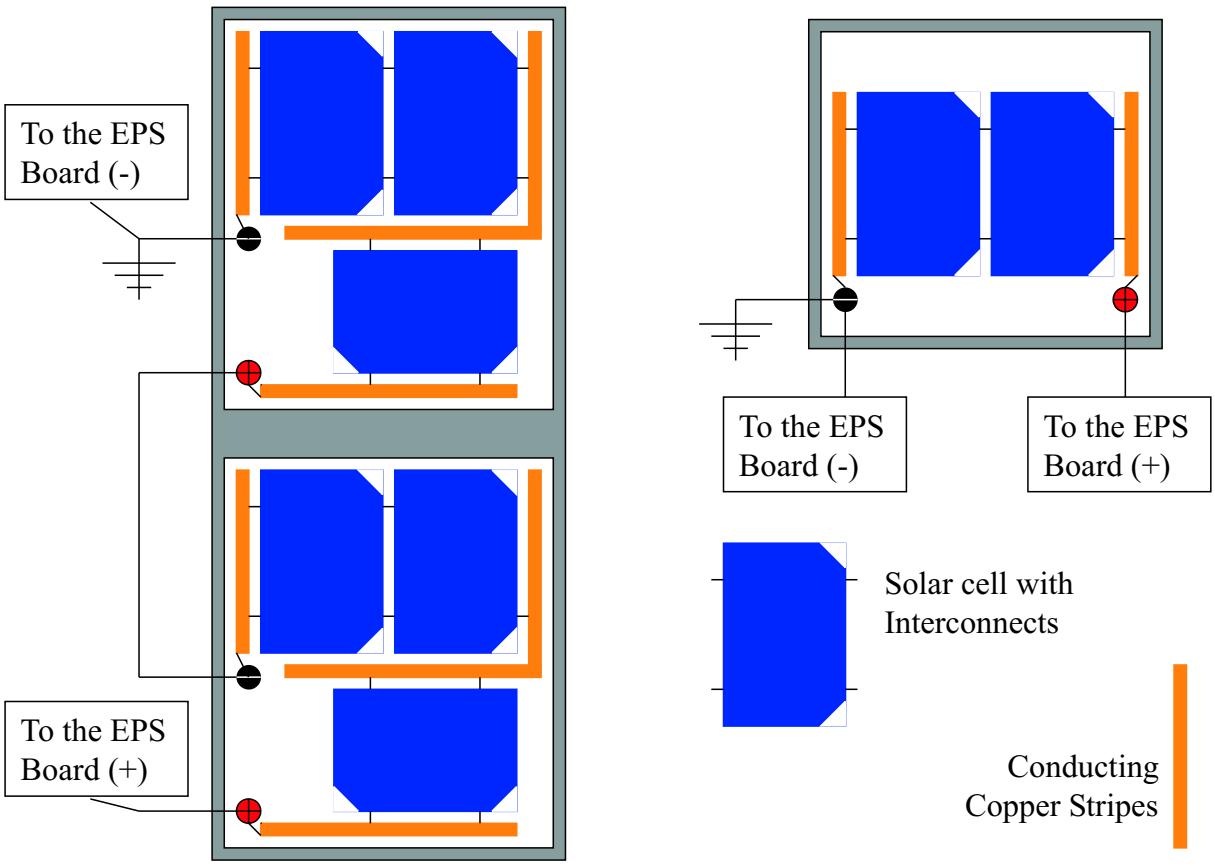

Figure 3.15: Solar Panel Design - The Panel's Electrical Configuration. Left: Two Large Panels in Series per Large Face of the Satellite. Right: One Small Panel per Small Face of the Satellite

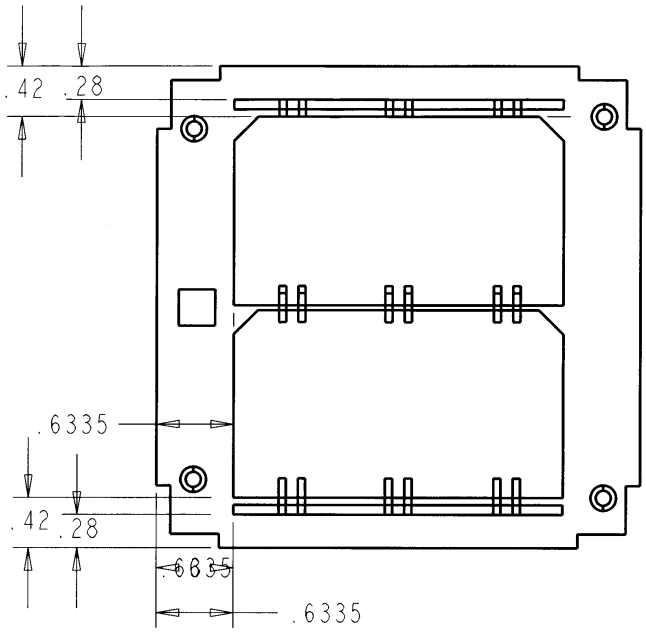

Figure 3.16: Solar Panel Design - The Small Panels (All Dimensions in Inch)

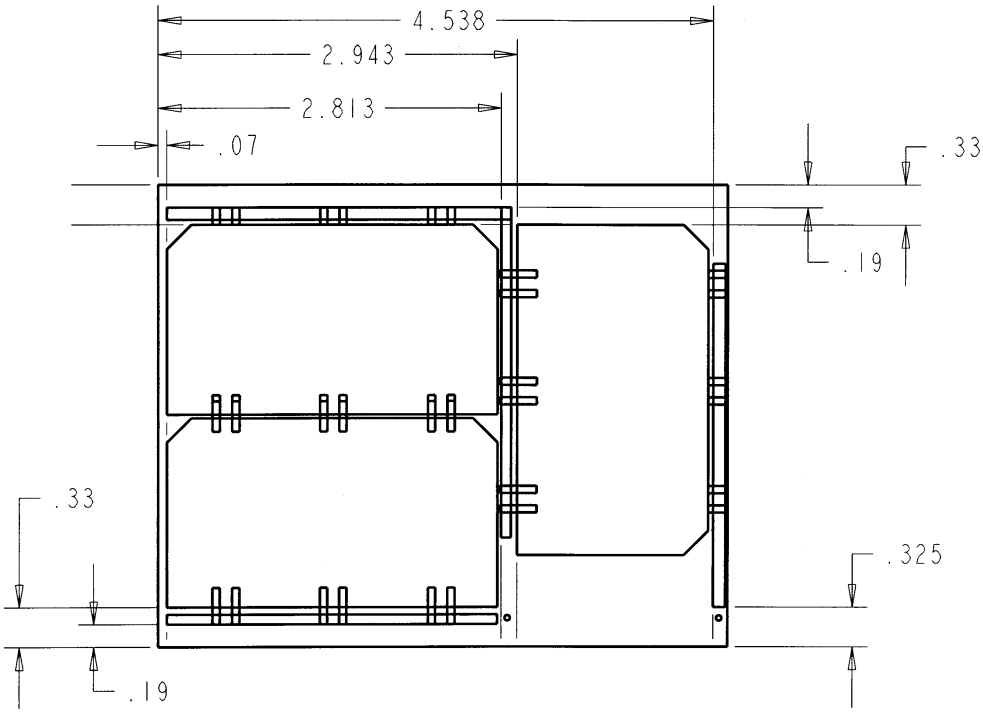

Figure 3.17: Solar Panel Design - The Large Panels (All Dimensions in Inch)

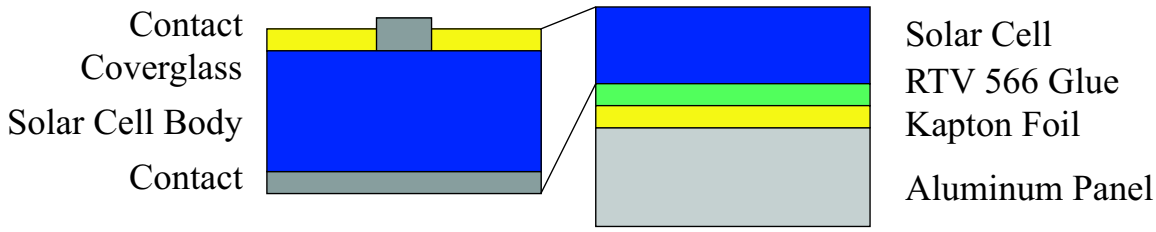

Figure 3.18: The Solar Panel Structure

3.8 Mounting the Solar Panels

In order to verify the design of the previous section, we decided to build solar panels for testing. The goal here was to augment the understanding of how solar panels are built, and also to find out, if the self-mounting of the final flight solar panels was a reasonable option.

For the test panels, we were using Spectrolab dual junction solar cells which Prof. Twiggs provided for us free of charge. These cells have the equivalent dimensions to the cells to be used for the final flight unit of the satellite.

The Mounting procedure

Figure 3.18 shows the general layer-structure we created. The procedure we followed for mounting the panels was:

1. We prepared the solar cells, in that we soldered the interconnects of the respective cells together. In order to later connect the end of each cell-string to one of the copper stripes on the bottom side of each string, we soldered ultra thin copper pads to the respective contacts on the backside of the cell (see Figure 3.19 for the cell without additional interconnects).

2. We prepared the Aluminum Panels, that is, we thoroughly smoothed and cleaned the surface

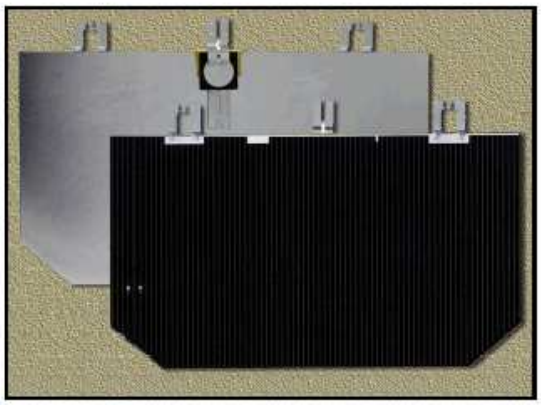

Figure 3.19: Solar Cell, Used for the Test Panels [15]

3. In order to facilitate the positioning of the components, we drew the outlines of the copper strips (see Figure 3.15) and the solar cells on the Aluminum plate with a thin pen.

4. Carefully avoiding air pockets, we stuck the Kapton foil (which is self-adhesive on one side) to the Aluminum plate.

5. In order to make sure there were no air pockets, we watched the panel in a customary vacuum jar, drained to about 100mbar.

6. Self-adhesive copper strips were bonded onto the Kapton tape at the previously marked positions.

7. As the space-rated RTV 566 glue by GE[3] was currently out of stock, we decided to use epoxy to bond the cells. We applied the glue to the backside of the solar cells, before carefully positioning the cells at the proper locations.

8. The current panel set up was transferred back into the vacuum jar. Applying light pressure to the cells by weighting them down, we had the glue hardening under 100mbar ambient pressure for several hours.

9. Finally, we cleaned the panel with acetone from small remnants of glue, and soldered the solar cell connectors to the copper stripe contacts.

10. After soldering customary cables to the copper stripes, the panels were ready for testing.

The Result

A total of four panels was built: The first panel was hardly success. One cell broke while bonding, the soldering connections were unsatisfactory and the too inaccurate placement of components lead to a short circuit.

Learning from the experiences above, three more panels were built with great care and thorough success. There, we built two large panels for one large face of the satellite and one small panel for the small face.

With these panels, we obtained the expected values for voltage and current. We mounted the panels to a dummy-satellite, to use it for representative EPS testing at a later time.

As to self-mounting the solar panels for the flight unit: Mounting the solar panels took very long time, i.e. a week, only for the panels described above (One person). As it is obvious that professional will obtain even better and more reliable results, the team decided to pass this job on to the Lockheed Martin Solar Array Center.

[3] General Electric

Chapter 4

RabbitSat EPS Power Storage

The Power storage is an important factor for the EPS design. We need power storage to make up for peak power requirements and to avoid losing excess power during times of high power availability. Power storage options for Aerospace applications include different kinds of secondary batteries[1]. The subsequent sections consider the power storage requirements, battery chemistry and configuration options, followed by a technical discussion of battery properties.

4.1 Power Storage Requirements

The following issues are of relevance for laying out the power source:

Mission Length The RabbitSat mission length shall be six months, potentially one year[2].

Primary or Secondary Power Storage RabbitSat will only use secondary batteries, as the mission type does not imply the need for primary batteries.

Orbital Parameters As listed in Table 2.1, the worst case eclipse duration is $T_e = 36min$, at 15.5 eclipses per day.

Power Use Profile From the power budget values of Figure 2.15, we created a showcase power use profile chart for a one orbit period (see Figure 4.1). These are the decisive numbers you can read from the show chart: The peak load that the battery has to be capable of providing is 11.5W, whereas the average load during eclipse will be in the order of 1.1W.

Battery charge/discharge limits Generally, the longer a battery will last, the less deeply you discharge it in each cycle. Depending on the battery chemistry, overcharging presents a serious problem. The limits are to be adapted to the battery type - please refer to the subsequent chapters.

[1] Secondary batteries refers to rechargeable batteries, whereas primary batteries are non-rechargeable

[2] Six month is a requirement, if the satellite will be operational after this period, it may be operated for another 6 months.

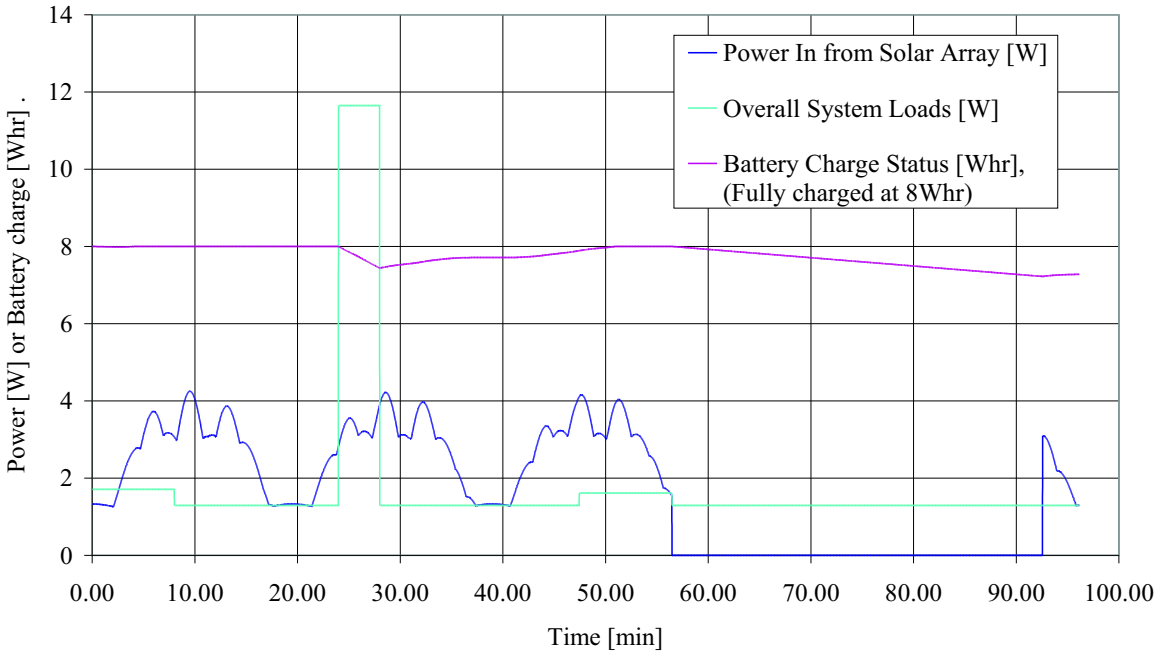

Figure 4.1: Showcase Power Usage Chart

4.2 Selection of the Battery Type

There are several types of batteries in usage for Aerospace applications. Figure 4.2 summarizes some facts about customary types.

As AgZn and NiH_2 batteries are not applicable for our size of satellite, our choice is limited to NiCd, NiMH, or LiIon batteries.

Out of these, the most common battery type is NiCd. NiCd batteries have been flown on satellites for many years and seldom showed any malfunction. They are the most tolerant towards overcharging and deep discharge. Whereas NiMH have similar characteristics, they are even more sensitive. The big advantage of NiMH is the higher energy density whilst the disadvantage is the low level of experience in NiMH chemistry in space applications. There is also the possibility of LiIon batteries where there is almost no experience in space systems. They are delicate to handle and require sophisticated charge control logic. Overcharging will quickly destroy the cells, that is, they will loose their ability to hold any charge. Nonetheless, there are three considerable advantages of LiIon batteries over all space rated secondary cells. The battery capacity is about two to three times as high as that of customary space batteries, whereby the cell volume is 60% lower. Additionally, LiIon batteries operate over a wider temperature range and have a higher cell voltage than required by most present-day aerospace applications. In particular for small pico-satellites like Cubesats, the higher cell voltage allows more flexibility in laying out the electrical configuration. Onboard the AAUSat as well as QuakeSat (see Section 2.1.2), the first LiIon batteries are now operational in space.

As for RabbitSat, the team decided to baseline selecting the NiCd chemistry due to its high level of robustness and reliability. Because of the similar properties of NiMH and

Battery	AgZn	NiH2	NiCd	NiMH	Li-Ion
Lifetime (cycles)	200+ (50%DOD)	45K+ (less than 20%DOD)	40K+ (less than 20%DOD)	300 to 500	500 to 1000
Watt-Hours/Kilogram	100	65	35	60 to 120	110 to 160
Discharge rate	High	Mod+	High	High	Low
Charge Retention	High	Low (best around 0degC)	Mod	Mod	not sensitive
Memory	No	No	Yes	No	No
Wet Shelf life	Short (Lifetime 90 to 200 days)	Mod	Mod	Long	Long
Failure Tolerance	High	High	Mod (High temperature buildup at high rate overcharge)	High	Low
Operating Temperature	0 to 45°C	0 to 20°C	0 to 50°C	-20 to 60°C (discharge only)	-20 to 60°C (discharge only)
Operating Cell Voltage	1.5	1.3	1.25	1.25	3.6
Experience Level	Low	Mod	High	Low	Low
Overcharge Tolerance	Not Specified	Not Specified	Mod	Low	Low--
Fast Charge Time	Not Specified	Not Specified	1 hr (typical)	2 to 4 hr	2 to 4 hr
Load Current peak/best result	Not Specified	Not Specified	20C/1C	5C/0.5C-	2C+/1C-
Notes	Activation required at time of use	Pressure vessel required; capacity loss concerns after storage	Very durable, many years of experience in Aerospace applications	Little experience in space applications, caracteristics similar to NiCd	Requires sophisticated charge control, little experience in Space applications

Figure 4.2: Common Battery Types

NiCd batteries[3], we consciously keep the option open to transition towards NiMH at a later point in the design. This might be useful in case the mass budget or the capacity requirements would later prescribe.

4.3 Determining the Battery Capacity

To determine the battery size, we first have to determine the desired depth-of-discharge (DOD). The DOD is defined as the percent of total battery capacity removed during a discharge period. The DOD represents a key factor for the battery cycle life, and differs depending on the battery chemistry. For instance, as shown in Figure 4.3, a NiH_2 battery would survive 10^4 cycles when discharging by 55% each cycle, whereas a NiCd battery would only survive about 2000 cycles at the same DOD.

Please note that the commonly utilized relationship shown in Figure 4.3 is a contentious point. It may be advisable to use this chart only as a good starting point for a design,

[3]NiMH and NiCd have the same cell voltage, a similar degree of robustness, and comparable charge/discharge characteristics

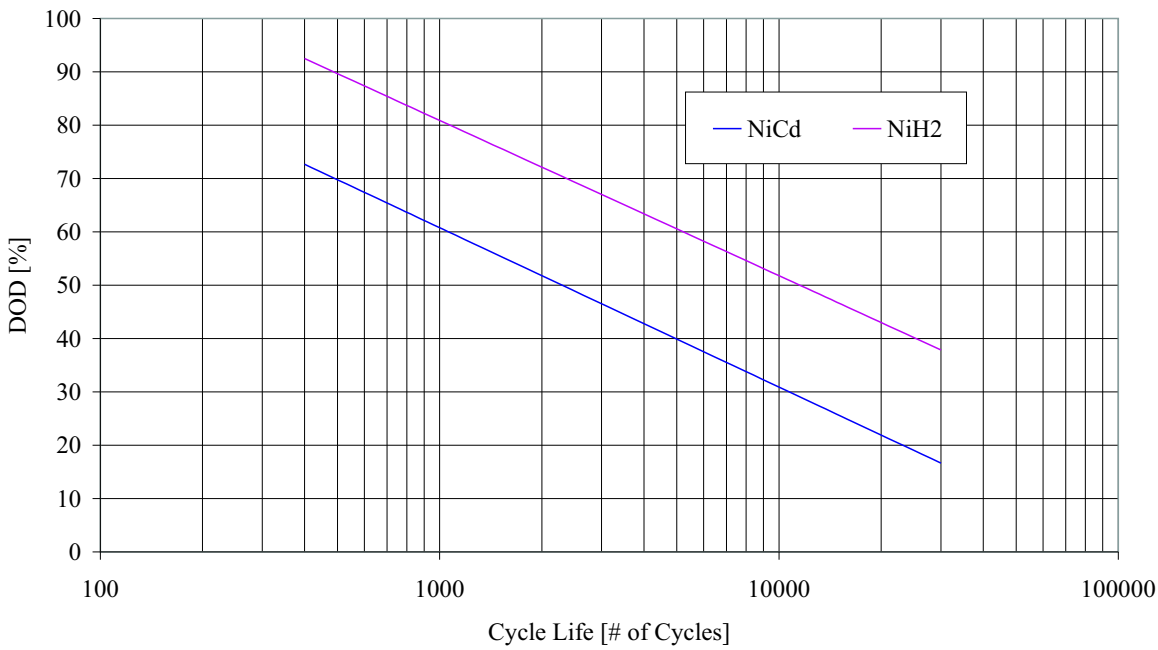

Figure 4.3: Depth-of-Discharge vs. cycle life for Secondary Batteries. Increased Cycle Life Reduces the Amount of Energy Available from the Batteries During Each Cycle - DOD Decreases with Cycle Life [11]

and not as design verification.

As for RabbitSat, the number of cycles for a 6 months period is 3000 (see Table 2.1). Hence, from Figure 4.3 we obtain a 46% allowable DOD for NiCd batteries.

With the eclipse power requirement P_e being 1.2W (Figure 4.1), we obtain

$$C_r = \frac{P_e \cdot T_e}{DOD \cdot n} = 1.7Whr, \tag{4.1}$$

where T_e is the eclipse period and n the efficiency from batteries to loads, here estimated to amount 90%.

Corresponding to our load voltage requirements and the solar array layout, a desirable nominal bus voltage for RabbitSat would be in the order of $V_n = 8.5V$[4], which translates into 7 to 8 NiCd cells in series.

Therefore, our required NiCd battery capacity in [AHr] will be

$$C_r, a = C_r/V_n = 202mAHr. \tag{4.2}$$

Accordingly, using AA-size NiCd cells, which have an average capacity of $300to1000mAHr$, we will satisfy our capacity needs with a single series string.

[4]Please refer to section 4.4 for an in-depth discussion of the optimum bus voltage

(a) NiCd Battery Charge Characteristics for Charging at 50mA

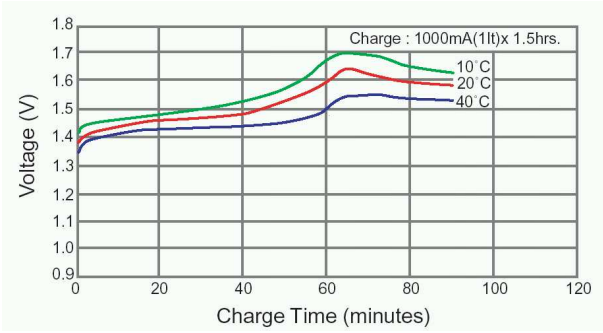

(b) NiCd Battery Charge Characteristics for Charging at 1000mA

Figure 4.4: Charging NiCd Batteries at Different Charge Currents [16]

4.4 Battery Charge/Discharge Characteristics

4.4.1 Battery Charging

The charge characteristics of NiCd batteries are affected by the current, time, temperature and other factors. Increasing the charge current and lowering the charge temperature causes the battery temperature to rise. Charge efficiency will vary with the current, time, and temperature [16]. Figure 4.4 shows characteristic charge curves for NiCd batteries at different charge currents and and varying temperatures. Generally, the battery charge current is given in [AHr] or in 'C' or 'lt', whereby [C] = [lt] refers to a multiple of the battery capacity. For, e.g., a charge current of 0.5A for a 1.2AHr capacity battery would equal a charge current of 0.6C.

4.4.2 Battery Discharging

The discharge characteristics of NiCd batteries will vary according to the current, temperature and other factors. Generally, in comparison with dry cell batteries, there is less voltage fluctuation during discharge, and even if the discharge current is high, there is very little drop in capacity. Among the various types of NiCd batteries, there are models that are specifically designed to meet the need for high current discharge, such as for power tools. There are also models which are designed to meet the need for high capacity, such as high-tech devices [16]. Figure 4.5 presents the voltage characteristics for battery discharging.

4.4.3 Battery Self Discharge

A drawback of NiCd batteries is the relatively high self discharge rate. According to Figure 4.6 though, we will be able to overcome long storage periods without losing a critical amount of power, as long as we can guarantee a controlled, low storage temperature.

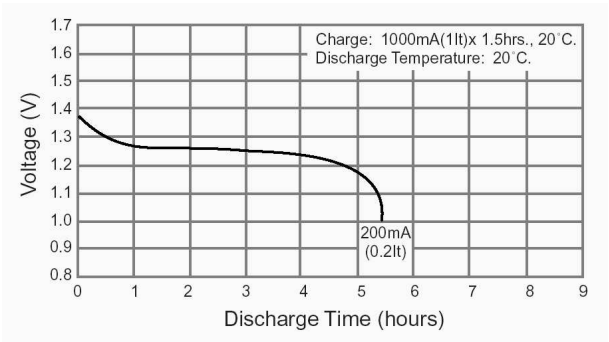

(a) NiCd Battery Discharge Characteristics a 200mA Current Draw

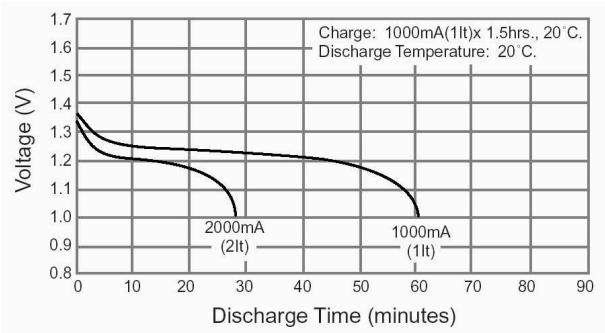

(b) NiCd Battery Discharge Characteristics for 1000 or 2000mA Current Draw

Figure 4.5: Discharging of NiCd Batteries [16]

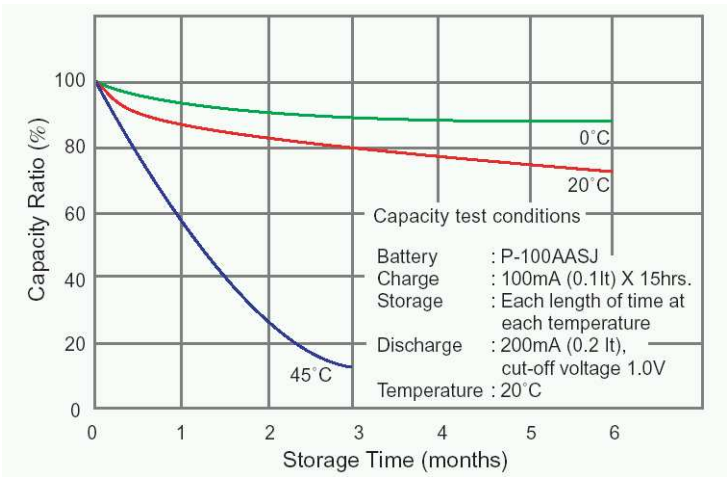

Figure 4.6: Typical NiCd self discharge characteristics [16]

4.5 Summary

This section led the reader through the different battery design steps. We found that the optimum power source for RabbitSat would be a single string of 7 to 8 AA-size standard NiCd secondary batteries. The similar characteristics of NiCd and NiMH batteries will facilitate a transition towards the latter chemistry, provided the further design process would require.

The following chapter will treat the satellite control scheme. From there, we will be referring back to this chapter and eventually finalizing the number of batteries.

Chapter 5

RabbitSat Power Regulation, and Control

After presenting an introduction to customary satellite power control schemes, the reader will be guided along the design path towards the control scheme for RabbitSat.

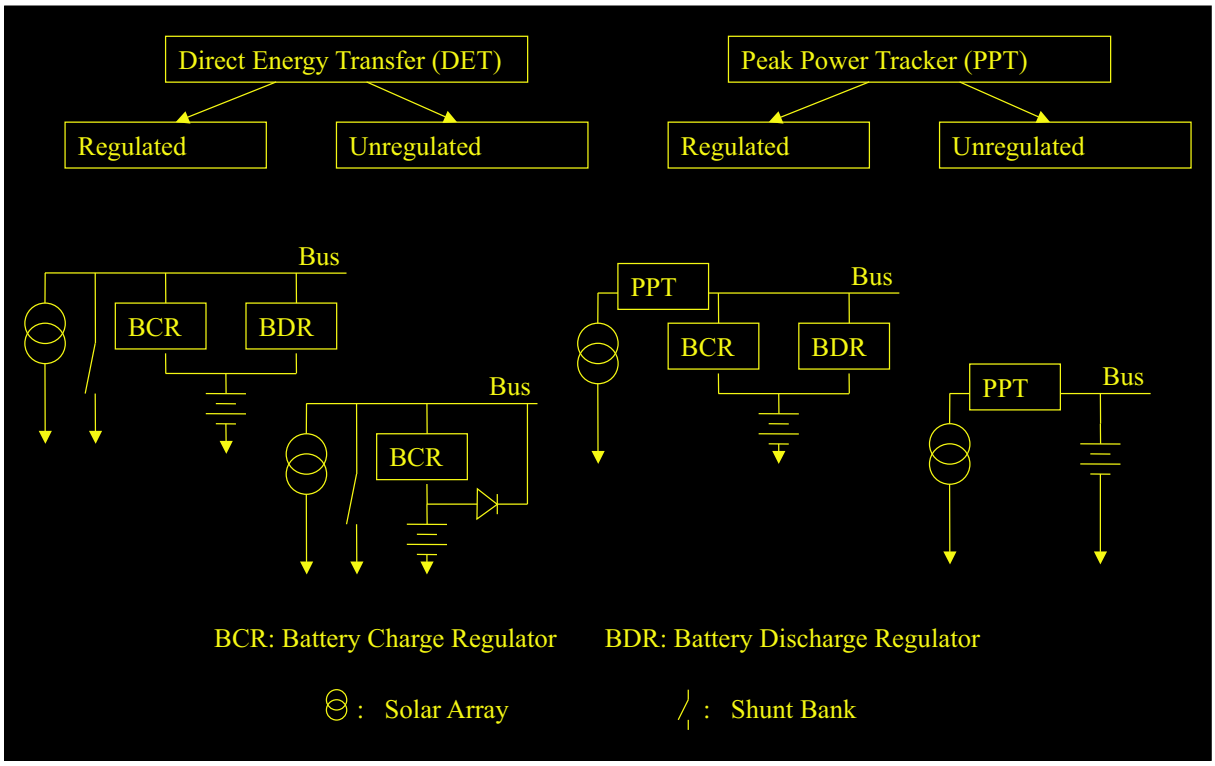

Figure 5.1: The Main Spacecraft Power Control Schemes; Derived from [11]

5.1 Customary EPS Control Schemes

The two main control schemes for spacecraft are

1. Direct Energy Transfer (DET) *and*
2. Peak Power Point Tracking (PPT)

where the bus may be unregulated or regulated, respectively.

Looking at Figure 5.1, for PPT, you will notice that the peak power point tracker is in series with the solar array, whereas for DET, the solar array is directly connected to the bus. Now, a peak power point tracker is a DC/DC converter that dynamically changes the operating point of the solar array. When energy demand exceeds the peak power, the PPT will track the peak power point.

Even though the PPT theoretically produces a slightly better solar array performance, the in-series DC/DC converter causes the overall energy conversion efficiency to decrease by the order of 4 to 7% [11].

The practical difference between the two methods is that the DET system generally "accepts" the entire solar panel current at the bus voltage[1], whereas the PPT would prevent the solar array from providing more current than currently required. This means,

[1]Please notice that a solar cell is to be seen as a current source. It provides current at the very voltage which the bus prescribes. The bus voltage, in turn, is driven by either the battery itself(unregulated case) or the battery discharge controller (regulated bus)

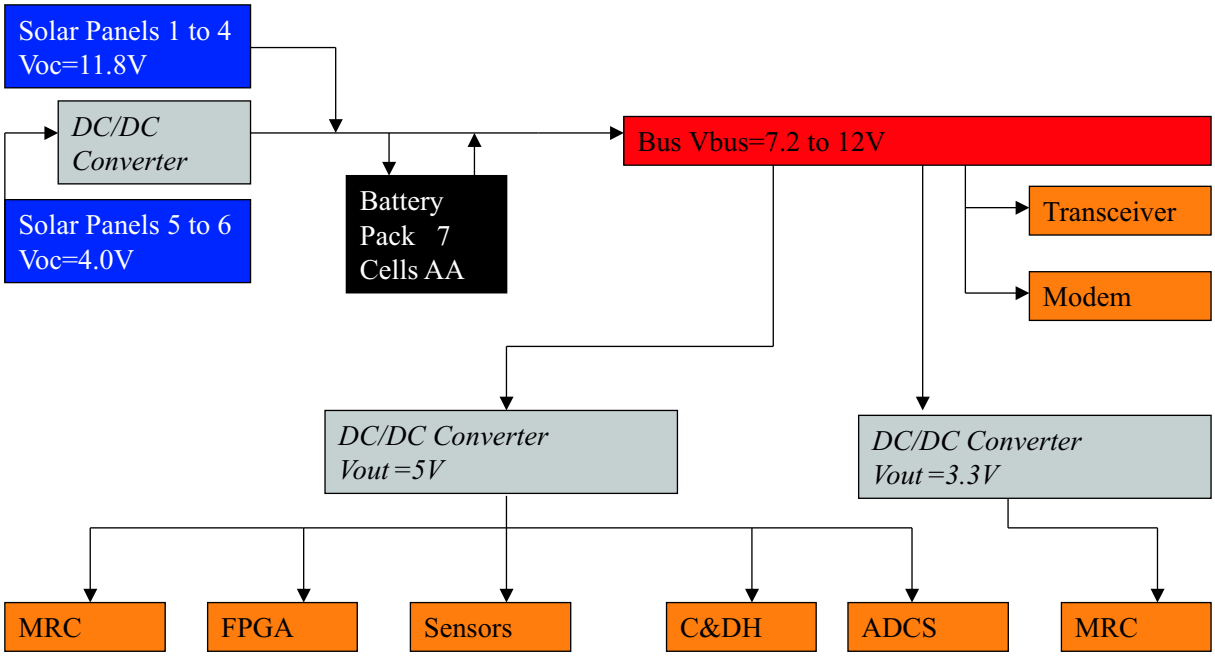

Figure 5.2: First-cut RabbitSat Control Scheme Configuration

that, contrary to DET, PPT does not require additional shunt regulation to get rid of excess power. DET needs shunt resistor banks in order to keep excess heat out of the satellite, whereas PPT uses the solar array for this purpose.

Hence, DET is also referred to as a *dissipative*, and PPT as a *nondissipative* system.

Techniques for controlling the bus voltage fall into three categories: unregulated, quasi regulated, and fully regulated systems. Unregulated systems directly connect the bus to the batteries. Quasi-regulated systems only employ a battery charge regulator, whereas fully regulated systems rely on both a charge regulator and a discharge regulator. It is obvious that the unregulated version is the most efficient, and the fully regulated system the most inefficient.

5.2 RabbitSat EPS Control Scheme

In order to maximize robustness and simultaneously keep complexity low, we decided to equip RabbitSat with DET and a completely unregulated bus voltage, as long as the specific requirements would allow. A PPT system would have required additional components and a micro-controlling unit. All this complexity, in series with the entire satellite's power source, appeared to be an unnecessary risk, diminishing the chances for success, at no gain. Nonetheless we explicitly acknowledge that PPT can be advantageous in similar satellites. For instance, the AAUSat uses PPT, as it has a micro-controlling-unit on its EPS anyway (see Section 2.1.2).

However, we analyzed our system with all the required components, creating a first-cut model for the power control configuration. The result of this analysis is illustrated in Figure 5.2. Contrary to the previously discussed DET control scheme, you will not see a shunt resistor bank here. This is because of two reasons:

1. The Cubesat concept, together with the especially tight time limit for RabbitSat, urges us to cut complexity, and hence to diminish the number of components wherever possible.

2. The high ratio of battery capacity to maximum incoming solar array power, together with the NiCd type batteries, makes critical battery overcharging hard anyway.

As we still have to have a way of getting rid of excess power, we decided to use the transmitter for this purpose. The transmitter is ideal here, because

1. it is the biggest satellite electrical load,

2. it radiates at least 25% of the total consumed power out of the satellite, *and*

3. it should be generally desirable to transmit often, as this is when someone will hear from our satellite.

The transmitter shall be controlled by the C&DH subsystem (see Section 2.2.3). Control drivers shall be the temperature increase rate dT/dt and the battery voltage.

5.3 RabbitSat Power Distribution

The power distribution system consists of cabling, fault protection and switching gear. Regarding the low level of complexity for RabbitSat, we can complete this section rather quickly.

5.3.1 Cabling

The design of the cabling system is, for RabbitSat, not the responsibility of the EPS, but of the systems integration subsystem. However, the following are the minimum requirements for harnessing the EPS:

1. Especially for all high current cables, the cable diameters shall be reasonably wide so as to keep the specific resistance, and thereby the I^2R losses low. High current cables are all cables connecting the solar panels, the battery pack, the transmitter, and the deployment switches[2].

2. The satellite will use one common ground for digital and analog, but nonetheless, we require additional separate ground cables for each load.

3. All cables shall be twisted pairs, so as to diminish noise propagation throughout the satellite.

[2]The deployment switches are mechanical switches activated upon deployment of the satellite from the launcher. They will be subject to the components discussion

5.3.2 Fault Protection

For complexity reasons, RabbitSat will not use explicit fault protection circuits to protect the different devices, but rather it will rely upon the current limiting functionality of the different DC/DC converters. These will shut down, as long as a connected load tries to draw a current, greater than the specified maximum current. To prevent all components under one DC/DC converter shutting down at the malfunction of one component, we split up the 5V loads and subordinated them to two 5V converters, as illustrated in Figure 5.3. The figure shows the maximum current values which we preset for the 5V and 3.3V DC/DC converters. To protect the solar panels from failing at the failure of a single cell within a respective series string, we are using solar cells with built-in back-bias diodes (see Section 3.4.1). As shown in Figure 5.3, the two small panels are connected in series with a DC/DC converter. Here, we employ two DC/DC converters, one for each of the small panels. We do not provide fault protection for the transceiver or the modem, as a failure in these devices would mean the loss of the satellite anyway.

5.3.3 Switching Devices

Several RabbitSat loads have to be switched on and off by the C&DH. As shown in Figure 5.3, these loads are

1. the MRC payload
2. the FPGA payload
3. the ADCS subsystem *and*
4. part of the sensors.

Loads that receive continuous power are

1. Modem
2. Transceiver
3. C&DH *and*
4. part of the sensors.

The Modem will be running continuously. The transceiver will be powered continuously, whereby the C&DH will trigger the PTT-line[3] in order to toggle between transmit and receive mode. The C&DH will be continuously powered up, whereby the C&DH subsystem is supposed to provide the capability of rebooting itself.

To switch the respective loads listed above, we will use p-channel Power MOSFETs[4]. The hardware selection will be part of the discussion in the subsequent chapters.

[3]PTT stands for Push-To-Talk. Mostly, PTT would be active (transmit mode), when the transceiver data line (TX) is pulled low.

[4]MOSFET stands for Metal Oxide Field Effect Transistor

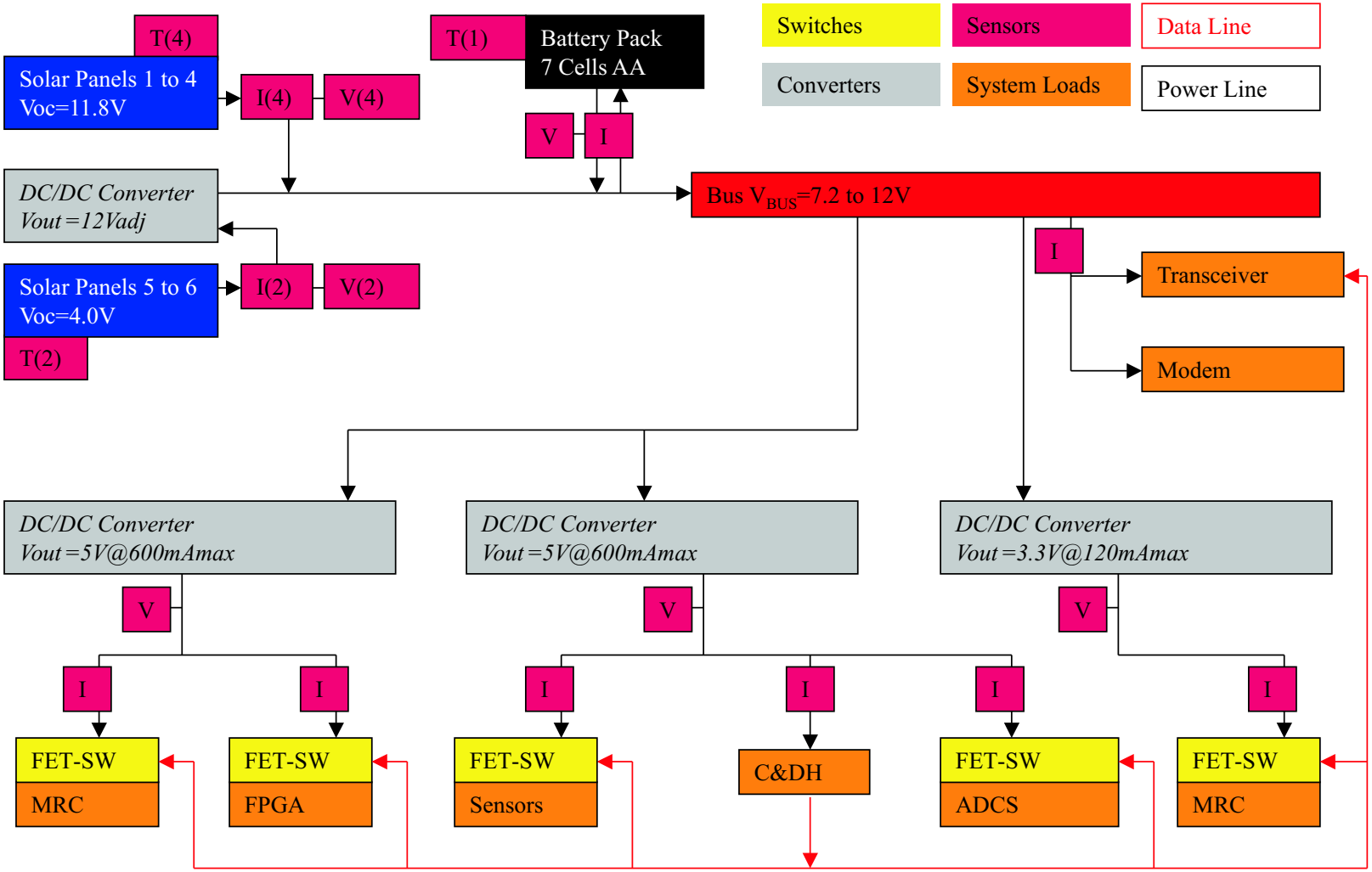

Figure 5.3: RabbitSat Power Control Scheme

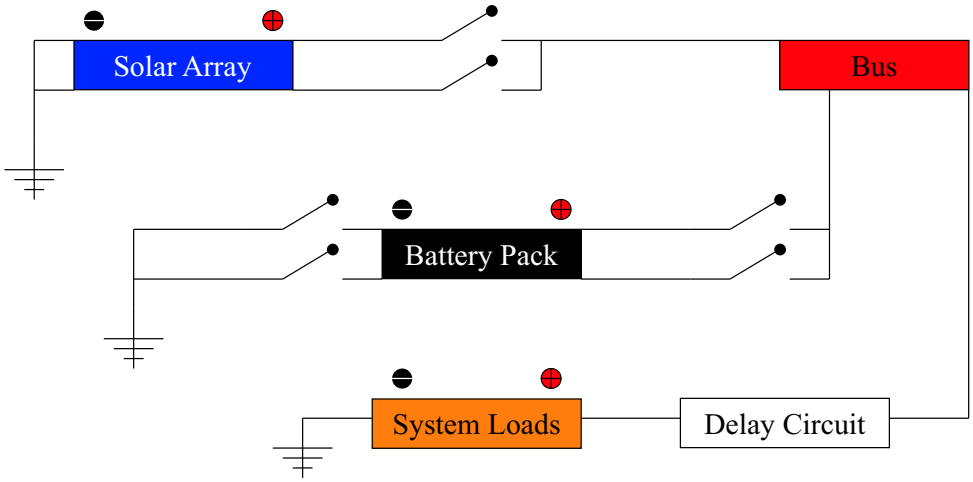

Figure 5.4: RabbitSat Power Control Scheme

Finally, this will discuss the deployment switches: in accordance with the requirements of the Cubesat, as well as those of the Space Shuttle, we decided for the deployment switching scheme as in Figure 5.4. The design includes two double redundant switches disconnecting the solar array and the battery anode from the bus. Another double redundant switch disconnects the battery cathode from the common ground. The loads will not be directly powered on by deployment. There will be a delay of several minutes before the loads will be activated.

Again, the hardware implementation of this functionality will be treated in the subsequent chapters.

Chapter 6

RabbitSat EPS Electronic Board Design

After having defined the functionality of the EPS system, the goal of this chapter is to guide the reader through the design process of the Electronic hardware.

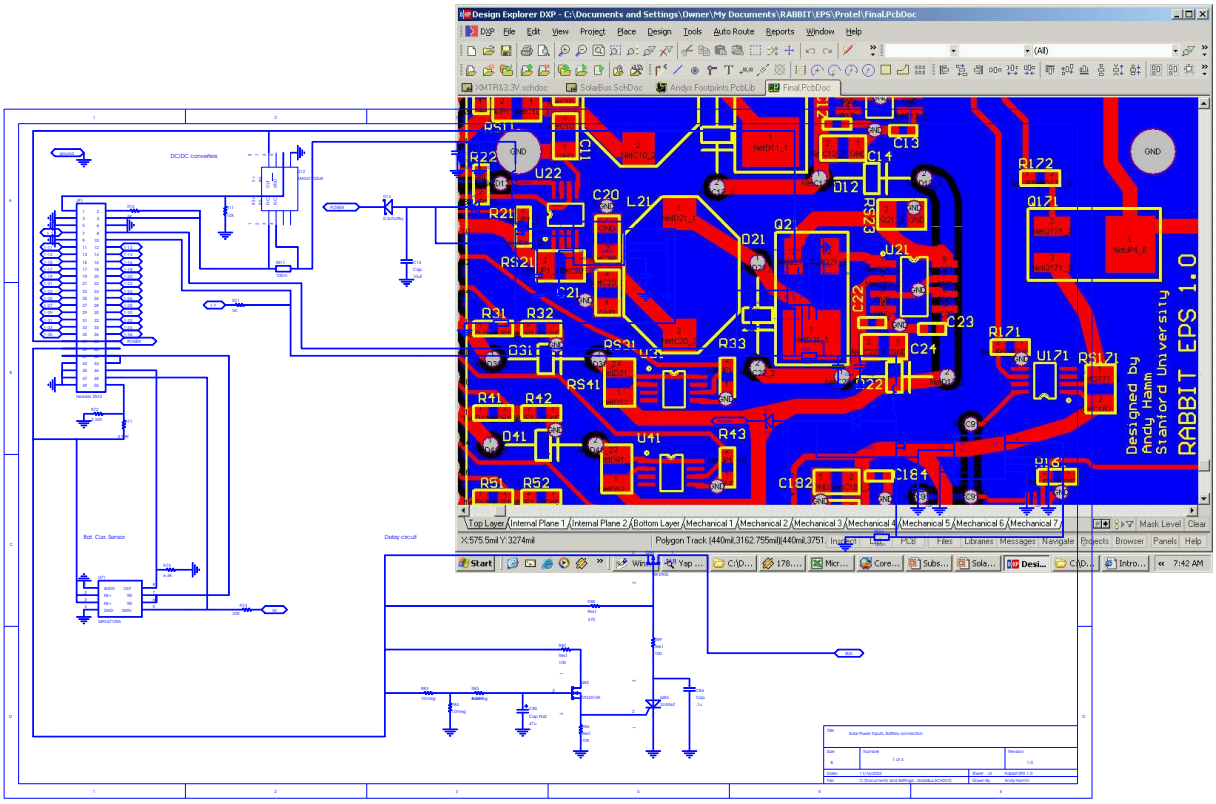

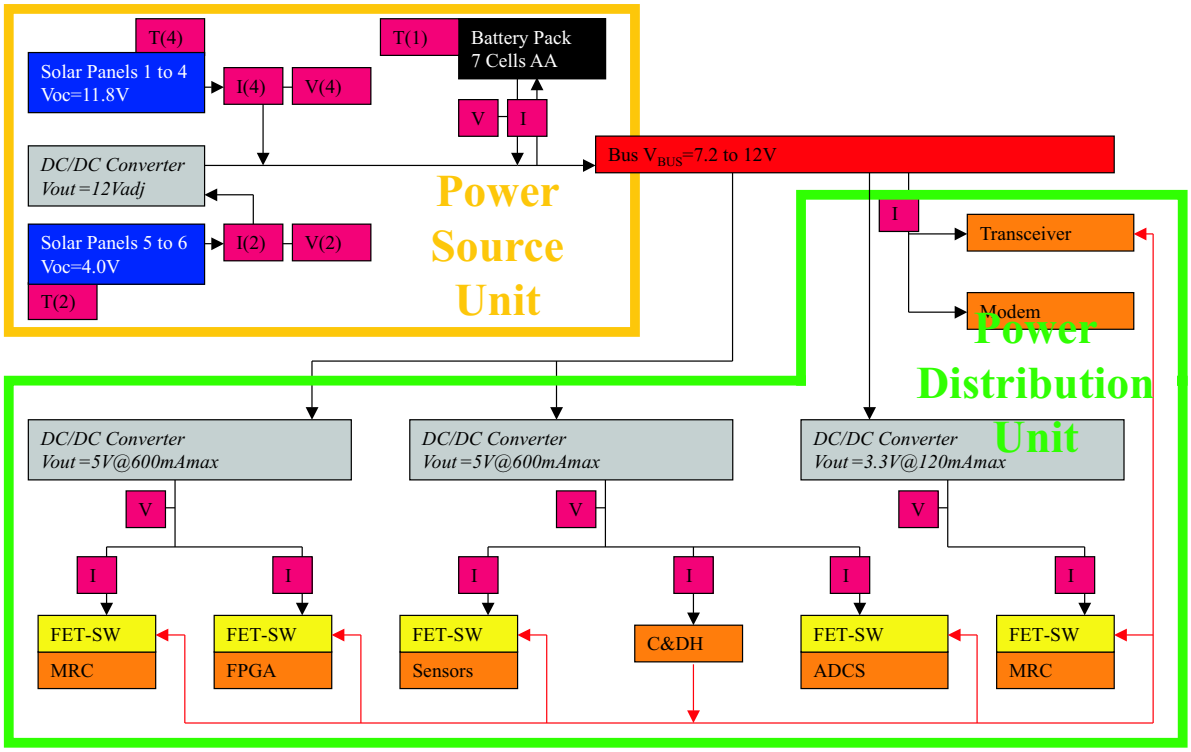

Figure 6.1: First-cut RabbitSat Control Scheme Configuration

In order to improve the overview here, we broke the system down into two units, the Power Source Unit and the Power Distribution Unit. The functional breakdown towards either unit is shown in Figure 6.1. The chapter will conclude by demonstrating and explaining the consolidation of all components onto a single EPS board.

6.1 The Power Source Unit

As Figure 6.1 shows, the power source unit essentially consists of the following components[1]:

1. 2 4V/12V - DC/DC Converter
2. Solar Array
3. Current Sensors
4. Battery Pack

The following will lead the reader through these components in the above order.

[1] The temperature sensors at the solar panels, as well as the battery, will be selected by the systems integration subsystem

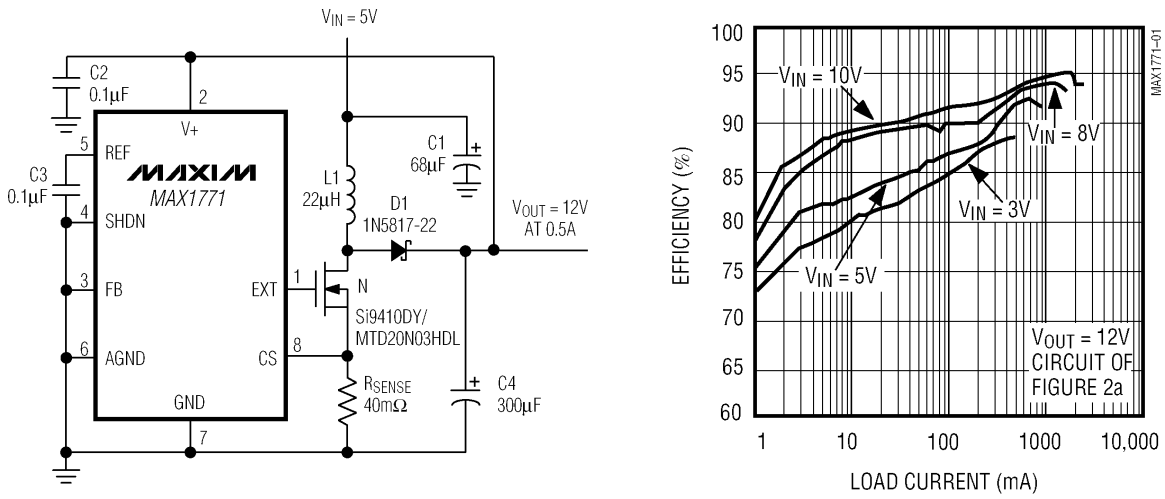

(a) Recommended Operating Circuit

(b) Efficiency Characteristics

Figure 6.2: The MAX1771 DC/DC Converter [17]

6.1.1 The DC/DC Converter

Description

The description will start off with the DC/DC converter as it is the most critical component of the power source unit. The DC/DC converter is critical, because it is a high frequency device and hence requires very careful layout. A poorly designed DC/DC converter does not work.

The reason that a DC/DC converter is required in the first place lies in the large potential difference of the small and the large solar panels. Using a linear regulator for adapting the voltages would only work downwards, i.e. 4V would have to be the bus voltage. A bus voltage this low, though, is undesirable. It would imply much higher currents; plus, the voltage would have to be boosted again for all connected system loads. Also, the power loss within a linear regulator would be 75% at this voltage ratio.

However, DC/DC converters are available as ready-made modules, mostly coming in radiation protected housings, or as Integrated Circuits (IC), which require more or less additional external circuitry. We tried to find a commercial converter, but this turned out to be very hard, considering our very specific and unusual voltage levels. Hence, the converters were self-designed.

When selecting the proper IC, our principal criterium was the conversion efficiency in our voltage ranges and the specific current levels. Therefore, we picked the MAX1771 converter by Maxim/Dallas. The efficiency characteristics are shown in Figure 6.2.

Design Procedure

The MAX1771 layout generally follows the MAXIM design recommendation as of Figure 6.2. For detailed information refer to the product data sheet [17].

Setting the Output Voltage The converter will be operated in bootstrapped mode with a preset output voltage of 12V. Therefore, FB has to be tied to GND.

Determining $\mathbf{R}_{SENSE}$ From the theoretical output current curves of Figure 6.3, we obtain $R_{SENSE} = 100m\Omega$. However, from experiments with a test unit we found that, for the successful operation of the converter with solar cells as a power source, we need to set the current limit even tighter. The final design shall use $R_{SENSE} = 180m\Omega$, at $I_{LIM} \approx 400mA$.

Determining the Inductor L The inductor value was determined using the equation

$$L \geq \frac{V_{IN}(max) \cdot 2\mu s}{I_{LIM}} = 20\mu H \tag{6.1}$$

where $V_{IN} = 4.5V$ is the maximum input voltage, and thus equal to the maximum output voltage of the small solar panel. We will use a $22\mu H$ inductor by Coilcraft (DO3316).

Power Transistor Selection The three important parameters when selecting the n-channel MOSFET (N-FET) are the total gate charge (Q_g), on-resistance ($r_{DS(ON)}$), and reverse transfer capacitance (C_{RSS}). We decided to use the MTD20N03HDL N-FET by On Semiconductor, with $(Q_g) = 13.4nC$, $(r_{DS(ON)}) = 35m\Omega$, and $(C_{RSS}) = 80pF(typ)to150pF(max)$.

Diode Selection The Max1771's high switching frequency demands a high-speed rectifier. Our design will use a customary 1N5817 Schottky barrier by Diodes Inc. This diode shows a low forward voltage in our applicable current range.

Output Filter Capacitor C4 Generally, the primary criterion for selecting the output filter capacitor is low effective series resistance (ESR). Unfortunately though, the best-suited capacitors here would be Polymer capacitors, which are not appropriate for vacuum applications. As Tantalum capacitors bear the risk of shorting, we will use a $10\mu F$ ceramic capacitor. This value may appear low, but it will be appropriate, since there is no sensitive load directly connected to the converter. The directly connected battery will act like a huge capacitor.

Input Bypass Capacitor C1, C2 The input bypass capacitor reduces peak currents drawn from the voltage source, and also reduces the noise at the voltage source caused by the switching action of the MAX1771. As with the output capacitor, low ESR capacitors are highly recommended. For the same reasons as above, we will go for ceramic capacitors, at $C1 = 2 \cdot 10\mu F$, bypasses by $C2 = 0.1\mu F$.

Reference Capacitor C3 As recommended by Maxim, we bypass REF with a $C3 = 0.1\mu F$ ceramic capacitor.

Our MAX1771 layout, as a result of the above discussion, is shown in Figure 6.4.

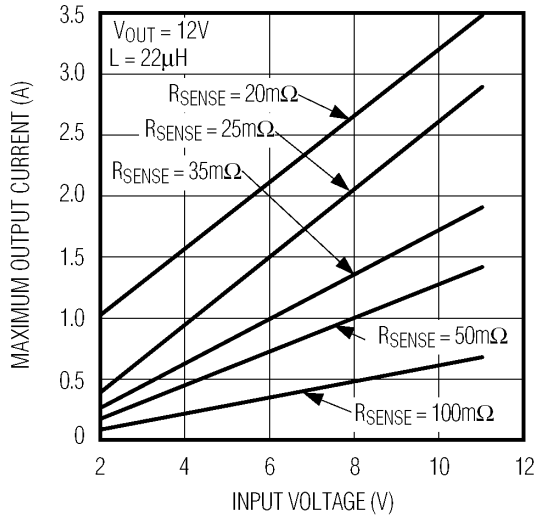

Figure 6.3: MAX1771 - Maximum Output Current vs. Input Voltage

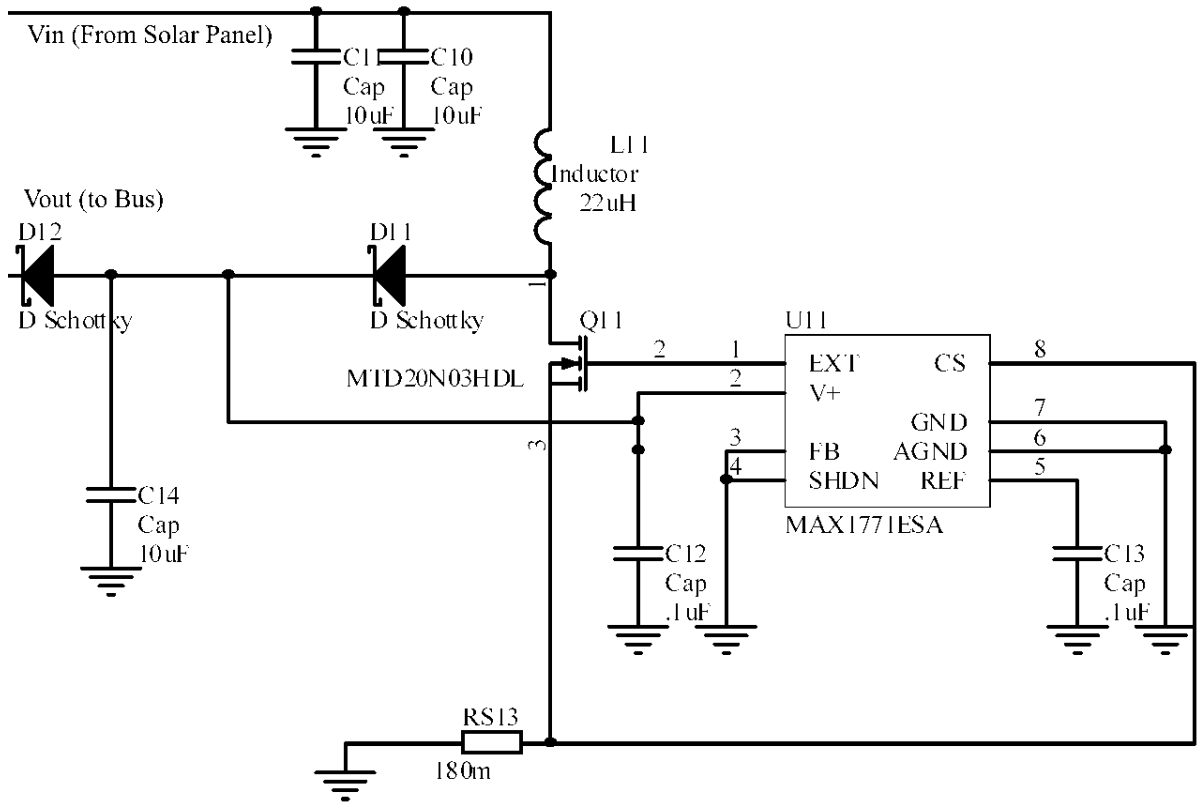

Figure 6.4: The RabbitSat MAX1771 Layout

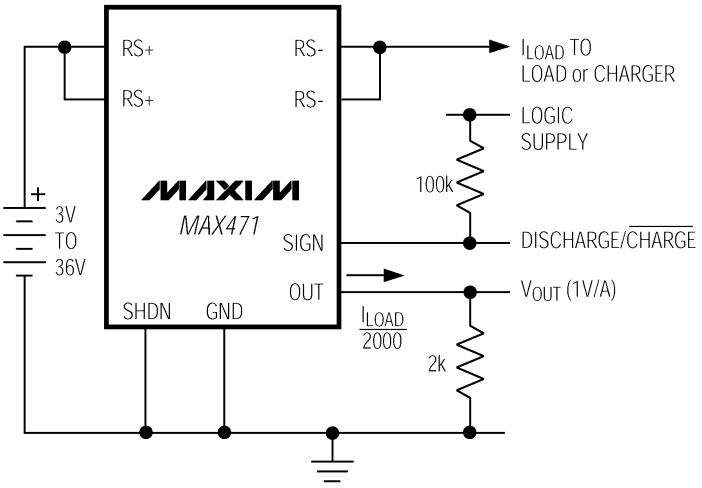

Figure 6.5: MAX471 Typical Operating Circuit [17]

6.1.2 The Current Sensors

Description

The RabbitSat EPS has to fulfill the requirement of measuring the current at different points, as shown in Figure 6.1. These are

1. the battery current in both directions *and*
2. the solar panel currents for each of the six faces, respectively.

As customary for our kind of application, we will be using high-side current-sense amplifiers. We choose the MAX4172 precision current sensor for the solar panel currents, and the MAX471 for the battery current. Contrary to the MAX4172, the MAX471 is capable of measuring the current in both directions. This feature is, of course, only useful for the battery. The MAX471 has considerably worse accuracy than the MAX4172, plus it does not come in the extremely small μmax package.

Design Procedure - MAX471

The MAX471 typical operating circuit is shown in Figure 6.5.

Setting the Gain Anticipating a maximum battery current of $I_{LOAD} = 1.5A$ and a full scale output voltage[2] $V_{OUT} = 5V$, as is customary[3] for most multiplexors (MUX) applications, we calculate the value for the output resistor R_{OUT}, and thus the gain, as

$$R_{OUT} = \frac{V_{OUT}}{I_{LOAD} \cdot 500\mu A/A} = 6.6K\Omega. \tag{6.2}$$

[2]The MAX471 output voltage
[3]At the time of writing, the C&DH design did not select the MUXs

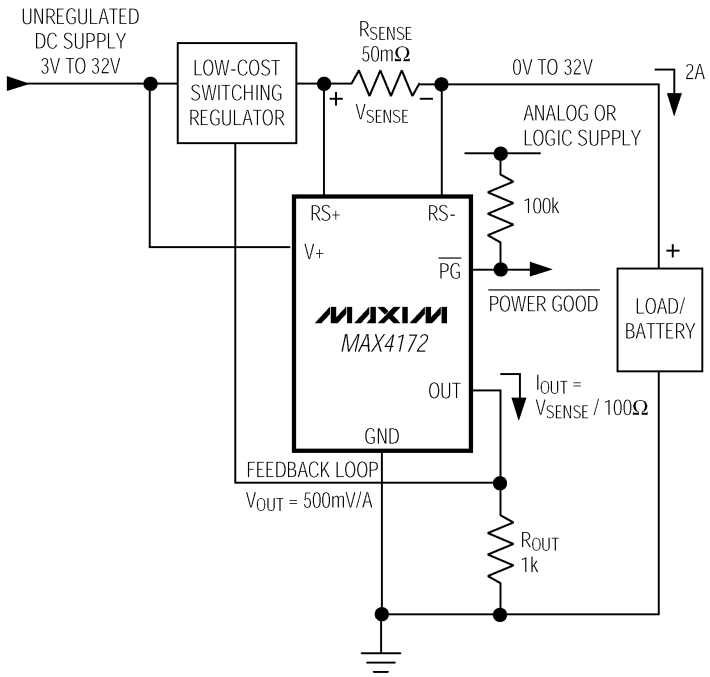

Figure 6.6: MAX4172 Typical Operating Circuit [17]

Logic Supply The MAX471 provides two different outputs, one analog and one logical output. The analog output, connected to OUT, represents the current, whereas the SIGN output goes low or high, depending on the current flow direction. The SIGN out will be pulled towards a TBD 5V line logic supply via a 100K resistor.

The Current The current may be calculated from the OUT voltage as

$$I = \frac{V_{OUT}}{R_{OUT} \cdot 500\mu A/A} \tag{6.3}$$

Design Procedure - MAX4172

Figure 6.6 shows a typical operating circuit for the MAX4172 current sensor.

Setting the Gain The solar panels' maximum current will be in the order of $I_{LOAD} = 500mA$ and the full scale voltage output again V_{OUT}, as for the MAX471. To set the gain, we fist have to determine the appropriate sense resistance R_{SENSE}, then size the output resistor accordingly. Now, the sense resistance depends on the full scale load current and is a trade between accuracy and I^2R loss. As a medium value, we pick $R_{SENSE} = 100m\Omega$. Then, we obtain

$$R_{OUT} = \frac{V_{OUT}}{I_{LOAD} \cdot R_{SENSE} \cdot G_m} = 10K\Omega, \tag{6.4}$$

where G_m is the transductance of $G_m = 10mA/V$.

The Current The current may be calculated from the OUT voltage as

$$I = \frac{V_{OUT}}{R_{OUT} \cdot R_{SENSE} \cdot G_m}. \tag{6.5}$$

.

Power Good Output PG The MAX4172 does have another output, the digital power good output. As we don't need this functionality, this pin will remain unconnected.

6.1.3 The Solar Array

The design of the solar array was the subject of Chapter 3. So as to integrate the solar array design in the EPS board, we need to provide for the harnessing, which is treated in Section 6.4. Other than that, we have to protect the solar panels from backward current flow. Otherwise, the current of the panels in daylight would flow through the panels in the shade, and thus dissipate all power. This protection is usually done by means of diodes, such as Schottky Barrier Rectifiers.

Because of their low forward voltage in our (low) current range, we will be using 1N5817 Schottky barrier of Diodes Inc.

For all panels, the diodes are arranged between the current sensors and the bus. Particulary for the small panels, this arrangement is doubly advantageous in terms of efficiency: The voltage level is higher than before the DC/DC converter, whereupon the current is lower[4].

Please see Appendix C.1 for the arrangement of the protection diodes.

6.2 The Power Distribution Unit

As Figure 6.1 shows, the power distribution unit essentially consists of the following components:

1. 2 12V/5V - DC/DC Converter
2. 1 12V/3.3V - DC/DC Converter
3. A total of 6 current sensors for the various electrical loads
4. Current Sensors
5. Five FET[5]-Switches

Subsequently, we will discuss these components in the above order.

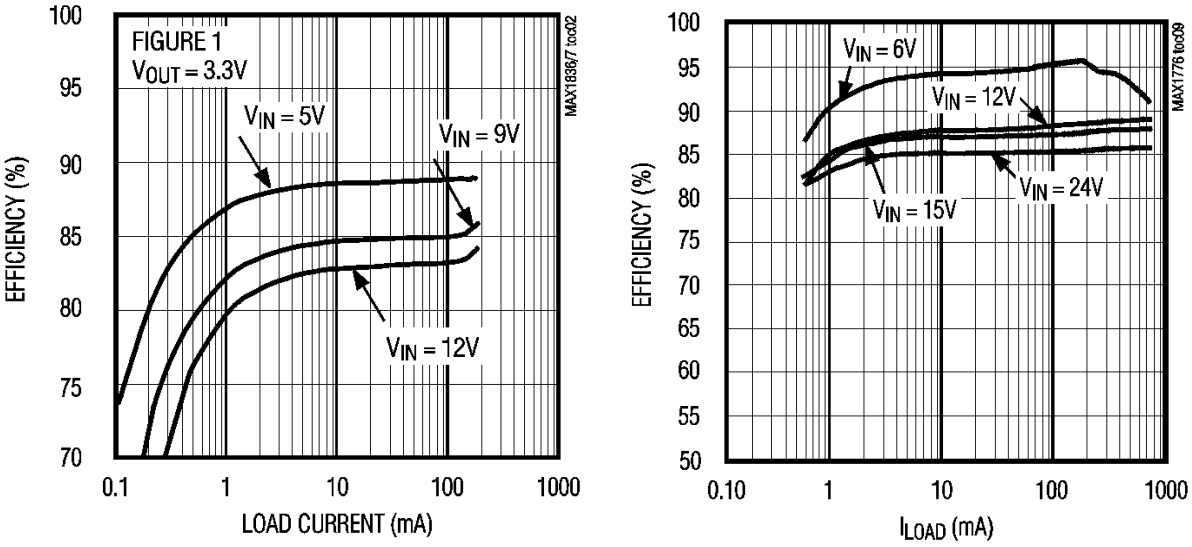

(a) MAX1836 Converter (b) MAX1776 Converter

Figure 6.7: DC/DC Converter Efficiency Characteristics of the below Discussed Parts [17]

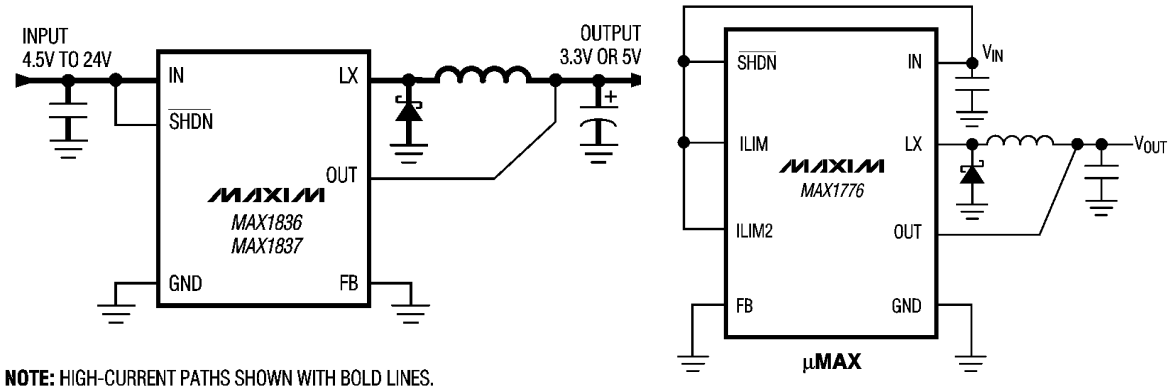

(a) MAX1836 Converter (b) MAX1776 Converter

Figure 6.8: DC/DC Converter Typical Operating circuits [17]

6.2.1 The DC/DC Converters

Description

Generally, the same issues as in Section 6.1.1 apply to the DC/DC converter selection for the power distribution unit. The large voltage ratio of up to 3.3V/11.5V precludes the possible usage of linear voltage regulators.

As one of the most efficient converters in our voltage/current range, we choose the MAX1836 and MAX1776 parts, for 3.3V and 5V output voltages respectively. The efficiency curves for both converters are shown in Figure 6.7.

Both converters provide internal current limiting functionality. As RabbitSat does not employ additional circuit protection, the converters will act as EPS short circuit protection. The setting of the current limits is part of the discussion below.

Figure 6.8 shows the typical operating circuits, on which the design procedure is based.

Design Procedure - MAX1776(5.0V)

Current Limits Before setting the current limit, we will take a look at the loads expected. As illustrated in Figure 6.1, the loads on the first converter (seen from left to right) are the MRC and FPGA payloads. Using the values from Figure 2.14, we obtain an operating current and $P_{max,1} \approx 250mA$, if both payloads are operated in high mode at the same time. To allow for short-time current peaks, we set the current limit for the first converter to $I_{LIM,1} = 600mA$. To set this current limit, we have to tie ILIM to IN, and ILIM2 to GND [17]. Equivalently, we find the maximum load for the second converter to be $P_{max,1} \approx 50mA$. Since, at the point of the design, the COMM subsystem requested to keep the option open of running the modem on 5V as well (and not on the unregulated bus, as previously assumed), we decided to add considerable margin here. We set the current limit to $I_{LIM,2} = 600mA$, as for converter 1.

Inductor Selection The factors to consider when selecting the proper inductor are the inductance, the saturation rating, series resistance and size. The minimum inductance value is

$$L_{MIN} = \frac{(V_{IN,MAX} - V_{OUT}) \cdot t_{ON,MIN}}{I_{LX,PEAK}} = 11.67\mu H, \tag{6.6}$$

where $t_{ON,MIN} = 1\mu s$, $V_{IN,MAX} - V_{OUT} = 7V$, and $I_{LX,PEAK} = 0.6A$. Accordingly, we selected a value for the CDRH6D28 series Inductor of $L = 22\mu H$.

The Output Capacitor The output capacitors reduce the noise (=voltage ripples). As explained in Section 6.1.1, we cannot use Polymer capacitors and should avoid using Tantalum capacitors. Therefore, we will try to use two $22\mu F$ ceramic capacitors[6] in parallel. I'd like to point out here that ceramic capacitors generally have another

[4] The diode implies a voltage drop of about 0.5V, negatively depending on the current

[5] FET stands for Field Effect Transistor

[6] Ceramic capacitors are not available with great capacitance values, $22\mu F$ is one of the highest possible.

advantage over Polymer and over Tantalum capacitors: The ceramic effective series resistance (ESR) is lower than either one (usually $\leq 0.015\Omega$)[7]. However, the output ripple consists of two components: variations in the charge stored in the output capacitor with each LX pulse, and the voltage drop across the capacitor's equivalent series resistance caused by the current into and out of the capacitor:

$$V_{RIPPLE} \cong V_{RIPPLE,ESR} + V_{RIPPLE,C}, \tag{6.7}$$

where the output ripple as a consequence of the ESR and output capacitance is:

$$V_{RIPPLE,ESR} = ESR \cdot I_{PEAK} = 25mV \tag{6.8}$$

$$V_{RIPPLE,C} = \frac{L \cdot (I_{PEAK} - I_{OUT})^2}{2C_{OUT} \cdot V_{OUT}} \cdot \frac{V_{IN}}{V_{IN} - V_{OUT}} \approx 81mV to 300mV^8 \tag{6.9}$$

where $I_{PEAK} \approx 1.7A$[9] is the peak inductor current. From these equations, we obtain a ripple voltage of about 150mV at a medium load. This is acceptable per se. However, it will be necessary to check the actual ripple experimentally. If then the ripple should be unacceptably great, the capacitor values have to be adapted. For fine filtering, two additional small ceramic capacitors in parallel are being employed, one at $0.1\mu F$ and a second one at $10,000pF$ (see the complete design drawing in Appendix C.1.

The Input Capacitor To filter peak currents from the power source, we use a customary $10\mu F$ capacitor. A Tantalum capacitor would be very risky at this point, because of the high inrush currents. This is particulary true, as the immediate power source here is the (low-impedance) battery.

Design Procedure - MAX1836(3.3V)

Current Limit For the MAX1836EUT33-T, the current limit is preset to 125mA.

Thermal-Overload Protection The MAX1836 has a built-in thermal overload protection, shutting the transistor down if the junction temperature exceeds $T_J = +160degC$ to allow the device to cool down.

Output Voltage By tying FB to GND, we choose the preset voltage of $V_{OUT} = 3.3V$.

Inductor Selection The inductor selection follows the same principle as described for the MAX1776. The minimum inductance is

$$L_{MIN} = \frac{(V_{IN,MAX} - V_{OUT}) \cdot t_{ON,MIN}}{I_{LIM}} = 48\mu H, \tag{6.10}$$

where $V_{IN,nominal} = 9.3V$. Therefore, we choose a $47\mu H$ inductor of the Sumida CDRH6D26 series.

Output Capacitor The selection of the output capacitor has been discussed at length in the previous section. We selected a $22\mu F$ capacitor in parallel with a $0.1\mu F$ capacitor.

[7] Typical for Tantalum: $ESR = 0.3to3.5\Omega$, for Polymer (OS-CON) $ESR = 0.04to0.07\Omega$ [18]
[9] For Sumida CDRH6D28 at $22\mu H$

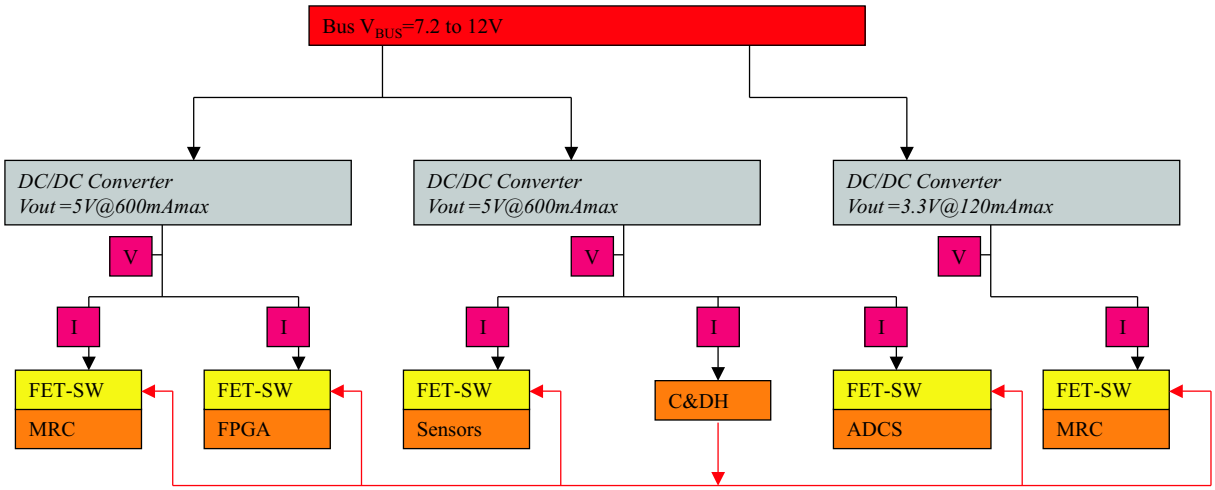

Figure 6.9: The EPS Switching Tasks

Input Capacitor As for the MX1776, we choose a $22\mu F$ capacitor for filtering the input current.

Diode Selection As for the MAX1771 converter, we choose the same low forward voltage diode, a N5817 Schottky Barrier Rectifier.

6.2.2 The Current Sensors

For the current sensors, we will be using the MAX4172 parts, which were discussed in detail in Section 6.1.1. R_{SENSE} and R_{OUT} have been set to $100m\Omega$ and $20K\Omega$ respectively for all current sensors of this unit. The output current is calculated from the voltage V_{OUT} by

$$I = \frac{V_{OUT}}{R_{OUT} \cdot R_{SENSE} \cdot G_m}, \tag{6.11}$$

with a transductance of $G_m = 10mA/V$.

6.2.3 The Switches

As mentioned earlier, in order to switch currents on the order of the RabbitSat loads, all switching may be performed simply using p-channel MOSFETs. We choose the IRF4905 MOSFET. With a static drain-to-source on-resistance of only $R_{DS(ON)} = 0.02\Omega$, a drain-to-source breakdown voltage of $V_{(BR)DSS} = -55V$, and a continuous drain current of $I_D = -74A$, the IRF4905 shows excellent performance for our needs. As a good compromise between heat dissipation and size, it was decided to use the D^{2}PAK package. Figure 6.10 shows the MOSFETs in the RabbitSat application. The left circuit uses the digital output voltage of the C&DH with a 10K series resistor for protection purposes. As the C&DH digital output uses 0V/5V switching levels, this layout is possible for all RabbitSat switches, switching 5V loads[10]. The exception here is the circuit on the right hand side of

[10] The gate voltage and the drain voltage must not differ considerably.

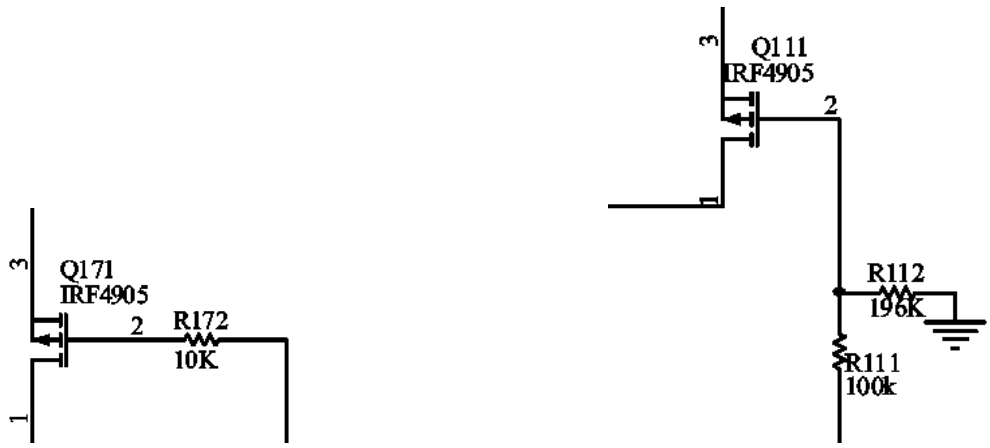

(a) The IRF4905 with Undivided Gate Voltage (b) IRF4905 with Voltage Divider at the Gate

Figure 6.10: IRF4905 - Application as Switches for RabbitSat

Figure 6.10. As here the 5V level data line has to switch 3.3V, we drop the gate voltage to 3.3V using a voltage divider, as shown in the Figure.

6.2.4 The Delay Circuit

Delay Functionality

The Cubesat requirements prescribe a several minutes delay before turning on any loads after deployment on orbit. As described in Section 5.3.3 and illustrated in Figure 5.4 the delay circuit will be activated upon deployment in orbit through mechanical switches[11]. As shown in Figure 5.4, the delay circuit will be electrically located between the loads and the batteries with solar panels. The following section describes the technical implementation od the delay.

Description

As commonly used for simple delay purposes, we employ a RC[12] time delay. Our circuit design is shown in Figure 6.11, where the left hand side includes the connection to the power source (batteries and solar panels), and the right hand side the connection to the common power bus and therefore the loads. Now, upon activation of the mechanical deployment switches, the "power source" side will see a voltage (the solar panel voltage = the bus voltage) of $V_{source} \approx 9.6V$. This is the time point "0" for the delay circuit. Now, capacitor C85 starts charging. Looking at the output of the delay circuit PSpice[13] simulation in Figure 6.12, you may watch C85 charging, represented by the voltage Vc (green line). By the time that Vc reaches a certain level, it triggers the gate of the n-channel MOSFET Q83 (pin 2). This, in turn causes current to flow from the Q83

[11]The switches will be selected by the structure team, according to what suits the structure best.
[12]RC stands for Resistance times Capacitance
[13]PSpice is a powerful circuit simulation package

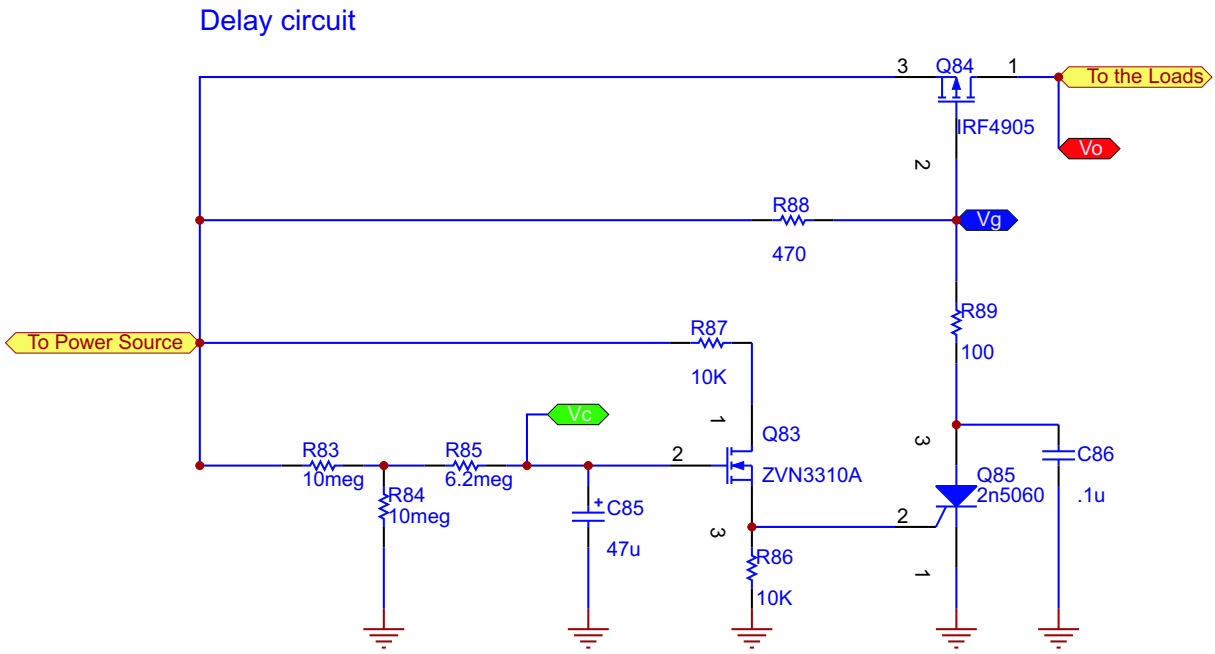

Figure 6.11: The EPS Delay Circuit

source(pin 3) to drain(pin 1) and the voltage at the SCR[14] gate slowly (Q 85, pin 2) starts ramping up. After about 200s, the SCR gate voltage will reach the SCR threshold voltage, and the SCR will be conducting current from Cathode (pin 1) to anode (pin 3). This current flow causes the gate of the p-channel MOSFET Q84 to go low (see the blue line in Figure 6.12), meaning, Q84 will be conducting and the loads will be electrically connected to the power source. Watch the load voltage coming up in Figure 6.12 (red line).

The beauty of this circuit is that it is extremely reliable. In the event of a latch-up through radiation, implying the failure of any semiconductor device of this circuit, the circuit will still provide power to the loads (semiconductors fail through shorting). At the same time, the probability of a latch-up occurring during launch or deployment is very low. This prevents an early activation of the loads.

The delay time is variable and may be arisen by increasing the value of C85. We set it to 320 seconds, as viewable in the PSpice graph in Figure 6.12.

[14]SCR means Silicon Controlled Rectifier

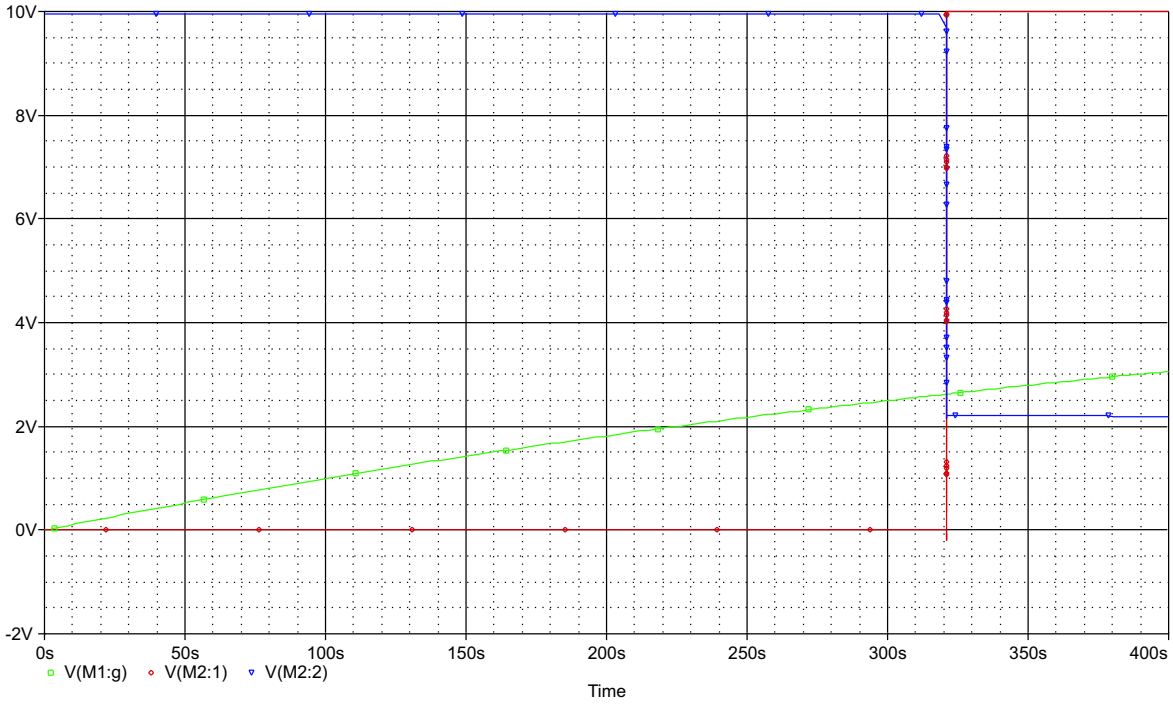

Figure 6.12: The EPS Delay Circuit

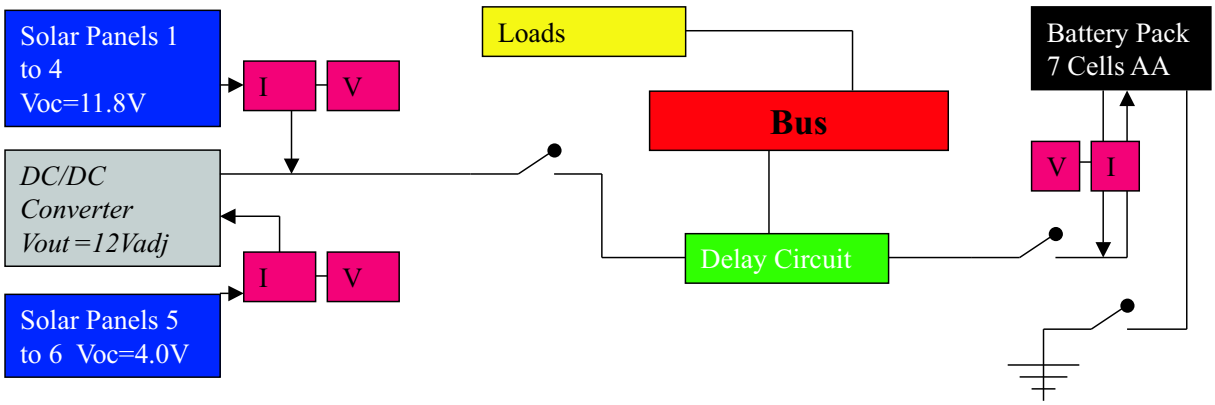

Figure 6.13: Functionality of the EPS Circuit Test Board

6.3 The EPS Test Board Design

The previous section described all sub-circuit designs in detail. Hardware-wise, we implemented this in two steps; Before building the *final EPS flight board*, we had to verify the functionality of the design concept using a *test board*, particularly with solar panels connected.

As for the test board, which is shown in Figures 6.15 and 6.14, we implemented the following:

1. The circuitry required to run two solar panels, this is, one large panel (consisting of two sub-panels) and one small panel respectively

2. The delay circuit as described in the previous section

3. Three current sensors, two MAX4271 parts for each of the solar panels and one (bidirectional) MAX471 sensor for the battery pack

4. Three mechanical deployment switches (Switching scheme as in Figure 6.9)

5. Connectors for the solar panels, the battery pack, the loads, and the sensor outputs

The test board functionality is illustrated in Figure 6.13. We used the board for all required electronic testing. As important result, we measured the efficiency of the MAX1771 DC/DC converter circuit to be between 75% and 81%[15].

We were able to increase the MAX1771 performance at low supply currents, while replacing the former sense resistor value of $100m\Omega$ to $180m\Omega$. We will be using the latter value for the final PCB.

[15] 75% was measured at 10mA, 81% at 200mA current output respectively.

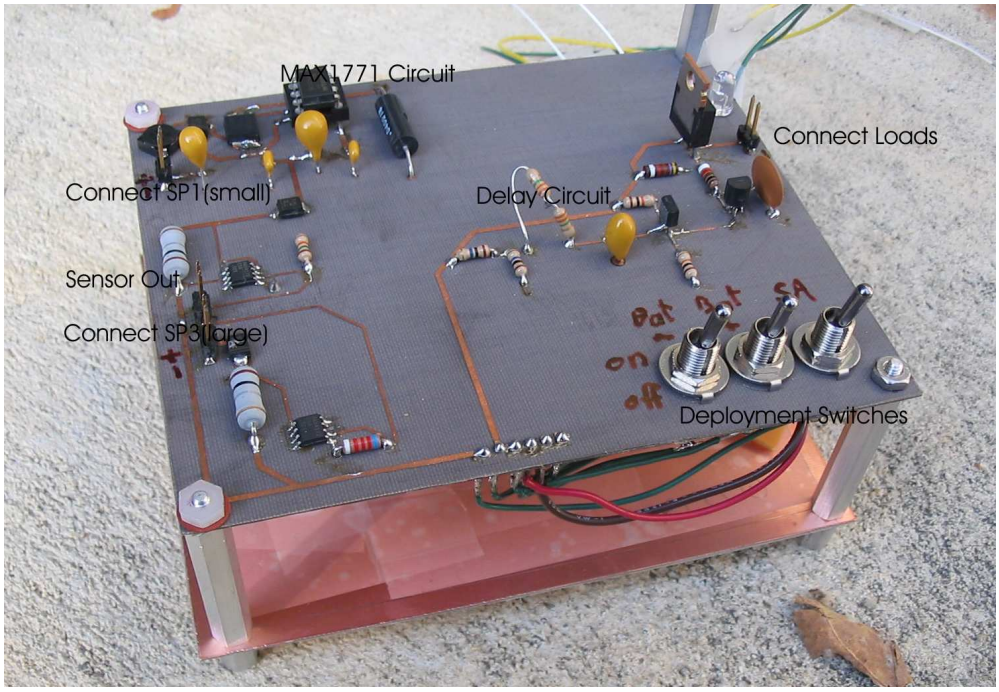

Figure 6.14: The EPS Circuit Test Board with Components

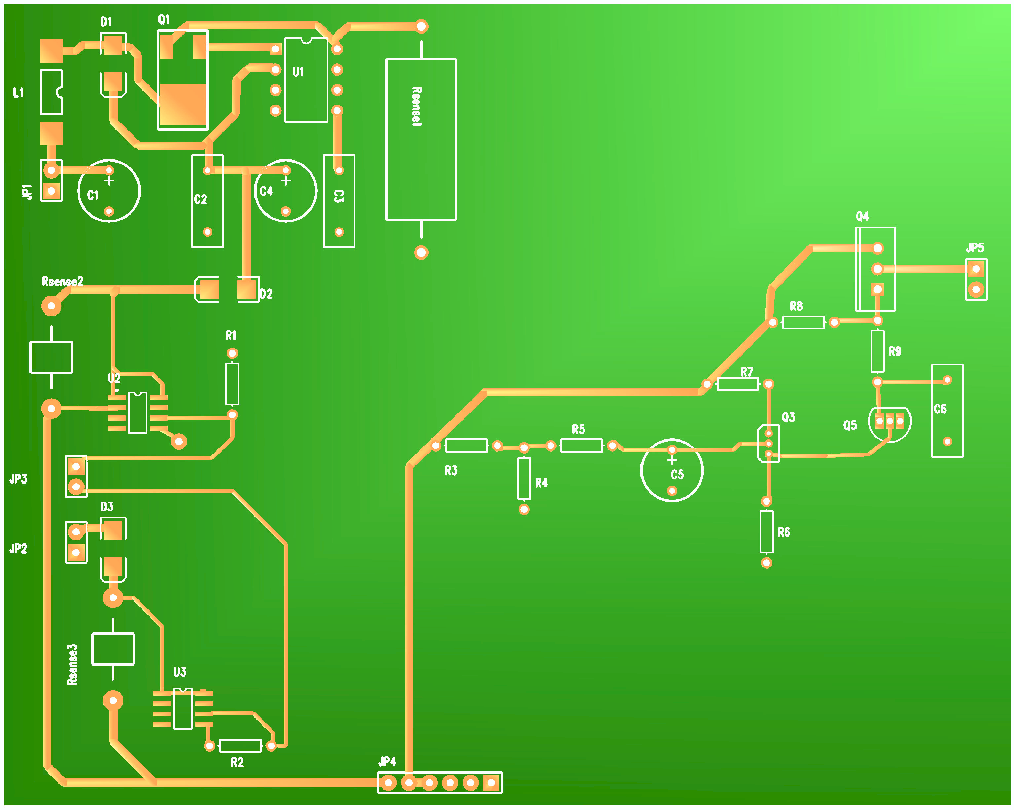

Figure 6.15: The EPS Circuit Test Board

6.4 The EPS Flight Board Design

The design of the final PC-board incorporates all practical experience from designing and experimenting with the previously discussed test board. These experiences particularly include the best layout of the traces and optimum placement of components around high-frequency devices, such as the DC/DC converters.

At the time of printing this document, the board is being built by PCBExpress of Portland, OR. The components have been ordered and are waiting to be mounted by Lockheed Martin of Sunnyvale, CA.

The final testing will be performed by my team members Mr. Scott Gorin and Mr. Mike Ingalls.

The complete set of schematics, as well as a copy of the PCB layout is included in Appendix C.1, whereas the complete set of project files is part of Appendix CD. Figure 6.16 shows the final board itself. The board has five (female) connector harnesses. All pins of these connectors are described in detail in Figure 6.17.

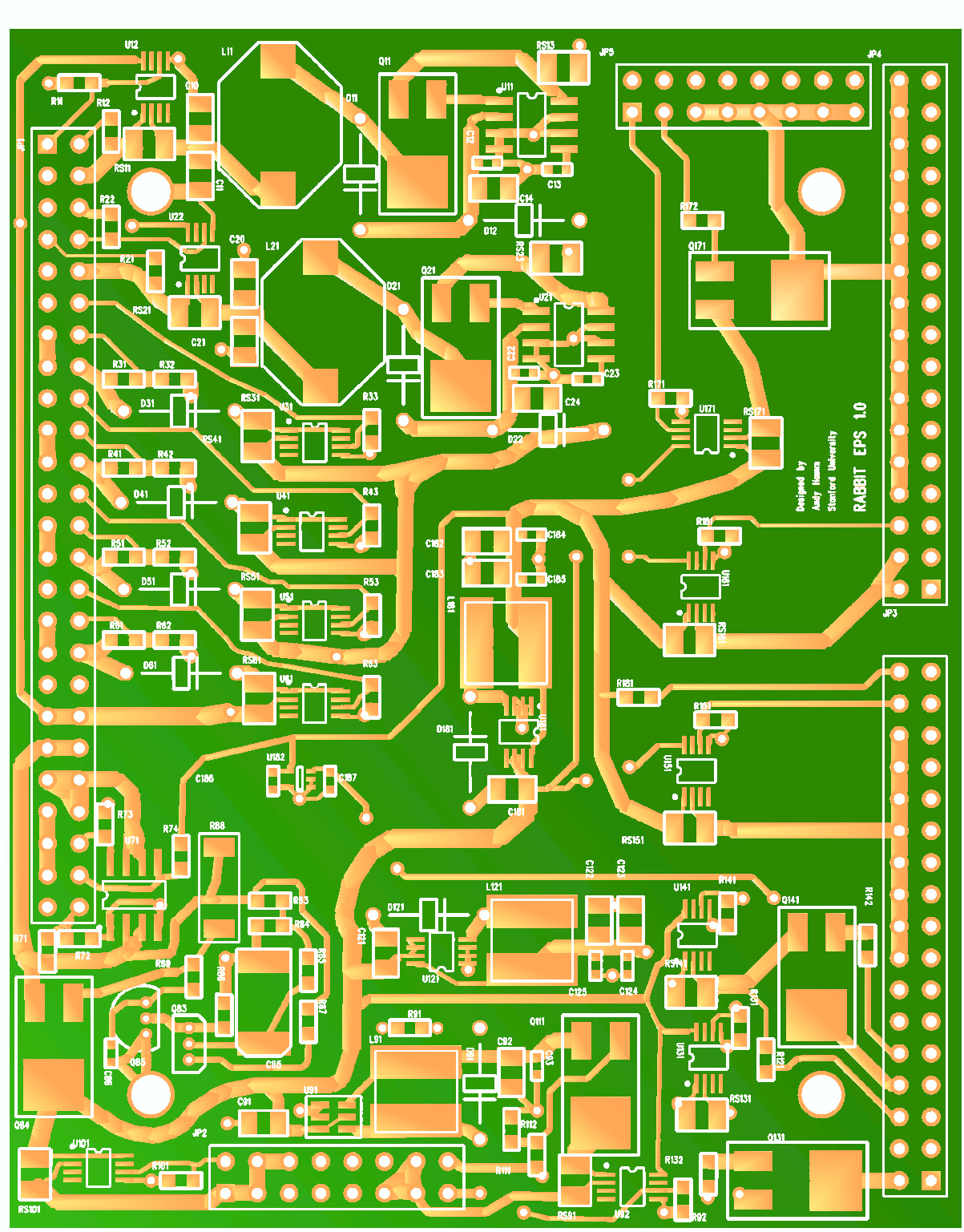

Figure 6.16: The EPS Flight Board

RABBIT EPS 1.0 - Connector JP 1							
#	Name	Description	Scale factor	#	Name	Description	Scale factor
1	Iout	Output of current sensor of SP 1	100*Vout[V] >> I[mA]	2	Vout	Voltage of SP1	1
3	GND	N/A	N/A	4	Pin	Power in from SP1	N/A
5	GND	N/A	N/A	6	GND	N/A	N/A
7	Vout	Voltage of SP2	1	8	Iout	Output of current sensor of SP 2	100*Vout[V] >> I[mA]
9	GND	N/A	N/A	10	Pin	Power in from SP2	N/A
11	GND	Connect to (-) side of SP3/a	N/A	12	Iout	Output of current sensor of SP 3	100*Vout[V] >> I[mA]
13	Pin	Connect to (+) side of SP3/a	N/A	14	Vout	Voltage of SP3	2.5*Vout>>Vsp3
15	Pout	Connect to (-) side of SP3/b	N/A	16	Pin	Connect to (+) side of SP3/b	N/A
17	GND	Connect to (-) side of SP4/a	N/A	18	Iout	Output of current sensor of SP4	100*Vout[V] >> I[mA]
19	Pin	Connect to (+) side of SP4/a	N/A	20	Vout	Voltage of SP4	2.5*Vout>>Vsp4
21	Pout	Connect to (-) side of SP4/b	N/A	22	Pin	Connect to (+) side of SP4/b	N/A
23	GND	N/A	N/A	24	GND	N/A	N/A
25	GND	Connect to (-) side of SP5/a	N/A	26	Iout	Output of current sensor of SP5	100*Vout[V] >> I[mA]

Figure 6.17: Connector Pin Allocation

RABBIT EPS 1.0 - Connector JP 1 *continued*							
#	Name	Description	Scale factor	#	Name	Description	Scale factor
27	Pin	Connect to (+) side of SP5/a	N/A	28	Vout	Voltage of SP5	2.5*Vout>>Vsp5
29	Pout	Connect to (-) side of SP5/b	N/A	30	Pin	Connect to (+) side of SP5/b	N/A
31	GND	Connect to (-) side of SP6/a	N/A	32	Iout	Output of current sensor of SP6	100*Vout[V] >> I[mA]
33	Pin	Connect to (+) side of SP6/a	N/A	34	Vout	Voltage of SP6	2.5*Vout>>Vsp6
35	Pout	Connect to (-) side of SP6/b	N/A	36	Pin	Connect to (+) side of SP6/b	N/A
37	Psw+	Connect to (+) side of switch 1a	N/A	38	Psw+	Connect to (+) side of switch 1b	N/A
39	Psw-	Connect to (-) side of switch 2a	N/A	40	Psw-	Connect to (-) side of switch 2b	N/A
41	Pbat+	Connect to (+) side of the battery (after switch 2a)	N/A	42	Pbat+	Connect to (+) side of the battery (after switch 2b)	N/A
43	Pext-	Connect to (-) side of external battery charger	N/A	44	Pext+	Connect to (+) side of external battery charger	N/A
45	Pbat-	Connect to (-) side of the battery (after switch 3a)	N/A	46	Iout	Output of battery current sensor (works in both directions)	303*Vout[V] >> I[mA]
47	Pbat-	Connect to (-) side of the battery (after switch 3b)	N/A	48	SIGNout	Logical output {5V - 0V} of the battery current direction/ Charge>>high, Discharge>>low (or the other way around)	N/A
49	GND	N/A	N/A	50	Vout	Output of battery Voltage	2.5*Vout>>Vbattery

Figure 6.18: Connector Pin Allocation

RABBIT EPS 1.0 - Connector JP 2							
#	Name	Description	Scale factor	#	Name	Description	Scale factor
1	Pout	Connect to XMTR	N/A	2	Iout	Output of XMTR current sensor	333*Vout[V] >> I[mA]
3	Pout	Connect any device running on bus voltage	N/A	4	Pout	Connect any device running on bus voltage	N/A
5	GND	N/A	N/A	6	Pout	Connect any device running on bus voltage	N/A
7	GND	N/A	N/A	8	GND	Connect to XMTR ground	N/A
9	GND	N/A	N/A	10	GND	N/A	N/A
11	Pout	Connect to MRC 3.3V		12	Vout	Voltage after 3.3V converter	1
13	Pout	Connect any device running on 3.3V {switched w/ MRC}	N/A	14	Pout	Connect any device running on 3.3V {switched w/ MRC}	N/A
15	Iout	Output of MRC 3.3V current sensor	50*Vout[V] >> I[mA]	16	SWin	Connect to Dig output of the C&DH, switches MRC 3.3V and 5V at the same time. High>>Off, Low>>On, Switching level: 5V/0V	N/A

Figure 6.19: Connector Pin Allocation

RABBIT EPS 1.0 - Connector JP 3							
#	Name	Description	Scale factor	#	Name	Description	Scale factor
1	GND	N/A	N/A	2	Pout	Connect to MRC 5V	N/A
3	GND	N/A	N/A	4	Iout	Output of MRC 5V current sensor	50*Vout[V] >> I[mA]
5	GND	N/A	N/A	6	Vout	Voltage of MRC/FPGA 5V	1
7	GND	N/A	N/A	8	Pout	Connect to FPGA (5V)	N/A
9	GND	N/A	N/A	10	SWin	Connect to Dig output of the C&DH, switches FPGA. High>>Off, Low>>On, Switching level: 5V/0V	N/A
11	GND	N/A	N/A	12	Iout	Output of FPGA current sensor	50*Vout[V] >> I[mA]
13	GND	N/A	N/A	14	Tout	Outputs the EPS board temperature	T[deg C]=(Vout-0.4V)/0.01953V
15	GND	N/A	N/A	16	Pout	Sensors 5V (continuously on)	N/A
17	GND	N/A	N/A	18	Pout	Sensors 5V (continuously on)	N/A
19	GND	N/A	N/A	20	Pout	Sensors 5V (continuously on)	N/A
21	GND	N/A	N/A	22	Pout	Sensors 5V (continuously on)	N/A
23	GND	N/A	N/A	24	Pout	Sensors 5V (continuously on)	N/A
25	GND	N/A	N/A	26	Pout	Sensors 5V (continuously on)	N/A
27	GND	N/A	N/A	28	Pout	Sensors 5V (continuously on)	N/A
29	GND	N/A	N/A	30	Pout	Sensors 5V (continuously on)	N/A
31	GND	N/A	N/A	32	Iout	Output of current sensor for the continuous 5V sensors	50*Vout[V] >> I[mA]
33	GND	N/A	N/A	34	Vout	Voltage of Sensors/C&DH/ADCS/Modem (5V)	1

Figure 6.20: Connector Pin Allocation

RABBIT EPS 1.0 - Connector JP 4							
#	Name	Description	Scale factor	#	Name	Description	Scale factor
1	GND	N/A	N/A	2	Pout	Connect to C&DH (5V)	N/A
3	GND	N/A	N/A	4	Pout	Connect to Modem (5V)	N/A
5	GND	N/A	N/A	6	Iout	Output of C&DH/Modem current sensor	50*Vout[V] >> I[mA]
7	GND	N/A	N/A	8	Pout	Sensors 5V (switched with ADCS)	N/A
9	GND	N/A	N/A	10	Pout	Sensors 5V (switched with ADCS)	N/A
11	GND	N/A	N/A	12	Pout	Sensors 5V (switched with ADCS)	N/A
13	GND	N/A	N/A	14	Pout	Sensors 5V (switched with ADCS)	N/A
15	GND	N/A	N/A	16	Pout	Sensors 5V (switched with ADCS)	N/A
17	GND	N/A	N/A	18	Pout	Sensors 5V (switched with ADCS)	N/A
19	GND	N/A	N/A	20	Pout	Sensors 5V (switched with ADCS)	N/A
21	GND	N/A	N/A	22	Pout	Sensors 5V (switched with ADCS)	N/A
23	GND	N/A	N/A	24	Pout	Sensors 5V (switched with ADCS)	N/A
25	GND	N/A	N/A	26	Pout	Sensors 5V (switched with ADCS)	N/A
27	GND	N/A	N/A	28	Pout	Sensors 5V (switched with ADCS)	N/A
29	GND	N/A	N/A	30	Pout	Sensors 5V (switched with ADCS)	N/A
31	GND	N/A	N/A	32	Pout	Sensors 5V (switched with ADCS)	N/A
33	GND	N/A	N/A	34	Pout	Sensors 5V (switched with ADCS)	N/A

Figure 6.21: Connector Pin Allocation

RABBIT EPS 1.0 - Connector JP 5							
#	Name	Description	Scale factor	#	Name	Description	Scale factor
1	Iout	Output of C&DH/Modem current sensor	50*Vout[V] >> I[mA]	2	GND	N/A	N/A
3	SWin	Connect to Dig. output of the C&DH, switches ADCS and Sensors High>>Off, Low>>On, Switching level: 5V/0V	N/A	4	GND	N/A	N/A
5	Pout	Connect to ADCS (5V)	N/A	6	GND	N/A	N/A
7	Pout	Sensors 5V (switched with ADCS)	N/A	8	GND	N/A	N/A
9	Pout	Sensors 5V (switched with ADCS)	N/A	10	GND	N/A	N/A
11	Pout	Sensors 5V (switched with ADCS)	N/A	12	GND	N/A	N/A
13	Pout	Sensors 5V (switched with ADCS)	N/A	14	GND	N/A	N/A
15	Pout	Sensors 5V (switched with ADCS)	N/A	16	GND	N/A	N/A

Figure 6.22: Connector Pin Allocation

Chapter 7

Summary and Conclusions

...This chapter is still under development
and will be completed very soon...

Bibliography

[1] Doerksen, K., Lvesque, J., Mas, I., *"Design, Modeling and Evaluation of a 2.4GHz FHSS Communications System for NarcisSat"*. Proceedings of the Small Satellite Conference, Logan, Utah, August 2003, p.1.

[2] Tapio, E., *"QuakeSat Online Documentation"*. <http://ssdl-delta.stanford.edu/LM-CubeSat/Team4> November 2003

[3] *"AAU-Cubesat Online Documentation"*. <http://www.cubesat.auc.dk> November 2003

[4] *"Design of Hardware and Software for the Powersupply for AAU Cubesat"*. <http://www.cubesat.auc.dk/documents/psu> November 2003

[5] Bhanderi, D., *"Mission Objectives"*. <http://ssdl-delta.stanford.edu/rabbit> October 2003.

[6] Gorin, S., *"RabbitSat Systems Requirements Document"*. RabbitSat Documentation, Document No RBT-1000, May 2003.

[7] Twiggs, B., Puig-Suari, J. *"Cubesat Design Specifications Document"*. Revision VIII <http://cubesat.calpoly.edu/documents> October 2003.

[8] Enoch, M., *"Agile Cubesat Mission - Technical Requirements Document"*. Advanced Technology Center, Space and Strategic Missile Operations, Lockheed Martin Space Systems Company, 2003.

[9] Enoch, M., *"Agile Cubesat Mission - Mission Requirements Document"*. Advanced Technology Center, Space and Strategic Missile Operations, Lockheed Martin Space Systems Company, 2003.

[10] Kahn, L., Bhanderi, D., Gorin, S., et alii, *"RabbitSat Subsystems Design Review"*. RabbitSat Reviews, September 2003.

[11] Wertz, J., R. ,Larson, W., J., *"Space Mission Analysis and Design III"*. Microcosm Press, 3rd edition, 1999

[12] Aldous, Scott *"How Solar Cells Work"*. <http://science.howstuffworks.com/solar-cell1.htm> October 2003.

[13] P. R. Sharps, M. A. Stan, D. J. Aiken, B. Clevenger, J. S. Hills, and N. S. Fatemi *"Multi-Junction Cells with Monolithic Bypass Diodes"*. <http://www.emcore.com/solutions/Photovoltaics> October 2003.

[14] Product Specifications *"InGaP/GaAs/Ge Triple-Junction Solar Cells"*. <http://www.emcore.com/solutions/Photovoltaics> October 2003.

[15] Product Specifications *"Improved Triple Junction Solar Cells"*. <http://www.spectrolab.com> October 2003.

[16] Panasonic Industial NiCd Batteries Product Specifications *"NiCd Batteries"*. <http://www.panasonic.com/industrial/battery/oem> November 2003.

[17] Maxim-IC Product Specifications *"DC/DC Converter Specification"*. <http://www.maxim-ic.com> November 2003.

[18] Adams, D., *"Introduction to Capacitors"*. <http://my.execpc.com/ endlr/ESR/> November 2003.

Appendix A

The Solar Panels

A.1 Mechanical Drawings

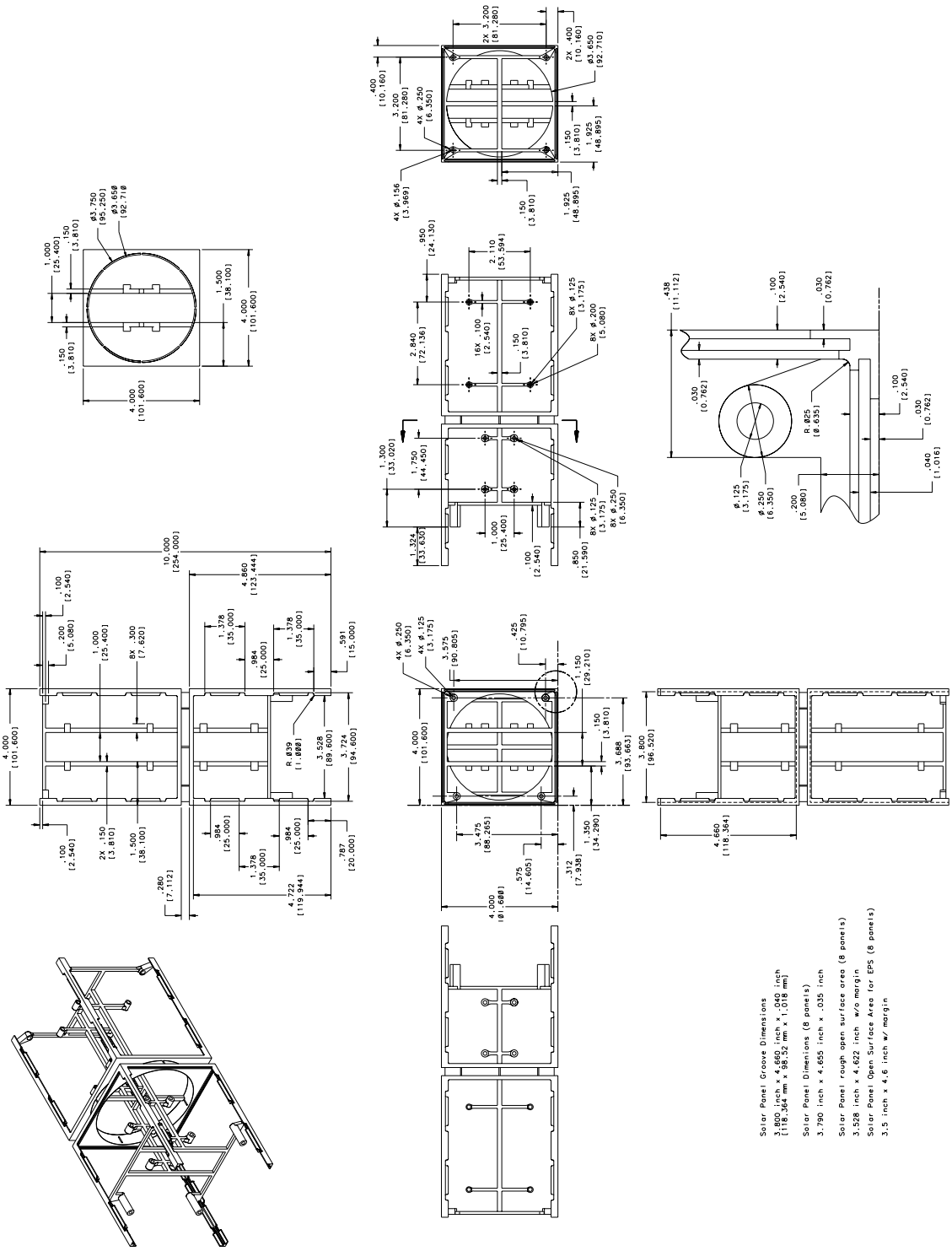
Solar Panel Groove Dimensions
3.800 inch x .040 inch x .040 inch
[96.520 mm x 1.016 mm x 1.016 mm]
Solar Panel Dimenions (8 panels)
3.790 inch x 4.655 inch x .035 inch
Solar Panel rough open surface area (8 panels)
3.528 inch x 4.622 inch w/o margin
Solar Panel Open Surface Area for EPS (8 panels)
3.5 inch x 4.6 inch w/ margin

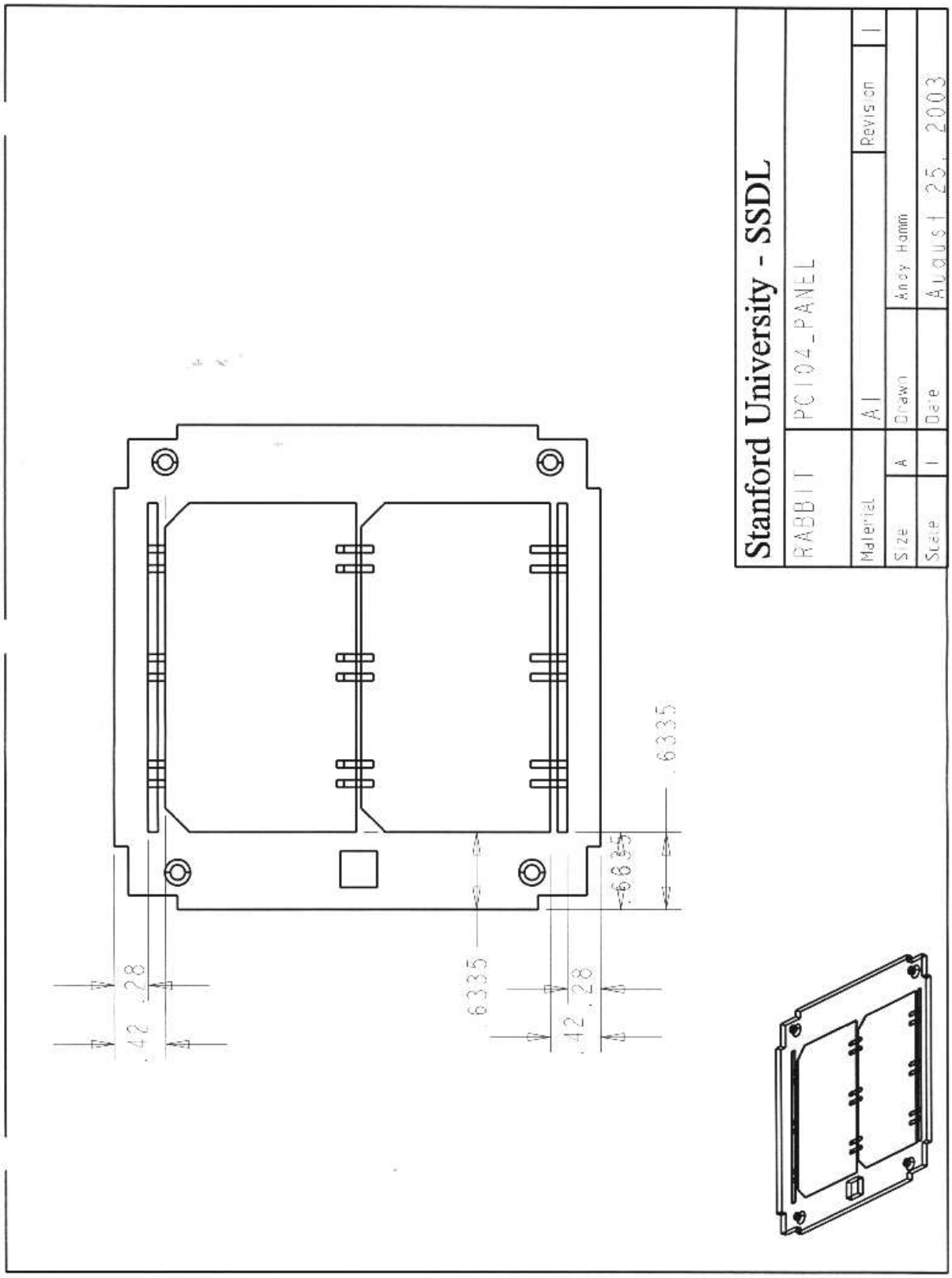
Stanford University - SSDL
RABBIT
PC104_PANEL
Material
Al
Revision
1
Size
A
Drawn
Andy Hamm
Scale
1
Date
August 25, 2003
.42
.28
.6335
.6335
.6335
.42
.28

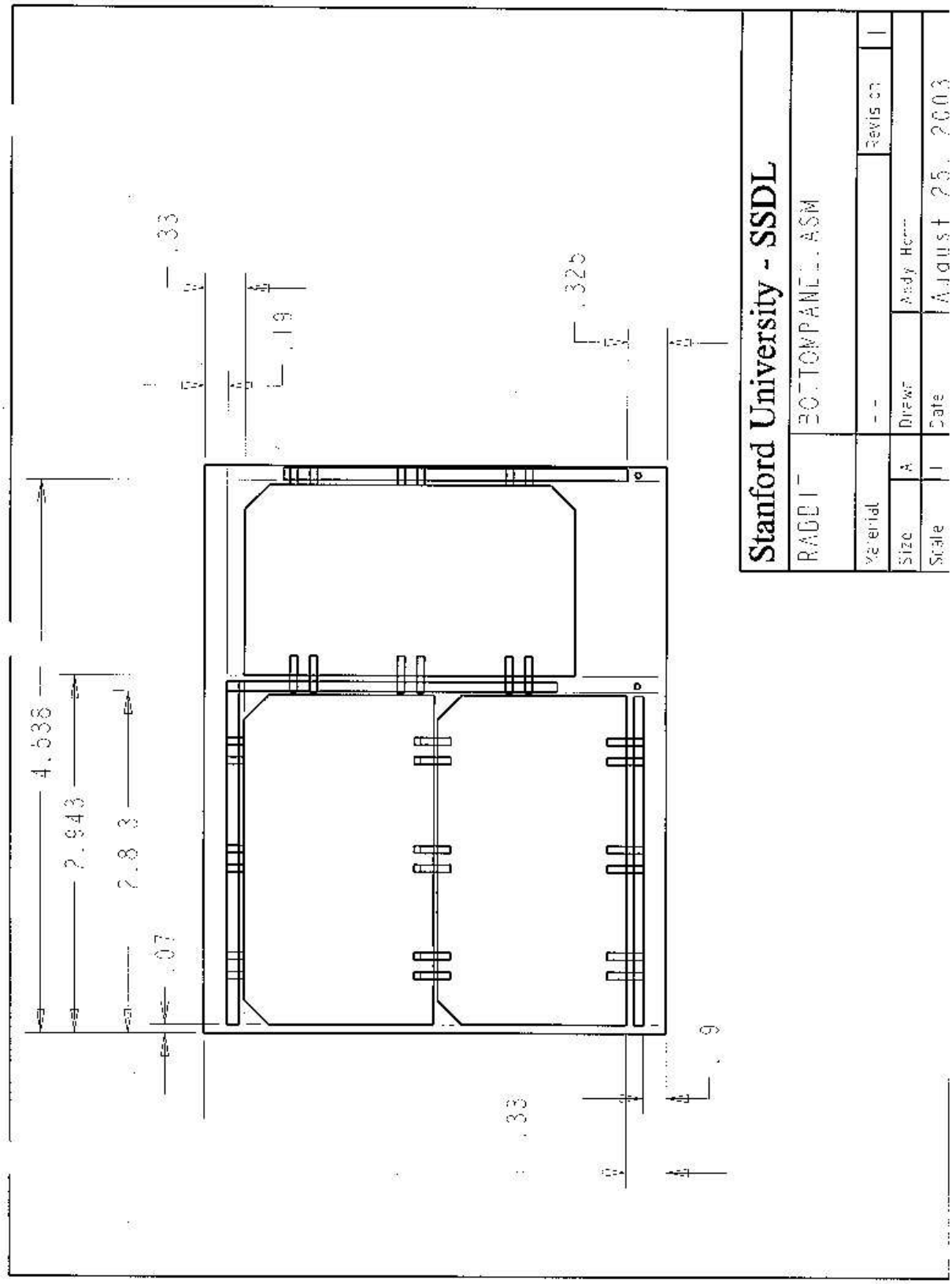
Stanford University - SSDL
RADDI
BOTTOMPANEL.ASM
Material
--
Revision
1
Size
A
Drawn
Andy Hem
Scale
1
Date
August 25, 2003
.33
.19
.325
4.938
2.943
2.83
.07
.33
.9

Appendix B

The EPS Test Board

B.1 Schematics

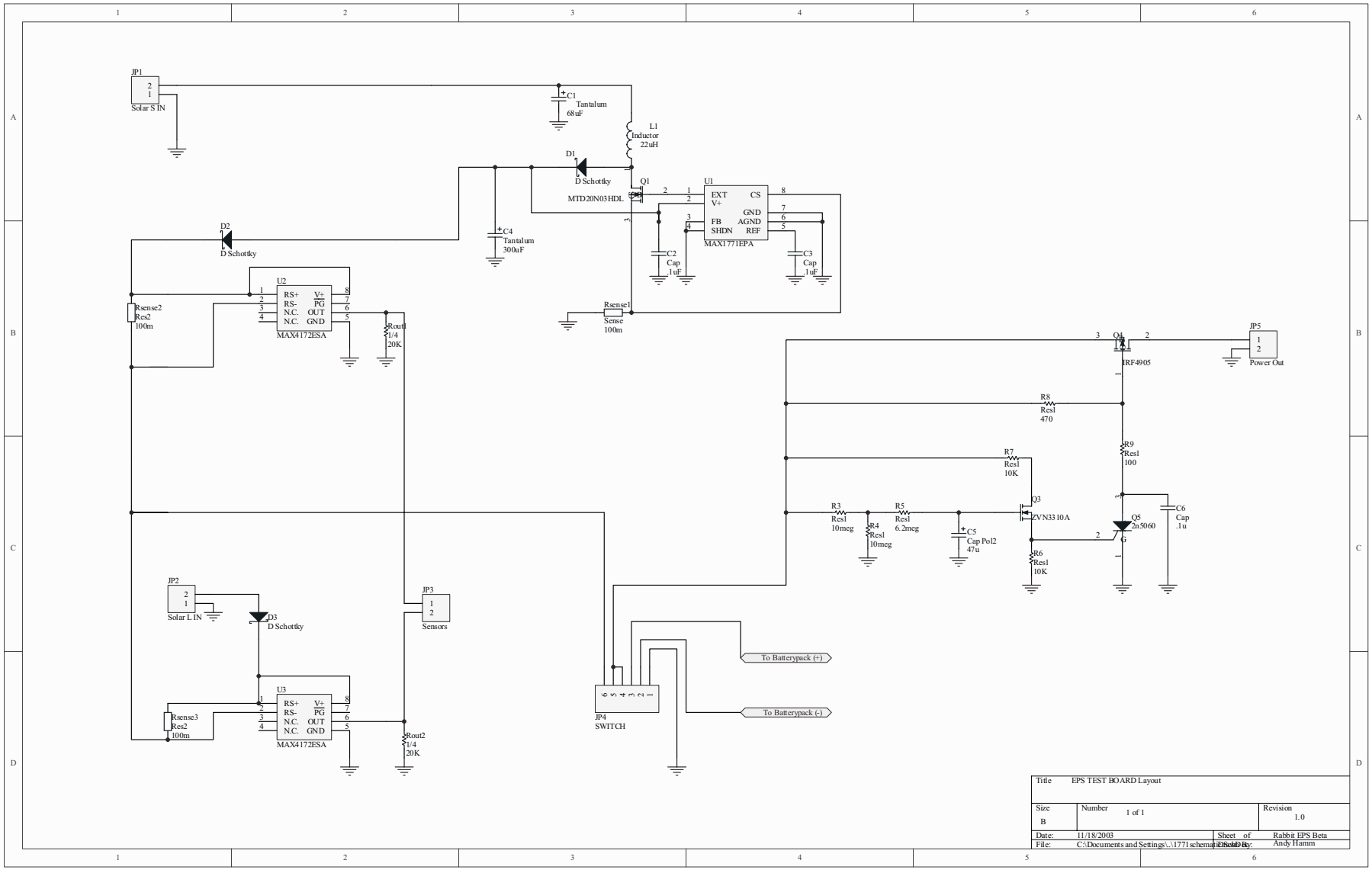
JP1
Solar S IN
C1
Tantalum
68uF
L1
Inductor
22uH
D1
D Schottky
Q1
MTD20N03HDL
U1
EXT
V+
FB
SHDN
CS
GND
AGND
REF
MAX1771EPA
C2
Cap
.1uF
C3
Cap
.1uF
C4
Tantalum
300uF
D2
D Schottky
U2
RS+
RS-
N.C.
N.C.
V+
PG
OUT
GND
MAX4172ESA
Rsense2
Res2
100m
Rout1
1/4
20K
Rsense1
Sense
100m
Q4
IRF4905
JP5
Power Out
R8
Resl
470
R9
Resl
100
R7
Resl
10K
Q3
ZVN3310A
R3
Resl
10meg
R5
Resl
6.2meg
R4
Resl
10meg
C5
Cap Pol2
47u
R6
Resl
10K
Q5
2n5060
C6
Cap
.1u
JP2
Solar L IN
D3
D Schottky
JP3
Sensors
U3
MAX4172ESA
Rsense3
Res2
100m
Rout2
1/4
20K
JP4
SWITCH
To Batterypack (+)
To Batterypack (-)
Title EPS TEST BOARD Layout
Size B
Number 1 of 1
Revision 1.0
Date: 11/18/2003
Sheet of
Rabbit EPS Beta
File: C:\Documents and Settings\..\1771schematic.SchDoc
Drawn By: Andy Hamm

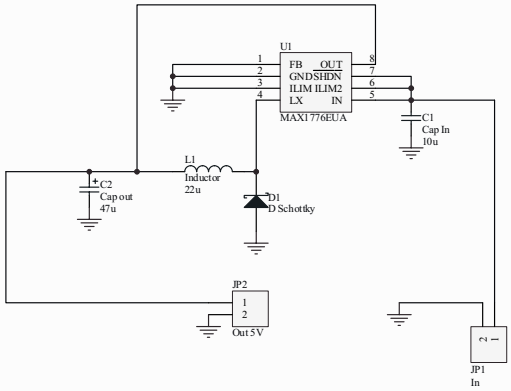

Title 5V DC/DC Converter

Size	Number	Revision
B	1 of 1	1.0

Date:	11/18/2003	Sheet of	Rabbit EPS 1.0
File:	C:\Documents and Settings\..\1776.SchDoc	Drawn By:	Andy Hamm

B.2 Printed Circuit Board

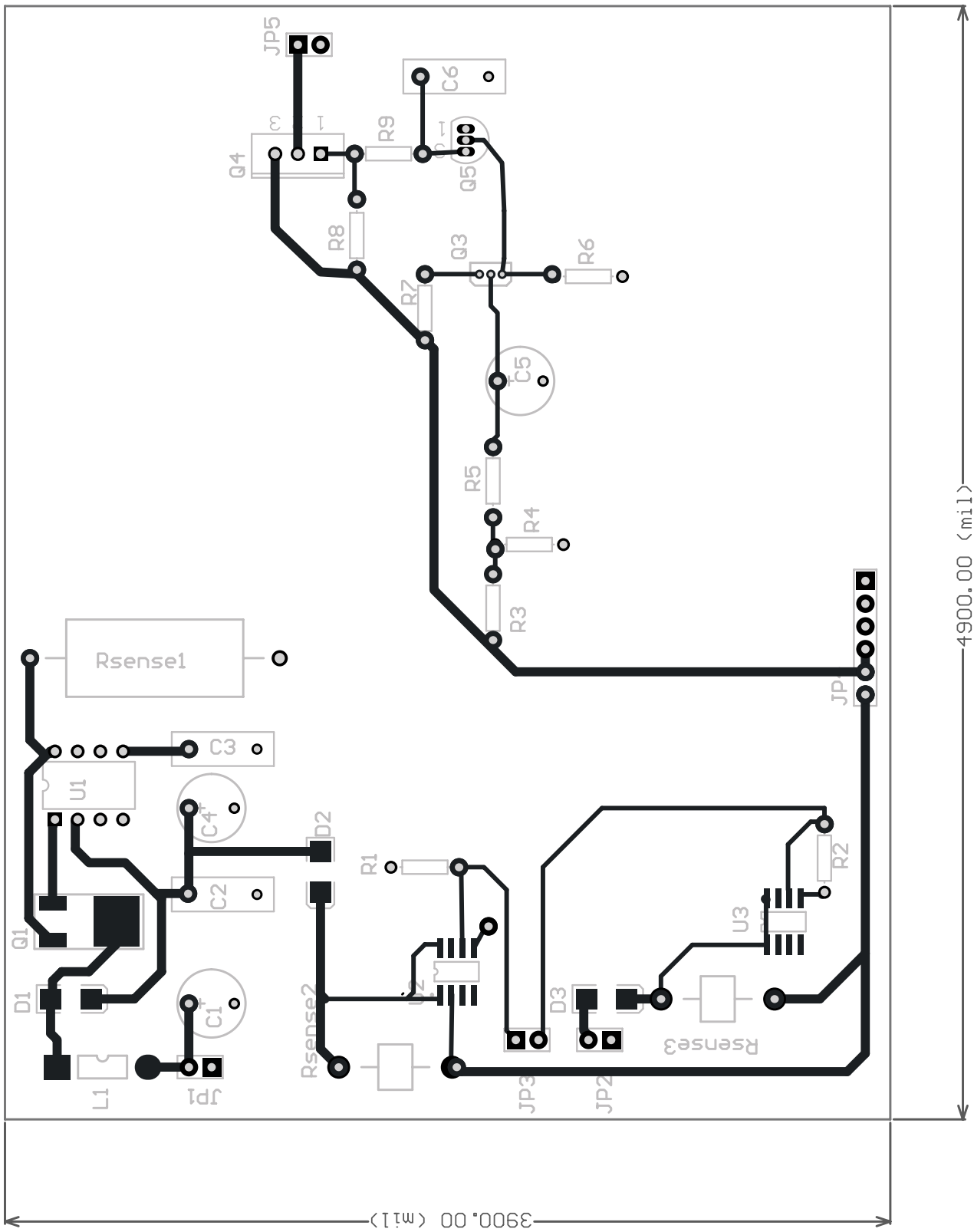
JP5
C6
R9
Q4
Q5
R8
Q3
R6
R7
C5
R5
R4
R3
JP4
Rsense1
C3
U1
C4
D2
R1
R2
C2
Q1
U3
D1
C1
U2
D3
Rsense3
Rsense2
L1
JP1
JP3
JP2
4900.00 (mil)
3900.00 (mil)

Appendix C

The EPS Flight Board

C.1 Schematics

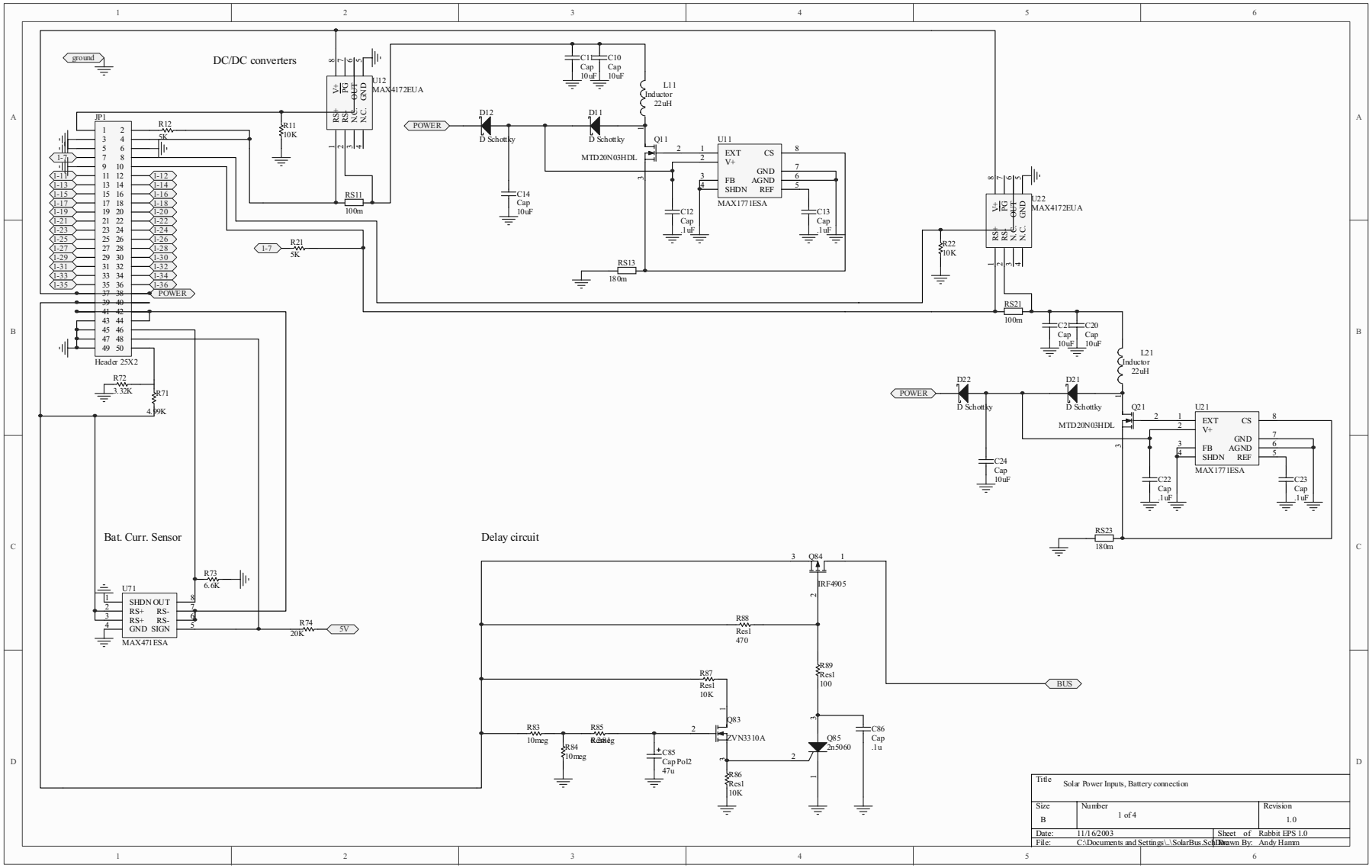
DC/DC converters
ground
U12
MAX4172EUA
JP1
Header 25X2
POWER
D12
D Schottky
D11
D Schottky
L11
Inductor
22uH
Q11
MTD20N03HDL
U11
MAX1771ESA
U22
MAX4172EUA
L21
Inductor
22uH
D22
D21
Q21
MTD20N03HDL
U21
MAX1771ESA
Bat. Curr. Sensor
U71
MAX471ESA
5V
Delay circuit
Q84
IRF4905
Q83
VN3310A
Q85
2n5060
BUS
Title
Solar Power Inputs, Battery connection
Size
B
Number
1 of 4
Revision
1.0
Date: 11/16/2003
Sheet of
Rabbit EPS 1.0
File: C:\Documents and Settings\..\SolarBus.Sch
Drawn By: Andy Hamm

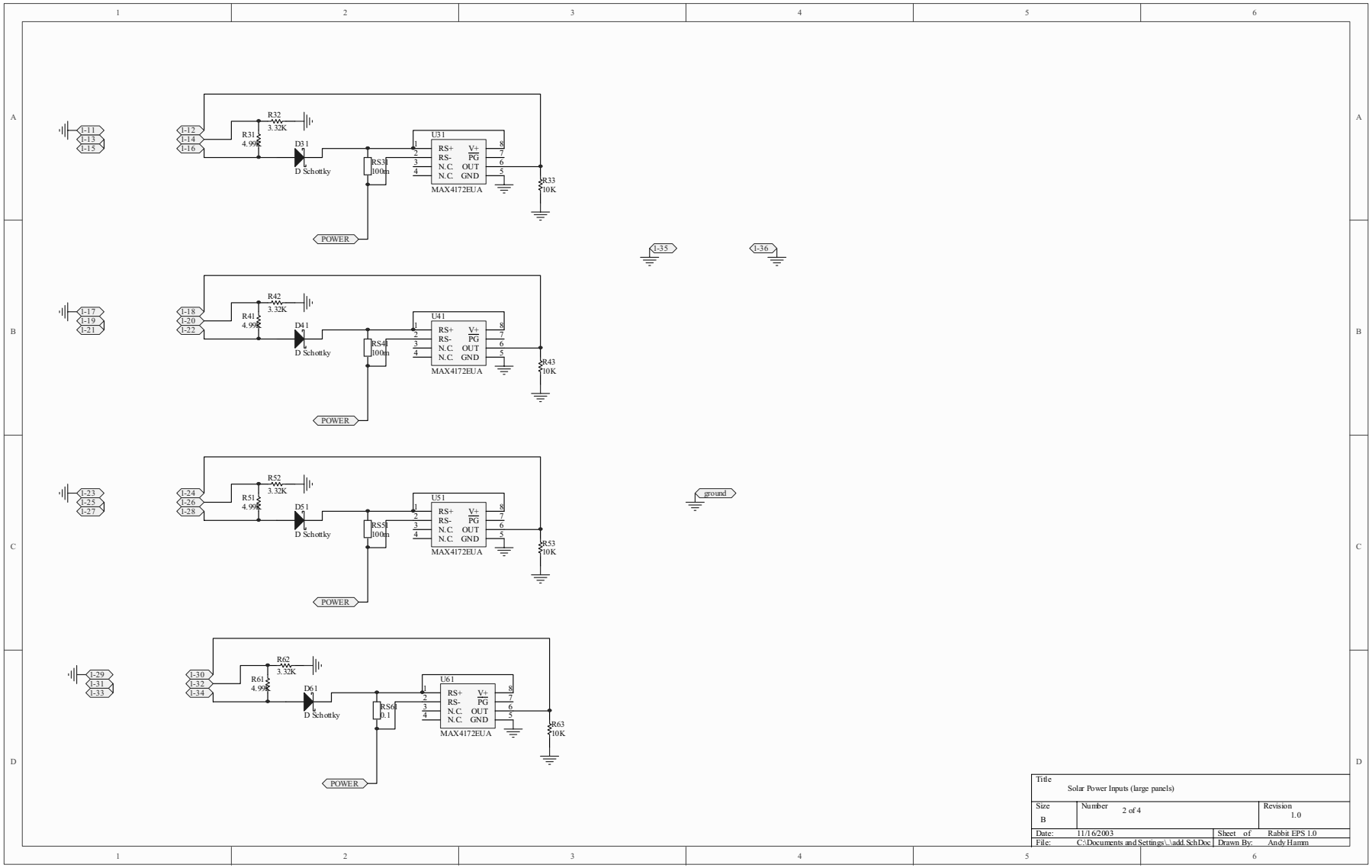
1-11
1-13
1-15
1-12
1-14
1-16
R32
3.32K
R31
4.99K
D31
D Schottky
RS31
100m
U31
RS+
RS-
N.C.
N.C.
V+
PG
OUT
GND
MAX4172EUA
R33
10K
POWER
1-35
1-36
1-17
1-19
1-21
1-18
1-20
1-22
R42
3.32K
R41
4.99K
D41
D Schottky
RS41
100m
U41
MAX4172EUA
R43
10K
POWER
1-23
1-25
1-27
1-24
1-26
1-28
R52
3.32K
R51
4.99K
D51
D Schottky
RS51
100m
U51
MAX4172EUA
R53
10K
POWER
ground
1-29
1-31
1-33
1-30
1-32
1-34
R62
3.32K
R61
4.99K
D61
D Schottky
RS61
0.1
U61
MAX4172EUA
R63
10K
POWER
Title
Solar Power Inputs (large panels)
Size
B
Number
2 of 4
Revision
1.0
Date:
11/16/2003
Sheet of
Rabbit EPS 1.0
File:
C:\Documents and Settings\..\add.SchDoc
Drawn By:
Andy Hamm

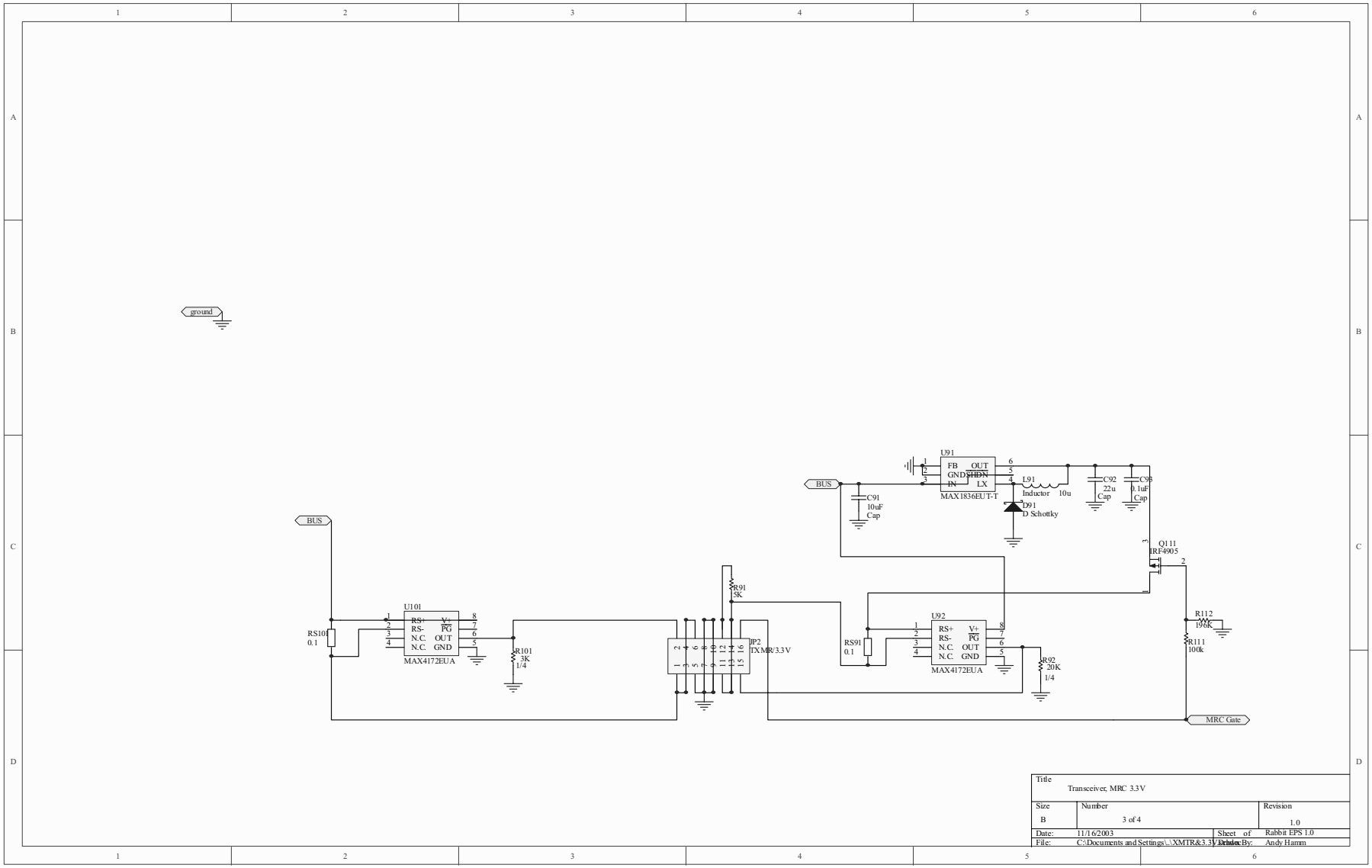
ground
BUS
U101
RS+ V+
RS- PG
N.C. OUT
N.C. GND
MAX4172EUA
RS101
0.1
R101
3K
1/4
R91
5K
JP2
TXMR/3.3V
U91
FB OUT
GND SHDN
IN LX
MAX1836EUT-T
C91
10uF
Cap
L91
Inductor 10u
D91
D Schottky
C92
22u
Cap
C93
0.1uF
Cap
Q111
IRF4905
RS91
0.1
U92
MAX4172EUA
R92
20K
1/4
R112
196K
R111
100k
MRC Gate
Title
Transceiver, MRC 3.3V
Size
B
Number
3 of 4
Revision
1.0
Date: 11/16/2003
Sheet of
Rabbit EPS 1.0
File: C:\Documents and Settings\..\XMTR&3.3V.Schdoc
Drawn By: Andy Hamm

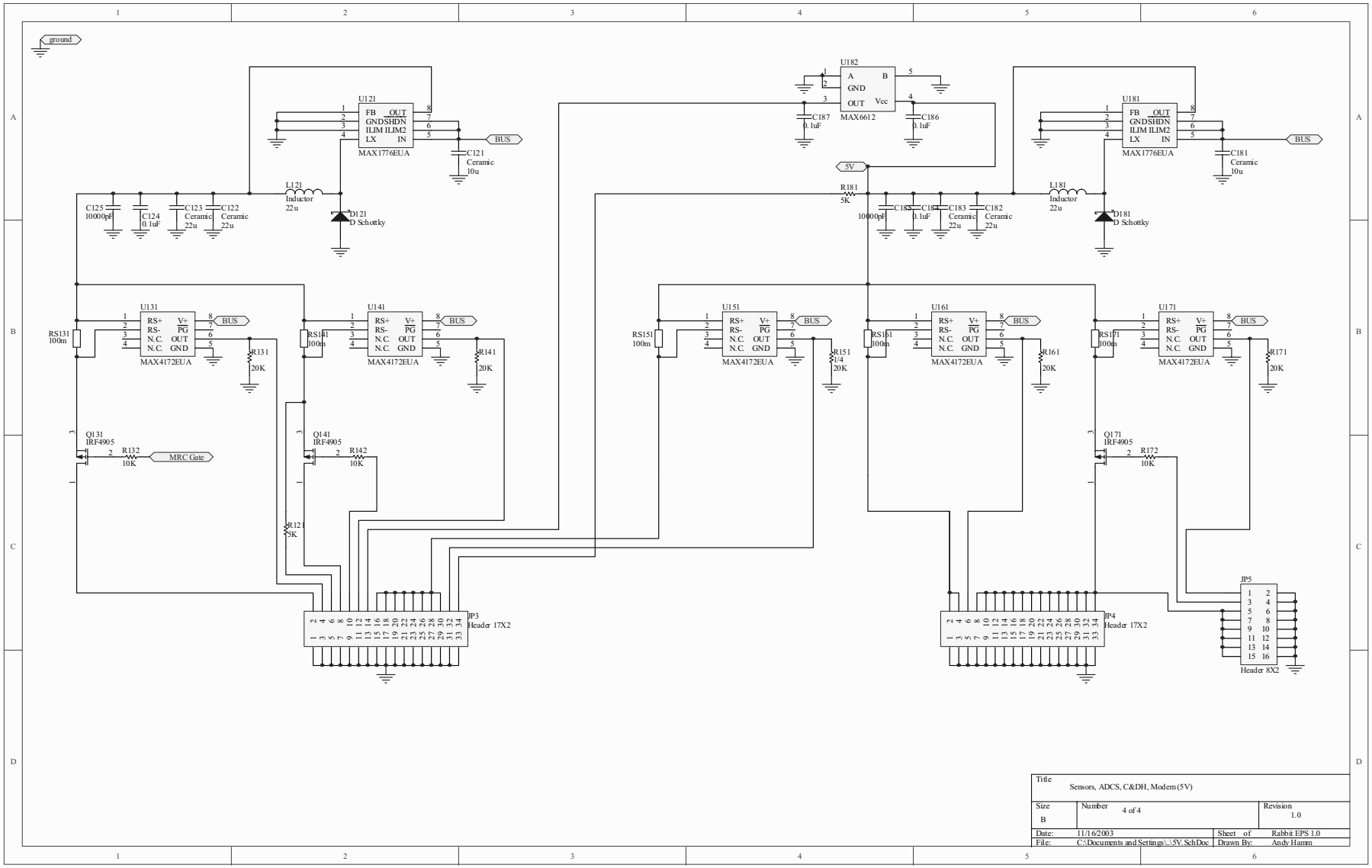
ground
U121
FB OUT
GND SHDN
ILIM ILIM2
LX IN
MAX1776EUA
BUS
C121
Ceramic
10u
L121
Inductor
22u
D121
D Schottky
C125
10000pF
C124
0.1uF
C123
Ceramic
22u
C122
Ceramic
22u
U182
A B
GND
OUT Vcc
MAX6612
C187
0.1uF
C186
0.1uF
5V
R181
5K
C185
10000pF
C184
0.1uF
C183
Ceramic
22u
C182
Ceramic
22u
U181
FB OUT
GND SHDN
ILIM ILIM2
LX IN
MAX1776EUA
C181
Ceramic
10u
L181
Inductor
22u
D181
D Schottky
U131
RS+ V+
RS- PG
N.C. OUT
N.C. GND
MAX4172EUA
RS131
100m
R131
20K
U141
RS141
100m
R141
20K
U151
RS151
100m
R151
20K
U161
RS161
100m
R161
20K
U171
RS171
100m
R171
20K
Q131
IRF4905
R132
10K
MRC Gate
Q141
IRF4905
R142
10K
R121
5K
Q171
IRF4905
R172
10K
JP3
Header 17X2
JP4
Header 17X2
JP5
Header 8X2
Title
Sensors, ADCS, C&DH, Modem (5V)
Size
B
Number
4 of 4
Revision
1.0
Date: 11/16/2003
Sheet of
Rabbit EPS 1.0
File: C:\Documents and Settings\..\5V.SchDoc
Drawn By: Andy Hamm

C.2 Printed Circuit Board

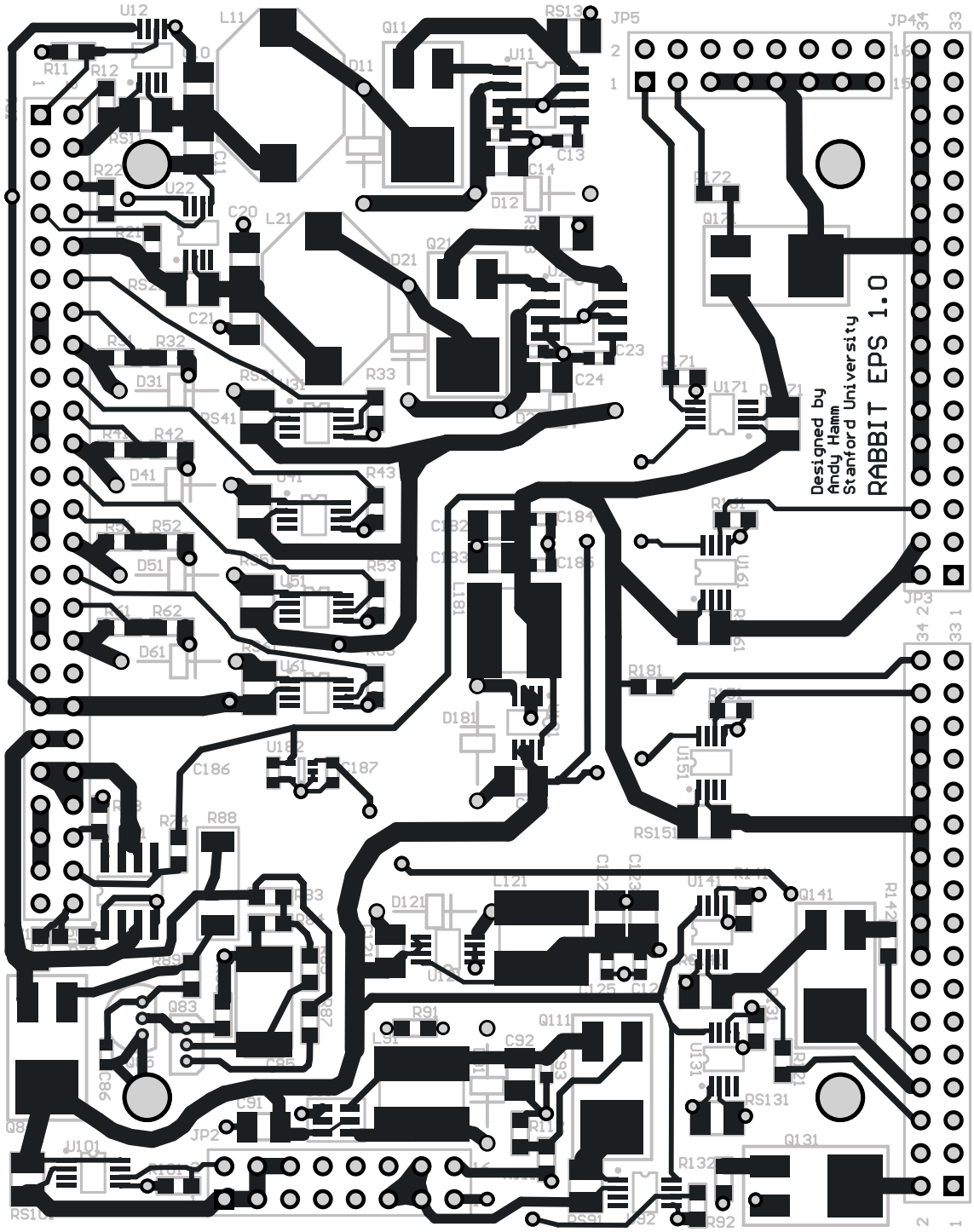

C.3 EPS Board Component Lists

Designator	DIGIKEY Part Number	Footprint	LibRef	Quantity	Value
C10	PCC2326CT-ND	Cap 1206	Cap	1	10uF
C11	PCC2326CT-ND	Cap 1206	Cap	1	10uF
C12	311-1088-1-ND	CAP CER 0.1u	Cap	1	.1uF
C13	311-1088-1-ND	CAP CER 0.1u	Cap	1	.1uF
C14	PCC2326CT-ND	Cap 1206	Cap	1	10uF
C20	PCC2326CT-ND	Cap 1206	Cap	1	10uF
C21	PCC2326CT-ND	Cap 1206	Cap	1	10uF
C22	311-1088-1-ND	CAP CER 0.1u	Cap	1	.1uF
C23	311-1088-1-ND	CAP CER 0.1u	Cap	1	.1uF
C24	PCC2326CT-ND	Cap 1206	Cap	1	10uF
C85	478-1773-1-ND	Cap AVX TPS C/D	Cap Pol2	1	47u
C86	311-1088-1-ND	CAP CER 0.1u	Cap	1	.1u
C91	PCC2326CT-ND	Cap 1206	Cap	1	10uF
C92	445-1393-1-ND	Cap 1206	Cap	1	22u
C93	311-1088-1-ND	CAP CER 0.1u	Cap	1	0.1uF
C121	PCC2326CT-ND	Cap 1206	Cap	1	10u
C122	445-1393-1-ND	Cap 1206	Cap	1	22u
C123	445-1393-1-ND	Cap 1206	Cap	1	22u
C124	311-1088-1-ND	CAP CER 0.1u	Cap	1	0.1uF
C125	311-1085-1-ND	CAP CER 0.1u	Cap	1	10000pF
C181	PCC2326CT-ND	Cap 1206	Cap	1	10u
C182	445-1393-1-ND	Cap 1206	Cap	1	22u
C183	445-1393-1-ND	Cap 1206	Cap	1	22u
C184	311-1088-1-ND	CAP CER 0.1u	Cap	1	0.1uF
C185	311-1085-1-ND	CAP CER 0.1u	Cap	1	10000pF
C186	311-1088-1-ND	CAP CER 0.1u	Cap	1	0.1uF
C187	311-1088-1-ND	CAP CER 0.1u	Cap	1	0.1uF
D11	1N5817DICT-ND	DIODE SCHOTTKY	D Schottky	1	
D12	1N5817DICT-ND	DIODE SCHOTTKY	D Schottky	1	
D21	1N5817DICT-ND	DIODE SCHOTTKY	D Schottky	1	
D22	1N5817DICT-ND	DIODE SCHOTTKY	D Schottky	1	
D31	1N5817DICT-ND	DIODE SCHOTTKY	D Schottky	1	
D41	1N5817DICT-ND	DIODE SCHOTTKY	D Schottky	1	
D51	1N5817DICT-ND	DIODE SCHOTTKY	D Schottky	1	
D61	1N5817DICT-ND	DIODE SCHOTTKY	D Schottky	1	
D91	1N5817DICT-ND	DIODE SCHOTTKY	D Schottky	1	
D121	1N5817DICT-ND	DIODE SCHOTTKY	D Schottky	1	
D181	1N5817DICT-ND	DIODE SCHOTTKY	D Schottky	1	
JP1	S2012-36-ND	HDR2X25	Header 25X2	1	
JP2	S2012-36-ND	HDR2X8	Header 8X2	1	
JP3	S2012-36-ND	HDR2X17	Header 17X2	1	
JP4	S2012-36-ND	HDR2X17	Header 17X2	1	
JP5	S2012-36-ND	HDR2X8	Header 8X2	1	
L11	In Stock of Stanford	Coil DO3316	Inductor	1	22uH
L21	In Stock of Stanford	Coil DO3316	Inductor	1	22uH
L91	308-1224-1-ND	CDRH6D28	Inductor	1	10u
L121	308-1228-1-ND	CDRH6D28	Inductor	1	22u
L181	308-1228-1-ND	CDRH6D28	Inductor	1	22u
Q11	In Stock of Stanford	CASE 369A	MOSFET-N	1	
Q21	In Stock of Stanford	CASE 369A	MOSFET-N	1	
Q83	In Stock of Stanford	TO-92	MOSFET-N	1	

Q84	IRF4905S	CASE 369A	MOSFET-P	1	
Q85	In Stock of Stanford	TO-92 - Round	SCR	1	
Q111	IRF4905S	CASE 369A	MOSFET-P	1	
Q131	IRF4905S	CASE 369A	MOSFET-P	1	
Q141	IRF4905S	CASE 369A	MOSFET-P	1	
Q171	IRF4905S	CASE 369A	MOSFET-P	1	
R11	P10KACT-ND	ResPan ERJ6EN	Res1	1	10K
R12	P4.99KCCT-ND	ResPan ERJ6EN	Res1	1	5K
R21	P4.99KCCT-ND	ResPan ERJ6EN	Res1	1	5K
R22	P10KACT-ND	ResPan ERJ6EN	Res1	1	10K
R31	P4.99KCCT-ND	ResPan ERJ6EN	Res1	1	4.99K
R32	P3.32KCCT-ND	ResPan ERJ6EN	Res1	1	3.32K
R33	P10KACT-ND	ResPan ERJ6EN	Res1	1	10K
R41	P4.99KCCT-ND	ResPan ERJ6EN	Res1	1	4.99K
R42	P3.32KCCT-ND	ResPan ERJ6EN	Res1	1	3.32K
R43	P10KACT-ND	ResPan ERJ6EN	Res1	1	10K
R51	P4.99KCCT-ND	ResPan ERJ6EN	Res1	1	4.99K
R52	P3.32KCCT-ND	ResPan ERJ6EN	Res1	1	3.32K
R53	P10KACT-ND	ResPan ERJ6EN	Res1	1	10K
R61	P4.99KCCT-ND	ResPan ERJ6EN	Res1	1	4.99K
R62	P3.32KCCT-ND	ResPan ERJ6EN	Res1	1	3.32K
R63	P10KACT-ND	ResPan ERJ6EN	Res1	1	10K
R71	P4.99KCCT-ND	ResPan ERJ6EN	Res1	1	4.99K
R72	P3.32KCCT-ND	ResPan ERJ6EN	Res1	1	3.32K
R73	P6.81KCCT-ND	ResPan ERJ6EN	Res1	1	6.6K
R74	P20.0KCCT-ND	ResPan ERJ6EN	Res1	1	20K
R83	P10MACT-ND	ResPan ERJ6EN	Res1	1	10meg
R84	P10MACT-ND	ResPan ERJ6EN	Res1	1	10meg
R85	P6.2MACT-ND	ResPan ERJ6EN	Res1	1	6.2meg
R86	P10KACT-ND	ResPan ERJ6EN	Res1	1	10K
R87	P10KACT-ND	ResPan ERJ6EN	Res1	1	10K
R88	PT470XCT-ND	RESPAN ERj1t	Res1	1	470
R89	P100ACT-ND	ResPan ERJ6EN	Res1	1	100
R91	P4.99KCCT-ND	ResPan ERJ6EN	Res1	1	5K
R92	P20.0KCCT-ND	ResPan ERJ6EN	Res1	1	20K
R101	P3.01KCCT-ND	ResPan ERJ6EN	Res1	1	3K
R111	P100KCCT-ND	ResPan ERJ6EN	Res1	1	100k
R112	P196KCCT-ND	ResPan ERJ6EN	Res1	1	196K
R121	P4.99KCCT-ND	ResPan ERJ6EN	Res1	1	5K
R131	P20.0KCCT-ND	ResPan ERJ6EN	Res1	1	20K
R132	P10KACT-ND	ResPan ERJ6EN	Res1	1	10K
R141	P20.0KCCT-ND	ResPan ERJ6EN	Res1	1	20K
R142	P10KACT-ND	ResPan ERJ6EN	Res1	1	10K
R151	P20.0KCCT-ND	ResPan ERJ6EN	Res1	1	20K
R161	P20.0KCCT-ND	ResPan ERJ6EN	Res1	1	20K
R171	P20.0KCCT-ND	ResPan ERJ6EN	Res1	1	20K
R172	P10KACT-ND	ResPan ERJ6EN	Res1	1	10K
R181	P4.99KCCT-ND	ResPan ERJ6EN	Res1	1	5K
RS11	RL12S.10FCT-ND	Res RL1220	Res2	1	100m
RS13	RL12S.18FCT-ND	Res RL1220	Res2	1	180m
RS21	RL12S.10FCT-ND	Res RL1220	Res2	1	100m
RS23	RL12S.18FCT-ND	Res RL1220	Res2	1	180m

RS31	RL12S.10FCT-ND	Res RL1220	Res2	1	100m
RS41	RL12S.10FCT-ND	Res RL1220	Res2	1	100m
RS51	RL12S.10FCT-ND	Res RL1220	Res2	1	100m
RS61	RL12S.10FCT-ND	Res RL1220	Res2	1	0.1
RS91	RL12S.10FCT-ND	Res RL1220	Res2	1	0.1
RS101	RL12S.10FCT-ND	Res RL1220	Res2	1	0.1
RS131	RL12S.10FCT-ND	Res RL1220	Res2	1	100m
RS141	RL12S.10FCT-ND	Res RL1220	Res2	1	100m
RS151	RL12S.10FCT-ND	Res RL1220	Res2	1	100m
RS161	RL12S.10FCT-ND	Res RL1220	Res2	1	100m
RS171	RL12S.10FCT-ND	Res RL1220	Res2	1	100m
U11	Sample ordered from MAXIM-IC, ask Prof. Twiggs	SO-G8	MAX1771ESA	1	
U12	MAX4172EUA-ND	TSSO3X5-G8/X.35	MAX4172EUA	1	
U21	Sample ordered from MAXIM-IC, ask Prof. Twiggs	SO-G8	MAX1771ESA	1	
U22	MAX4172EUA-ND	TSSO3X5-G8/X.35	MAX4172EUA	1	
U31	MAX4172EUA-ND	TSSO3X5-G8/X.35	MAX4172EUA	1	
U41	MAX4172EUA-ND	TSSO3X5-G8/X.35	MAX4172EUA	1	
U51	MAX4172EUA-ND	TSSO3X5-G8/X.35	MAX4172EUA	1	
U61	MAX4172EUA-ND	TSSO3X5-G8/X.35	MAX4172EUA	1	
U71	In Stock of Stanford	SO-G8	MAX471ESA	1	
U91	In Stock of Stanford	SO-G6/P.95	MAX1836EUT-T	1	
U92	MAX4172EUA-ND	TSSO3X5-G8/X.35	MAX4172EUA	1	
U101	MAX4172EUA-ND	TSSO3X5-G8/X.35	MAX4172EUA	1	
U121	Sample ordered from MAXIM-IC, ask Prof. Twiggs	TSSO3x5-G8/X.35	MAX1776EUA	1	
U131	MAX4172EUA-ND	TSSO3X5-G8/X.35	MAX4172EUA	1	
U141	MAX4172EUA-ND	TSSO3X5-G8/X.35	MAX4172EUA	1	
U151	MAX4172EUA-ND	TSSO3X5-G8/X.35	MAX4172EUA	1	
U161	MAX4172EUA-ND	TSSO3X5-G8/X.35	MAX4172EUA	1	
U171	MAX4172EUA-ND	TSSO3X5-G8/X.35	MAX4172EUA	1	
U181	Sample ordered from MAXIM-IC, ask Prof. Twiggs	TSSO3x5-G8/X.35	MAX1776EUA	1	
U182	Sample ordered from MAXIM-IC, ask Prof. Twiggs	SC70	MAX6612	1	